4 Code Assessment Activities [Sensitivity Studies]

Sensitivity studies are required to investigate uncertainties in the analytical simulation modeling (ASM) of an experiment, or postulated plant accident. The ASM, defined in Section 3, has three modeling components: user, code, and accident (experiment) scenario. Uncertainties in the ASM can be found in each component; these uncertainties should be identified, as much as practical, within each component. The results of sensitivity studies provide important feedback for the ranking of phenomena, identified in Section 2, which in turn helps to focus these types of investigations. Therefore, some of the studies in the following subsections are intended as confirmation of the high ranking given to certain phenomena, other studies are provided to show that phenomena are less important for establishing accurate predictions of pressure, temperature, and gas concentration in containments during design basis or beyond design basis accidents. In most experiments, sensitivities studies are paramount to an understanding of the physics occurring in the experiments, and in this regard, the CONTAIN code is well structured to provide the needed flexibility for investigating uncertainties in each ASM component. Many of these types of sensitivities are explored in this section so that we have a better understanding of controlling processes in an assessment experiment. Clearly, a good series of sensitivity studies depends on how well certain basic phenomena are simulated by the code; therefore, feedback from sensitivity studies is used to improve physical modeling, which in turn benefits the studying of user, initial and boundary condition uncertainties, etc.

Listings of the various types of sensitivity studies described in the following subsection for separate and integral effects testing are given in Tables 4.1 and 4.2, respectively. Fifteen of the twenty reference tests are used as a basis for over 80 sensitivity calculations. In the tables, an attempt is made to catagorize the type of study according to the primary code model(s) involved, and the ASM component most applicable to the parametric variation. For some studies, one or more ASM components are involved. The variables (comparison of data to calculated, or variation in calculated), on which assessments may be rendered, are listed in the last column of the each table.

Table 4.1 Listing of separate effects sensitivity studies described in Section 4.				
Experiment	Code Model	ASM type	Sensitivity	Dependent variable (comparisons)
Wisc. Flat Plate	HMTA	Code	mixed convection algorithm	condensation heat transfer coefficient
		Code	film theory correction for mass rate effects	
		User/Code	condensate film thickness	
Phebus FPT0	HMTA	Expr.	condenser wall temp.	pressure
		User/Code	condensate film thickness	
	HMTA/ Atmos. T.H.*	Code	convective heat and mass transfer	pressure and condensation rate
JAERI Spray Tests	Spray	User	spray region nodalization	pressure and temperature
		User/Code	spray droplet diameter	pressure, temperature, and saturation ratio
	film tracking /HMTA	User/Expr./ Code	spray water washdown	pressure and temperature
	HMTA	User	forced convection	
	Flow solver	User/Code	stratification	
	Pool-gas HMTA	Code	sump-gas heat and mass transfer	pressure

* Thermal Hydraulics

Table 4.2 Listing of integral effects sensitivity studies described in Section 4.				
Experiment	Code Model	ASM type	Sensitivity	Dependent variable (comparisons)
HDR:				
V44 (ISP16)	HMTA	User	forced convection	pressure
	Flow solver		nodalization	pressure and temperature
	HMTA		structure heat transfer	pressure
	Atmos. T.H.*		atmospheric liquid water	
	HMTA		energy velocity methodology	
	Atmos. T.H./ Flow solver		atmospheric liquid water	pressure, and pressure differential
	Flow solver		loss coefficient/inertia length	
T31.5 (ISP23)	HMTA	User	forced convection	pressure
	Atmos. T.H. / Flow solver	User/Code	atmospheric liquid water	pressure and pressure differential
T31.5 (benchmark)	Flow solver	User	nodalization	pressure, temperature, and hydrogen concentration
		Code	stratification stable vs. metastable	temperature and hydrogen concentration
E11.2 (ISP29)	1-D transient conduction	Expr.	thermal conductivity of concrete (water absorption)	pressure
	Atmos. T.H.	Expr.	Instrument cooling	
	Atmos. T. H./ HMTA	Expr.	presents of shell-to-concrete gap heat sinks	
	Atmos. T. H.	Expr.	steam injection rate	
	Flow solver	User	nodalization	
	Flow solver	Code	stratification	pressure, temperature, and hydrogen concentration

Table 4.2 Listing of integral effects sensitivity studies described in Section 4. (Cont.)				
Experiment	Code Model	ASM type	Sensitivity	Dependent variable (comparison)
E11.4 (benchmark)	Flow solver	User	nodalization	pressure
	1-D conduction / HMTA	Expr.	initial temperature of heat sinks	
	1-D conduction	Expr.	thermal conductivity of concrete (water absorption)	
CVTR:				
CVTR Test #3	Flow solver	User	nodalization	pressure and temperature
	HMTA	Expr.	steel and concrete heat sink amounts	
	1-D conduction	Expr.	containment shell-to-concrete air gap	
	Atmos. T.H.	Expr.	steam enthalpy	
	Atmos. T.H.	User/Code	atmospheric liquid water	
	Atmos. T.H. / spray	User	water carry over	
	HMTA	User	forced convection	
NUPEC Tests:				
M-8-1	Flow solver	Code	stratification	pressure, temperature, and hydrogen concentration
M-7-1	HMTA / Spray	User	forced convection	
	Spray / film tracking	User	spray washdown	
	Spray / flow solver	User	nodalization	

* Thermal Hydraulics

4.1 Separate Effects

4.1.1 Wisconsin Flat Plate Condensation Tests

Default mixed convection algorithm.

The CONTAIN default mixed convection algorithm for the average Nusselt number is given as

$$N_{Nu} = \max\left[N_{Nu,c}, N_{Nu,f}\right]$$

where $N_{Nu,c}$ and $N_{Nu,f}$ are the Nusselt numbers determined by natural and forced convection, respectively. In Huh93 the condensation heat transfer coefficients were calculated locally using a 1-D condensation model consistent with the averaged CONTAIN forced convective model for flat plates. It was apparent in that analysis that at low velocities, the heat transfer coefficient was significantly under predicted. We believe that under prediction is the result of the neglect of natural convection effects when the forced convection velocities are ~ 1 m/s. To show this, the reference calculation was rerun for two cases: the first run duplicated the Huh93 analysis, with $N_{Nu} = N_{Nu,f}$; the second case was run with $N_{Nu} = N_{Nu,c}$. These results are shown in Table 4.3, as h_{calc}(forced) and h_{calc}(nat), along with the default mixed convective run denoted by h_{ref}. Cases #1, 3, 5, and 6 are conducted at a low velocity of 1 m/s. In each of these cases, we see that the reference calculation predicted $N_{Nu} = N_{Nu,c}$; furthermore, the heat transfer coefficients determined in this manner were consistently within the ± 10% instrument error for Cases #1, 3, and 6, and within ± 14% for Case #5, Table 4.4. In contrast, when these cases were calculated using only the forced convective option, the resulting coefficients were found to be significantly lower than the natural convective contribution, and below the instrument error as shown in Table 4.4.

At the high velocity, 3 m/s, the default mixed convective correlation gave a Nusselt number that was equal to the forced convective Nusselt number, Cases #2 and #4. In these two instances, using the natural convective Nusselt number produces a heat transfer coefficient that is significantly under predicted, shaded in Table 4.4; whereas, the forced convective Nusselt number selection in the mixed algorithm resulted in excellent agreement with the measurements.

Film theory correction for mass rate effects.

In CONTAIN, the heat and mass transfer analogy (HMTA) is used to determine the mass transfer (condensation/evaporation) with a correction, based on film theory[1], for high mass rate effects. The correction factor, F, was separated out of the CONTAIN equations and presented in Table 3.9. These correction factors can be used to calculate uncorrected heat transfer coefficients from the CONTAIN results. In Table 4.3, these uncorrected coefficients are denoted by h_{calc} (mix)*, where the "(mix)" designation indicates that the default mixed convection algorithm is used, and the "*" shows that the coefficient are uncorrected for mass rate effects. Shown in Table 4.5 are the associated errors that would be obtained had the correction factor not been included in the CONTAIN modeling. The errors are significant, especially for the cases with the highest measured heat fluxes (i.e., highest mass transfer rates). Had the CONTAIN model not included the correction for mass rate effects, the calculated heat transfer coefficients would have been significantly under predicted.

Condensate Film Thickness.

The reference calculation was modeled using the condensate film tracking option. The effect of this option is also compared in Table 4.3 with the default options that sets the maximum film thickness to 0.0005 meters. In another assessment effort [Til96], it was found that the default film thickness may be too large for fluxes in the range measured for these tests. Therefore, the film tracking option was used in the reference calculation. To investigate the sensitivity of the calculated coefficients to film thickness, a run was made using the default film thickness, h_{calc} (film). If the default film thickness is increased, the resistance to heat transfer is increased and the heat transfer coefficient is accordingly reduced. We can see that this is the case from Table 4.3. The errors shown in Table 4.6 are not large however, and we can conclude that for these tests film thickness is not a sensitive parameter, except when the total resistance to heat transfer is relatively small (i.e., high heat transfer coefficient) as in Case #6.

[1] Bird, R. B., Stewart, W. E., and Lightfoot, E. N., Transport Phenomena, 6th Printing, John Wiley & Sons, Inc., pp. 658-668, 1965.

Table 4.3 Sensitivity of CONTAIN average heat transfer coefficients in the Wisconsin flat plate condensation experiments.

Case #	T_{mix}, C	T_w, C	m_{air}/m_{steam}	V, m/s	h_{calc}(ref) [h_{calc}(forced)] |h_{calc}(nat)| {h_{calc}(mix)*} <h_{calc}(film)>	h_{exp}	$h_{exp(max, min)}$ (error band)
1	70	30	3.5	1	**103.8** [88.6] |103.8| {88.49} <98.6>	111.1	122.2 99.99
2	70	30	3.5	3	**210.7** [210.7] |103.8| {180.0} <196.5>	213.9	235.3 192.5
3	80	30	1.78	1	**165.4** [125.5] |165.4| {125.0} <154.7>	163.9	180.3 147.5
4	80	30	1.78	3	**296.9** [296.9] |165.4| {224.2} <273.2>	305.6	336.2 275.0
5	90	30	0.68	1	**292.1** [198.9] |292.1| {173.3} <265.6>	255.5	281.1 229.95
6	95	45	0.29	1	**501.5** [340] |501.5| {238.5} <424.7>	546.	600.6 491.4

Table 4.4 Comparison of condensation heat transfer coefficient, calculation errors for the Wisconsin flat plated tests with the default mixed (reference), forced, and natural convective algorithms in the CONTAIN code.

Case #	V, m/s	Calculation Error, % [a]		
		h(ref)	h(forced)	h(nat)
1	1	6.57	20.3	6.57
2	3	1.5	1.5	51.5
3	1	-0.92	23.4	-0.92
4	3	2.85	2.85	45.9
5	1	-14.3	22.2	-14.3
6	1	8.15	37.7	8.15

[a][(exp.)-(calc.)/(exp.) * 100]

Table 4.5 Comparison of calculation errors for the Wisconsin flat plate tests when mass rate effects are not taken into account.

		Calculation Error, % [a]	
Case#	Energy Flux, W/m^2	h(ref)	h (uncorrected)
1	4444	6.57	20.3
2	8556	1.5	15.8
3	8195	-0.92	23.7
4	15280	2.85	26.6
5	15330	-14.3	32.2
6	24570	8.15	56.3

[a][(exp.)-(calc.)/(exp.) * 100]

Table 4.6 Effect of film thickness on the calculation errors for heat transfer coefficients in the Wisconsin flat plate tests.

Case #	Measured h	Calculation Error, % [a]	
		h(ref)	h(default film)
1	111.1	6.57	11.3
2	213.9	1.5	8.1
3	163.9	-0.92	5.6
4	305.6	2.85	10.6
5	255.5	-14.3	-3.9
6	546.	8.15	22.2

[a][(exp.)-(calc.)/(exp.) * 100]

4.1.2 Phebus Test FPT0

Condenser Wall Temperature.

Condenser wall temperatures are controlled during the Phebus test to maintain a nearly constant temperature. However, there are a few degrees variation as the condensation rate varies due to changes in the steam injection. Since the variation is relatively small, a user may choose to use a constant, "average" condenser wall temperature instead of the variable temperature input for the reference calculation. A sensitivity calculation is run with a constant wall temperature of 353.15 K. Shown in Figure 4.1 is the comparison of measured and calculated vessel pressure. After the first pressure increase, the pressure relaxes as the steam injection is reduced. The measured condenser wall temperature during this relaxation period is about 3 degrees less than the averaged temperature used in the sensitivity run. Since this constant temperature used in the calculation is too high during this period, the condensation rate is reduced too much and the calculated pressure is over predicted. The rest of the transient however is calculated with good accuracy, except at the end where again the measured wall temperature is less than the averaged temperature, and the pressure is over predicted again.

Condensate Film Thickness.

The reference calculation was run using the film tracking option for estimating condensate thickness on the condenser wall. Shown in Figure 4.2 is the pressure variation that results when the default maximum film thickness of 0.0005 meters is used. As with the Wisconsin tests, using the default film thickness for this test results in an over prediction of pressure at high condensation rates. The film tracking option gives better results.

Natural Convective Condensation.

The default natural convective correlation used for turbulent heat transfer to wall surfaces in CONTAIN is

$$N_{Nu,c} = 0.14\left(N_{Gr}N_{\mathrm{Pr}}\right)^{0.33}$$

where, $N_{Nu,c}$ is the Nusselt number for natural convection; N_{Gr} is the Grashof number; and, N_{Pr} is the Prandtl number. This relationship is also used in the HMTA with the Nusselt number replaced by the Sherwood number N_{Sh} and the Prandtl number replaced with the Schmidt number N_{Sc}. In more recent heat transfer texts, the leading coefficient in the correlation is 0.10 instead of 0.14. To examine how changing the natural convective correlation leading coefficient affects the Phebus calculation, the coefficient was changed in the input to 0.10 using the N_{Nu}

and N_{Sh} multiplier keyword HMXMUL. Shown in Figure 4.3 is the pressure variation with this change. The smaller coefficient results in an increase in the calculated pressure which is consistently greater than the measured pressure in the test. The variation of the condensation rate, Figure 4.4 also shows that change is in the direction of a larger deviation from measured condensation rates for periods when the steam injection is highest. Overall, the better thermal hydraulic performance is obtained using the default natural convection correlation.

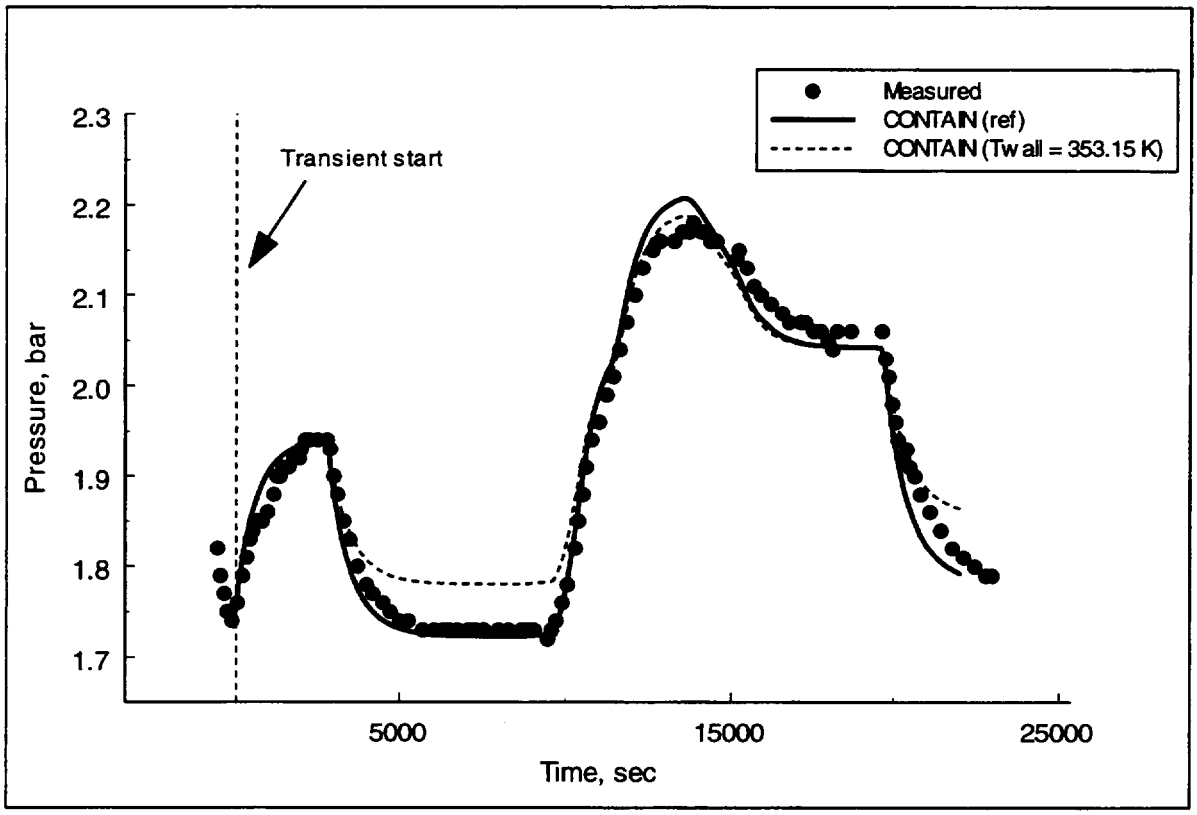

Figure 4.1 Comparison of measure and calculated vessel pressures for Phebus test FPT0 showing the effect of condenser wall temperature on pressure.

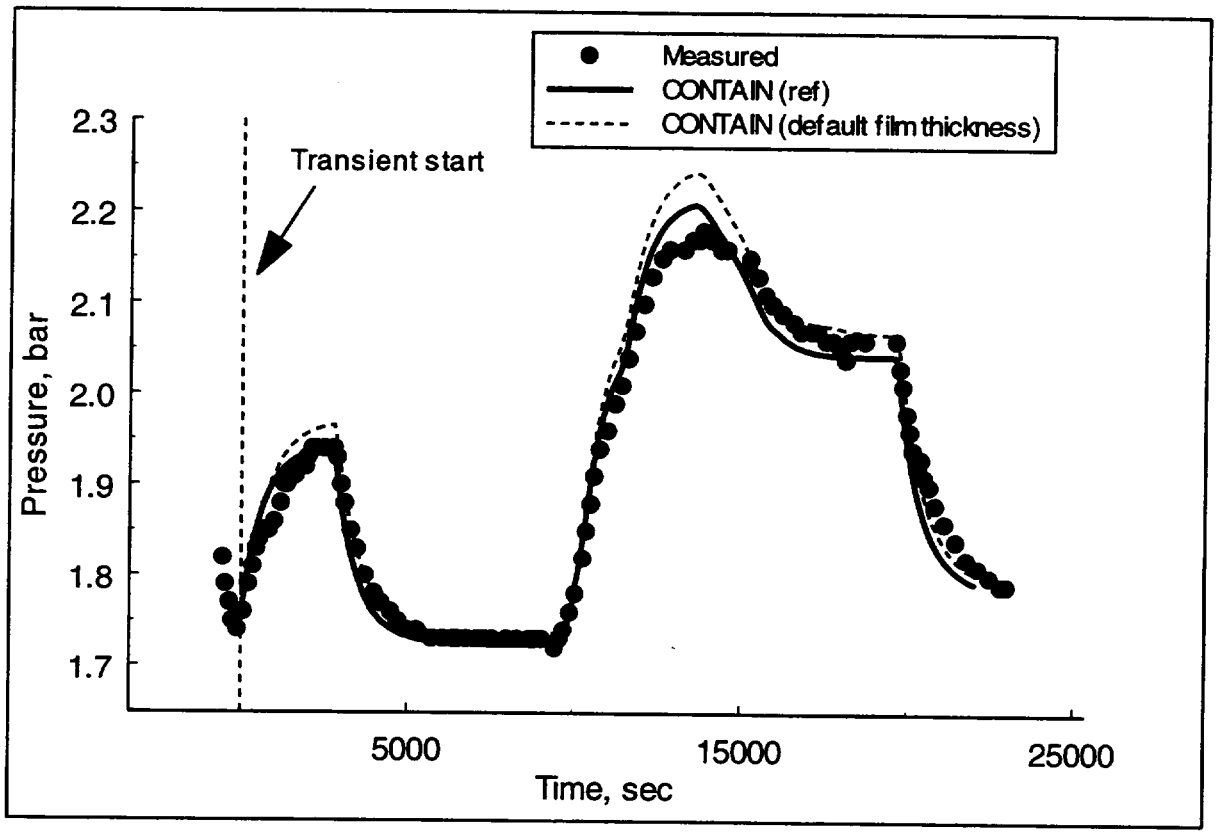

Figure 4.2 Comparison of measured and calculated vessel pressure for Phebus test FPT0 showing the effect of condensate film thickness on pressure.

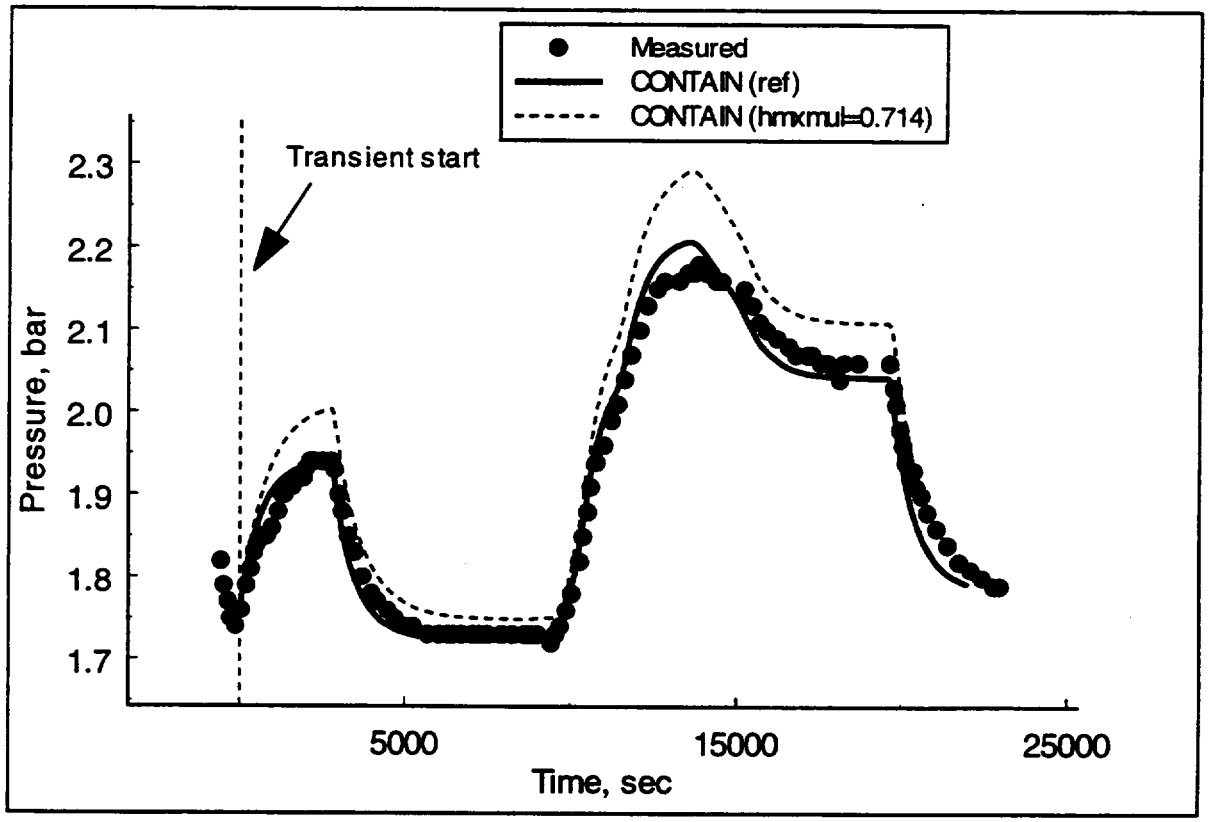

Figure 4.3 Comparison of measured and calculated vessel pressure for Phebus test FPT0 showing the effect of a reduction in the leading coefficient of the natural convective correlation from 0.14 in the reference calculation to 0.10 for the case hmxmul=0.714.

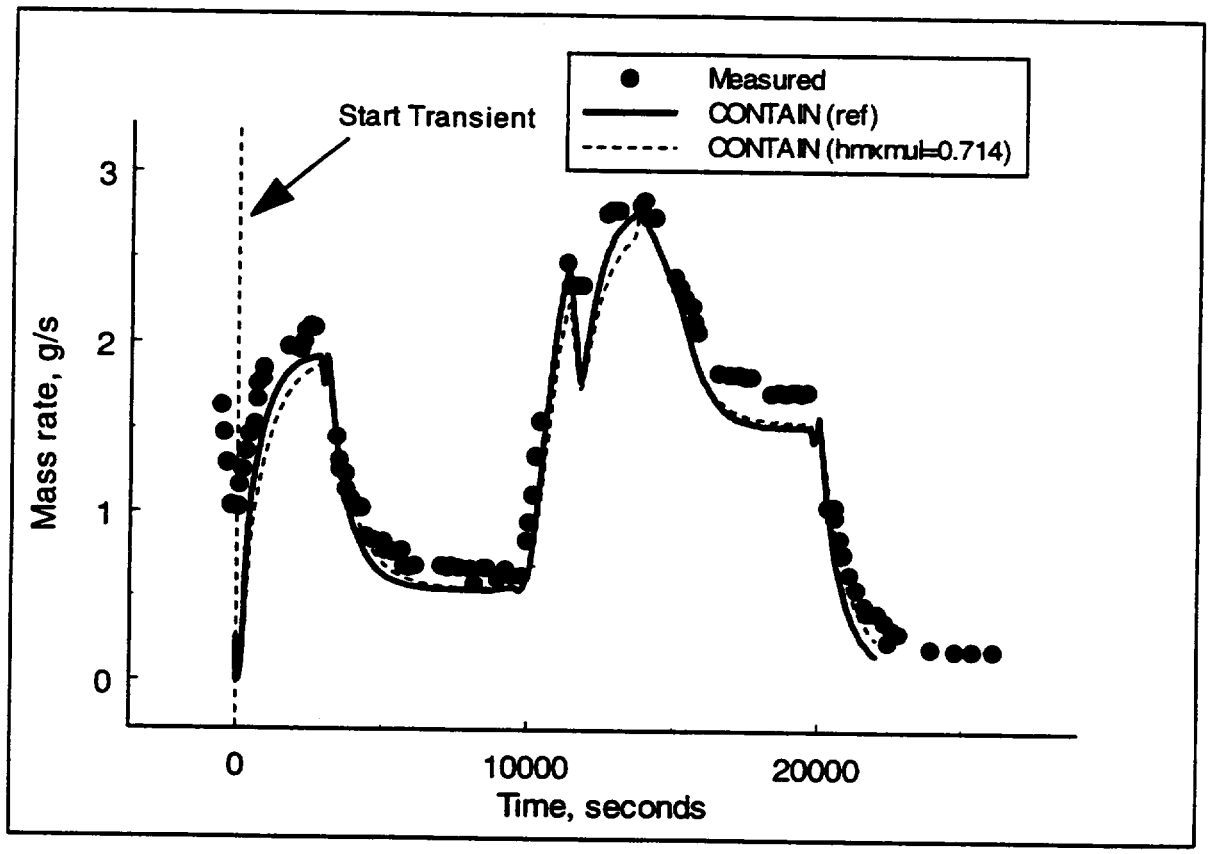

Figure 4.4 Comparison of measured and calculated condensation rates for Phebus test FPT0 showing the effect of a reduction in the leading coefficient of the natural convective correlation from 0.14 in the reference calculation to 0.10 for the case hmxmul=0.714.

4.1.3 JAERI Pressure Suppression Spray Tests

Spray region nodalization.

The CONTAIN spray model restricts the interaction of spray droplets and atmosphere within a spray region to the cell in which the spray source is specified, that is, there is no spray fall-through capability between cells. During the time that sprays are activated, the turbulence that the sprays impose on the atmosphere will induce mixing such that the spray region is essentially uniformly mixed and modeling the spray region with one cell is adequate for predicting pressure and temperature within the region during these periods. This observation is supported by the good results obtain in the reference calculations for the JAERI tests. However, limiting the spray region to a single cell may, in some cases, be too restrictive; for example, regional stratification may occur during periods before or after sprays are activated, and to model these cases, a multi-cell nodalization for the region needs to be considered. An alternative to the single spray cell is investigated here to show how a variation on input allows a multi-cell treatment of a spray region. Because the CONTAIN spray model restricts sprays to the cell in which the spray injection is defined, adjustments in the multi-cell input must be made to approximate the effect of droplets falling through a series of vertically aligned cells. To accomplish this, pseudo pools feed sprays in "fall-through" cells; each pool (without heat transfer to the atmosphere) feeds a spray source in an adjoining cell below through a pump. Water is pumped from each pseudo pool at a rate equal to or slightly greater than the spray injection rate to prevent accumulation of water in the cells.

Shown in Figure 4.5 is a 16-cell nodalization of the JAERI test vessel. Pressure and temperature histories of the air/steam mixture in the vessel for the single nozzle spray test PHS-6 for the single and multi-cell models are shown in Figures 4.6 and 4.7, respectively. The pressure follows very closely the single cell pressure which, as noted in the reference calculation, is in very good agreement with measurements. Additionally, the temperature in the spray region for the multi-cell model is also in very good agreement with the data. The slight over prediction in the pressure at the end of the transient, compared to the single cell calculation, is due to differences in predicted mixing in the non-spray region above the spray source. In the CONTAIN multi-cell calculation, cell #1 is an unmixed region but in the actual test the region just above the spray elevation is also mixed. Turbulence created by the spray/gas interaction is large enough that mixing extends above the spray nozzle elevation. CONTAIN does not model this interaction and therefore predicts the region to be unmixed with a higher temperature causing the pressure calculation to be over predicted slightly. The small reduction of the temperature in the spray region compared to the single cell calculation is due to differences in the sensible heat transfer calculation between spray droplet and atmosphere in the single and multi-cell models. In the single cell case, the number of spray droplets are determined by the injected water rate and the specified spray droplet diameter. As the spray droplets fall through the atmosphere, vapor condenses on the droplets, increasing the diameter accordingly. With the nodalized vessel cascading water sources are defined at each cell level in the spray region; each of these water

sources re-initialize the spray droplet size distribution so that the entire spray region is populated with sprays of smaller diameter than for the single cell model. The result of this variation in droplet size modeling is that the surface area for sensible heat transfer between droplet and atmosphere is somewhat greater for the nodalized vessel than for the single cell model. Increased sensible heat transfer, eliminates the small degree of superheating predicted in the single cell reference calculation. The additional sensible heat transfer keeps the gas mixture temperature at saturation, which is in agreement with the thermal condition in the vessel estimated from the pressure and temperature measurements (see below).

Spray droplet diameter and fall height.

The phenomenon of water spray pressure suppression can be explained by using a two-phase T-V diagram for steam. In Figure 4.8, a diagram with the region of interest is expanded for discussion purposes, where in actuality P1 is only slightly greater than P2. When sprays are introduced into a vapor space that is saturated, point B on the diagram, the gas mixture temperature during depressurization tends to follow the saturation line B-E. We can think of this occurring as a two step process for discussion; the first process being condensation of vapor on the droplet (B-C) and then the second process being sensible heat transfer from a slightly superheated vapor space to the colder surface of the droplets (C-D-E). When the sensible heat transfer is large enough, the saturation curve is intersected (point E), and we observe the atmosphere temperature following the saturation curve during the depressurization process. This process is demonstrated in the single nozzle test PHS-6. Since the containment space for this test is well mixed we can estimate the saturation temperature of the gas mixture and compare that temperature to the measured temperature. Shown in Figure 4.9 is the comparison that shows that for this test the depressurization process is indeed following the saturation curve.

In most cases, energy transfer by sensible heat transfer is not large enough to cause homogeneous condensation in the atmosphere, E-F; and, in other cases when the sensible heat transfer is too small (relative to the condensation rate) the transfer rate will not be high enough to bring the atmosphere down from a superheated state (C) to saturation (E). When the latter occurs the atmosphere remains superheated during the spray pressure suppression process. One of the ways to observe this effect is to inject sprays of various spray droplet sizes. By varying the droplet size, the surface area for sensible heat transfer is also varied. The larger droplet sizes with less surface area per mass injected will tend to represent cases of superheat while the cases with smaller droplets will produce a saturation condition.

A typical spray drop distribution from a containment spray nozzle is shown in Figure 4.10 [Pas71]. As condensation occurs the distribution is shifted to slightly larger spray droplets, Figure 4.11. And, as the spray droplets fall, some coalesce, reducing the number of smaller droplets. Pas71 has estimated the effect of coalescence in the spray region in a typical containment to be less than 10%, as indicated by the change in the surface area per unit volume of the droplets during the fall, Figure 4.12. Shown in Figure 4.13 is a regression analysis of the

mass distribution for the SPRACO 1713A nozzle [BW74]. The median spray droplet diameters (50% cumulative mass) for this distribution is approximately 0.001 meters, while the mean diameter (based on the count or frequency distribution) is 0.000658 meters.

Shown in Figures 4.14 and 4.15 are the temperature and pressure sensitivities to a range of spray diameters. Shown in Figure 4.16 are the saturation ratios (humidity ratios) for the various spray diameters. We see from these figures that spray diameters $\leq$0.001 meters are required to match experimental data for pressure and temperature. Diameters of this size also are in agreement with representative diameters for a typical spray distribution. Figure 4.17 provides a comparison of measured and calculated gas mixture temperatures using the mass median (0.001 meters) and the count mean (0.000658 meters) diameters, represented by the typical spray droplet distribution mentioned above. In addition, Figure 4.17 also includes a case with four spray sources, each represented by the mean count diameter for the size segment of the typical spray droplet distribution. The spray droplet diameter segments for the multiple spray case are 0.0001 - 0.0005 meters, 0.0006 - 0.001 meters, 0.0011 - 0.0015 meters, and 0.0016 - 0.002 meters. Representative spray droplet diameters based on either the mass median, count mean, or the segmented distribution gives reasonably good agreement with the data. The better agreement however corresponds to the case where the representative droplet diameter is less than either of these averages, as indicated for the calculation were the representative diameter is taken as 0.0002 meters.

The ratio of sensible to condensation heat transfer can also be affected somewhat by the extending the time that a single droplet remains suspended in the containment. A long residence time will provide more time for sensible heat transfer to occur when the atmosphere becomes superheated as a result of a condensation process that occurs mainly during the first few meters of fall. For example, extending the fall height of an initial 0.001 meter diameter droplet from 18 to 50 meters increases the saturation ratio in the JAERI vessel for test PHS-6 from 0.9 to 0.96, and reduces the degree of superheating by approximately 55% (3 degrees superheat reduced to 1.3 degrees).

Spray water washdown/forced convection.

In a rapid pressurization event, sprays may be activated shortly after an initial blowdown period. Activation will therefore follow a period of significant pre-heating of structural steel in the containment (containment shell and miscellaneous support structure). When and if spray water contacts these hot surfaces, some water may be evaporated. The evaporation effectively transfers energy from the pre-heated structures back into the atmosphere, while increasing the water vapor content of the atmosphere. These two effects tend to 1) increase the atmospheric pressure and 2) maintain the atmosphere near saturation. In addition to these effects, the action of the falling spray droplets on confined gases in the containment may also setup significant gas flows or circulation currents within open regions near hot surfaces. The gas flows can increase both

sensible heat and, if water is present on the surfaces, mass transfers from walls through the process of forced convection. If the gas flows are significant they may also be responsible for entraining and carrying suspended spray droplets to wall surfaces, and therefore may also be responsible in part for water deposited on the surfaces of structures. To investigate the effects of these transfer processes on predicted containment loads, the JAERI tests are analyzed using separate and combined effects of spray water washdown and forced convection from hot wall surfaces during the pressure suppression period.

In the single nozzle test, spray water would not contact the vessel wall if we assume an unconfined spacial distribution for the injected water. However, some analytical analyses of confined sprays suggest that strong vortexes may form, and these flows may entrain water, depositing a portion of the spray water onto the vessel wall [Mar88]. The effect of spray water contacting containment surfaces is referred to as a washdown effect. A 15% washdown means, for example, that 15% of the introduced spray water comes into direct contact with the vessel wall of the containment. Clearly, the determination of the amount of washdown or even the gas flow along surfaces in the containment is not within the scope of the CONTAIN code assessment effort; however, through sensitivity studies using CONTAIN an understanding of the possible implications on containment loads either by washdown or internal circulation currents can be assessed. Such an assessment may be important for developing a knowledge of the importance of certain processes and become an explanation of the thermal hydraulic behavior observed in the spray tests .

The washdown effect is simulated in the CONTAIN model by using the film tracking model for water films on the vessel wall; a 15% washdown is modeled by including a water source for the film equal to 15% of the spray mass rate. The interaction of the 15% of the spray water with the atmosphere prior to contact with the vessel wall can be modeled in two ways: the first method would be to assume no significant interaction with the atmosphere such that the mass rate of water injected into the atmosphere is effectively reduced by 15%; the second method would assume some significant interaction prior to deposition such that the effective spray injection into the atmosphere is maintained at 100%. In the each case, variations on the temperature of the water deposited onto the vessel walls may also be considered. For example, if the sprays do not interact with the atmosphere, the spray water contacts the structures with a temperature equal to the injected spray water; if the interaction is significant, the water contacts the walls with a temperature equal to the gas temperature in the facility.

Shown in Figures 4.18 and 4.19 are the pressure and temperature plots for the atmosphere in test PHS-6 for a case of 0% and 15% spray washdown, assuming no interaction of water with the atmosphere prior to deposition. The plots indicate that a 15% washdown effect, by itself, results in a significant over prediction of pressure and gas temperature. Figures 4.20 and 4.21 show the effects of gas flow on the vessel thermal hydraulics using an estimated forced convective velocity along the vessel wall ranging from 5 to10 m/s. Although the pressure over predications for the 5 and 10 m/s cases are not very much, the temperature over predictions are significant since they

represent a degree of superheating that is not observed in the test. As noted in the description of the reference case, the spray droplet size is input as 0.001 meters. We showed above that a small spray droplet size will tend to produce a more saturated atmosphere. This effect is also indicated in Figures 4.20 and 4.21 for the case with a spray droplet of 0.0005 meters. However, while the smaller droplet size decreases the superheating, the pressure over prediction increases significantly.

To further analyze some of the sensitivities resulting from spray washdown and gas flows a number of additional cases are considered where the pressure and gas temperatures at 5000 seconds after spray activation are the focus of the comparisons. Shown in Table 4.7 are a number of CONTAIN sensitivity studies. Case 1 is the reference calculation described in Section 3.3, and denoted as 0% washdown in Figures 4.18 and 4.19. Case 4, with 15% washdown is also plotted in these figures. Cases 2 through 5 represent those cases with no interaction of the deposited water with the atmosphere prior to deposition. As indicated in the table, only a small amount of water deposition, ~ 5%, is required to reach a maximum pressure and temperature condition at 5000 seconds; additional water deposition - up to 30% - does not increase the pressure further. Therefore, within a reasonable range of spray washdown values, pressure and gas temperature are relatively insensitivity to this parameter.

Recall that Cases 2 to 5 are calculated by reducing the spray mass rate by the amount of spray washdown. The importance of mass transfer versus spray rate reduction is shown through a comparison of Cases 3 and 15. In Case 15, with only a 5% spray rate reduction the pressure increase above the measurement is minimal (~ 0.06 bar), while in Case 3, with both deposition and spray reduction, the increase is significant (~0.4 bar). Therefore, for small amounts of water deposited on the vessel wall, the mass transfer process is important. The significance of the comparison is reduced as the amount of spray washdown percentage increases; compare Cases 4 and 14.

As the deposition rate increases, the evaporation rate effects become a smaller contributor to the pressure increase compared to the effect of spray rate reduction. This trend is demonstrated from a comparison of pressure and gas temperature as predicted for Cases 5 and 9; for example, Case 9 shows a noticeable decline in pressure when the washdown is not attended by a similar reduction in the spray rate.

When the spray rate does not reduce as a result of washdown (assuming that a significant spray/atmosphere interaction has preceded the deposition, i.e., Cases 6 to 9), the pressure and temperature loads are maximized for a certain percent washdown. The effect is especially noticed for Cases 6 to 9 where the deposited water has a temperature equal to the spray injection. In these cases, which may be considered somewhat unphysical, the low temperature water is responsible for relatively large sensible energy at the wall as contrasted to Cases 10 to13 where the deposited water temperature is higher and a great portion of the energy transfer goes to water evaporation. Where the deposited water temperature is increased to approximately account for

spray water/atmosphere energy exchange, the percent washdown for maximum loads at 5000 seconds occurs over a broad range of washdown rates (5-15%); this is contrasted to the more rapid decline in loads observed for washdown percentages greater than 5% in the case of the low temperature water.

In reference Mar88, an analytical experiment is presented showing that under certain conditions (very small droplet size and high injection rates) spray droplet/gas dynamic drag processes can drive strong airflow velocities in an open spray region producing a ringed vortex (flowing down in the center of the vessel and upwards along the vessel wall). Cases 16-18 show the approximate effect of including forced convection effects along the walls of the vessel for test PHS-6, assuming no water deposition. An estimate on the magnitude of the induced airflow has been used in Mar88 using the simple equation $u = \sqrt{2gh}$ where u is a representative velocity, g is the acceleration due to gravity, and h is the effective spray head height above the floor. Accordingly, this equation can give relatively accurate estimates if the effective spray head height is given by $0.75 * h$. For a spray head height of 19.5 meters, the estimate airflow velocity is ~ 17 m/s. From Figures 4.20 and 4.21 it was concluded that forced convection with an assumed velocity of 10 m/s along the vessel walls produces a degree of superheating that is not in agreement with the data. Cases 16-18 show that the sensitivity of superheat to a reasonable range of velocities, including the estimate from the simple equation above, is minimal.

Cases 19 to 21 show the combined effects of gas flow and varying spray droplet size. As indicated in Figures 4.20 and 4.21, while a small spray droplet size decreases gas temperatures, bringing the atmosphere closer to saturation, the pressure increases at the same time thereby increasing the over prediction of vessel pressure.

Combining both the forced convection and washdown effect, significantly elevates the containment pressure and temperature, as observed in Case 22; therefore, this combination (which might be considered assuming that the air currents may entrain and thereby carry spray droplets to the wall surfaces) is discounted on the basis of comparisons of measured and calculated pressure and gas temperature.

There are a number of reasons why the air flows in test PHS-6 may not be adequately estimated by the ringed vortex model simulated in Mar88, and estimated by the simple equation above. First, the vessel aspect ratio, height/diameter, is more than twice the aspect ratio of the vessel used in the analytical experiment and this may affect the behavior of the spray induced vortex; secondly, the spray flux is more than an order of magnitude less than the flux used in the simulation of reference Mar88 (see Table 3.7 for a comparison of spray fluxes, $\dot{M} / A$). A reduced spray flux means that laminar viscous drag effects become more important and these drag effects can retard the development of a ring vortex. Further with a reduced flux, droplet coalescence and the residence time of small diameter droplets in the atmosphere increases; these

small droplets tend to retard the development of a ring vortex.

One of the important conclusions from the sensitivity studies on JAERI test PHS-6 is that, on the basis of measured and calculated thermal hydraulic conditions of the vessel atmosphere, it is unlikely that vessel wall heat and/or mass transfer is a factor in the prediction of this single nozzle spray test. However, in spray test PHS-1, the number of spray nozzles is increased to six, located nearer to the vessel walls, and the spray flux is six times greater than for the single nozzle test. As a consequence, the probability of spray water contacting the vessel wall is much higher than for test PHS-6.

Shown in Figures 4.22 and 4.23 are the containment pressure and temperature comparisons (in the 7.5-16 meter region) using various assumptions regarding washdown and air flows. Assuming no washdown or airflow affecting heat and mass transfer at the wall surface does not produce results representative of the thermal hydraulic conditions within the vessel. As noted in the figures, the case with 0% washdown and no forced convection causes the predicted containment pressure and temperature to decrease rapidly, leading to an under prediction of pressure and temperature loads. Using a 10% washdown rate gives very good pressure agreement, as does the assumption of a 10% washdown with a force convective velocity of 10 m/s. We note that a case with just forced convection also improves the agreement between measured and CONTAIN calculated results. Figures 4.24 and 4.25 show pressure and temperature results for a range of forced convection velocities along the vessel surface. Figure 4.24 shows that even with very high velocity profile (17 m/s), predicted pressures are still below the measurements; however, they are much closer to the data than cases having 0 and 10 m/s velocities. And, in Figure 4.25, it is indicated that the temperature agreement with a velocity of 17 m/s is in relatively good agreement with measurements. The temperature comparisons however can be somewhat misleading as shown in Table 4.8. In the table, both gas and saturation temperatures are compared. The measured saturation temperature is back calculated assuming a uniform distribution of air in the vessel; the calculation shows that the atmosphere is saturated since both the gas temperature and saturation temperature are approximately equal. CONTAIN results for a velocity equal to 17 m/s show that the atmosphere is superheated (as a consequence of the large amount of sensible heat addition from the vessel surface) with the saturation temperature under predicted by about 15 degrees. Therefore, although it would appear that the forced convective results give relatively good gas temperature agreements with measurements for the higher velocity case, a closer examination reveals that the apparent agreement is due to a significant degree of superheating exists for the calculation while further analysis of the measurements indicate that the atmosphere is saturated. From previous sensitivity analyses concerning saturation conditions during sprays, it was also revealed that smaller spray droplet sizes will tend to produce a saturated atmospheric condition. When the droplet diameter is reduced from 0.001 to 0.0002 meters, the pressure, gas temperature, and saturation temperature at 2000 seconds, for the calculation with a surface velocity of 17 m/s, are 1.46 bar, 341.8 K and 341.3 K, respectively. Compared to results with the larger droplet size, the pressure variation is small, and the gas temperature, while now also near saturation, is somewhat reduced, and

approximately 10 degrees below the measured gas temperature.

Table 4.9 gives a comparison of various assumptions for spray and washdown effects on pressure and temperature based on a snapshot at 2000 seconds. The importance of the washdown effect is shown for cases where the washdown water is assumed not to interact with the atmosphere prior to deposition (2a-5a) and for cases were interaction is assumed (6a-9a). In the first grouping the spray mass rate is reduced by the amount of water put onto the vessel wall. The second grouping, by assuming interaction with the atmosphere does not have the spray mass rate reduced but does have the temperature of the spray water contacting the vessel walls increased above the injection temperature to approximate thermal contact with the atmosphere prior to deposition. In the comparison of both groupings, either assumption concerning atmospheric interaction appears inconsequential, as does the percentage of spray water that is deposited (within the reasonable range of 5-30%). When we compare the cases calculated with only the spray rate reduction (10a-13a) with the cases where a portion of the spray water contacts the vessel surfaces (i.e., cases 2a-5a -- washdown effect with spray rate reduction), we see that the evaporation effect is significant for keeping the atmosphere saturated and increasing both pressure and temperature in agreement with the measurements.

Temperature stratification and spray induced mixing.

Shown in Figure 4.26 is the 16-cell nodalization showing the spray injection locations for JAERI test PHS-1 (six nozzle test). As noted in the reference calculations for hydrogen distribution tests, HDR T31.5, E11.2, and NUPEC M-8-1, the default flow solver can predict stable stratifications during mid-level injections. In the case of PHS-1, the region below the sprays will be cooled and a temperature stratification will develop. This is also shown in the measurements; however, turbulence induced by the spray interactions with the air/steam mixture causes some mixing to occur above the spray elevation. This induced mixing is not modeled in the CONTAIN code. Therefore, the effective region of spray cooling is slightly under estimated with the 16-cell nodalization such that the multi-cell calculation over predicts late time pressure by a small amount, as shown in Figure 4.27. Note, that the reference calculation for PHS-1 is the single cell calculation with 10% washdown and reduced spray rate (90% of injection). In this instance, the single-cell representation (uniformly mixed vessel) gives a good pressure prediction, in part, because there is significant mixing above the injection location.

Sump mass and heat transfer.

When sprays are activated, the spray droplets quickly come into thermal equilibrium with the atmosphere that they are falling through. As the spray droplets plus condensed water deposit into a sump, this water is initially quite hot. It cools slowly as lower temperature spray water deposits as the transient progresses, as energy is transferred to the underlying structure, and as liquid is transported from the sump through liquid pathways. While the steam partial pressure in the

atmosphere decreases due to sprays, the mass and heat transfer from hot water in the sump can also be a source of vapor through evaporation. If the sump is not modeled, this source of delay energy addition to the atmosphere is omitted and the pressure is under predicted. This is shown, in the case of JAERI test PHS-6 (single nozzle test), where the CONTAIN calculations with and without a pool are modeled and the pressure results are compared to measurements in Figure 4.28. In the figure, the late time pressure is significantly under predicted for the case without the sump pool modeled.

Table 4.7. Sensitivity analysis for JAERI test PHS-6 based on vessel wall interactions with spray water and gas flows (time = 5000 seconds).*

Case #	Description	Vessel Atmosphere Thermal Hydraulics			
		Pressure, bar	Tgas, K**	Tsat, K	Sat. Ratio
----	Measured	2.1	367	367	1
1	no washdown, no forced convection, 100% spray rate	2.1	370.7	367	0.9
washdown effect with spray rate reduction:					
2	2%, 98% spray	2.26	372.	373.3	0.96
3	5%, 95% spray	2.47	377.3	377.3	1
4	15%, 85% spray	2.47	377.4	377.4	1
5	30%, 70% spray	2.48	377.6	377.6	1
washdown effect with no spray rate reduction (film source temperature = 313.15 K):					
6	2%	2.24	372.8	371.5	0.96
7	5	2.43	376.5	376.5	1
8	15	2.37	374.9	374.9	1
9	30	2.27	372.5	372.5	1
washdown effect with no spray rate reduction (film source temperature = 360. K):					
10	2	2.24	373	371.6	0.96
11	5	2.45	376.9	376.9	1
12	15	2.43	376.4	376.4	1
13	30	2.39	375.6	375.6	1
spray rate reduction effect:					
14	85% spray	2.26	371.8	374.4	0.91
15	95% spray	2.16	371.9	369.	0.9

Table 4.7. (continued)					
Case #	Description	Vessel Atmosphere Thermal Hydraulics			
		Pressure, bar	Tgas, K**	Tsat, K	Sat. Ratio
gas flow effect:					
16	5 m/s	2.22	376	370.5	0.83
17	10	2.26	378	371.5	0.81
18	17	2.29	379.1	372	0.79
gas flow and spray droplet diameter effect:					
19	10m/s, spdiam = 0.001m	2.27	378	371.5	0.81
20	10m/s, spdiam = 0.0005 m	2.33	375.5	373.77	0.94
21	10m/s, spdiam = 0.0002 m	2.35	374.	374	1
gas flow and washdown effect:					
22	10m/s, 15% washdown***	2.49	377.7	377.7	1

* All cases, except cases 20 and 21, have spray droplet diameter, spdiam = 0.001 meters.
** Gas temperature is uniform
*** 85% spray, assumes no interaction of washdown water with atmosphere prior to deposition

Table 4.8 Sensitivity analysis for JAERI test PHS-1 based on the gas flow along the vessel wall (time = 2000 seconds).*

Flow velocity m/s	Pressure bar	T_{gas} K	T_{sat} K	Sat. Ratio
measured:				
---	1.68	351.5	352.5**	~1
CONTAIN:				
0	1.26	328	325	0.87
10	1.38	341	334	0.76
17	1.44	345	338	0.78

* CONTAIN analysis performed using a single cell representation of the vessel atmosphere
** based on uniform mixing

Table 4.9. Sensitivity analysis for JAERI test PHS-1 based on vessel wall interactions with spray water (time = 2000 seconds).*

Case #	Description	Vessel Atmosphere Thermal Hydraulics		
		Pressure, bar	Tgas, K**	Sat. Ratio
----	Measured	1.66	349	~1
1a	no washdown, no forced convection, 100% spray rate	1.26	328	0.87
washdown effect with spray rate reduction:				
2a	5%, 95% spray	1.66	351.8	1
3a	10%, 90% spray	1.66	351.8	1
4a	15%, 85% spray	1.66	351.9	1
5a	30%, 70% spray	1.67	352.3	1
washdown effect with no spray rate reduction (film source temperature = 350. K):				
6a	5%	1.64	351	1
7a	10%	1.62	350	1
8a	15%	1.61	349.5	1
9a	30%	1.57	347.4	1
spray rate reduction effect:				
10a	95% spray	1.28	330	0.87
11a	90% spray	1.31	332	0.87
12a	85% spray	1.34	334.7	0.88
13a	70% spray	1.48	344.3	0.9

* CONTAIN analysis performed using a single cell representation of the vessel atmosphere
** based on uniform mixing

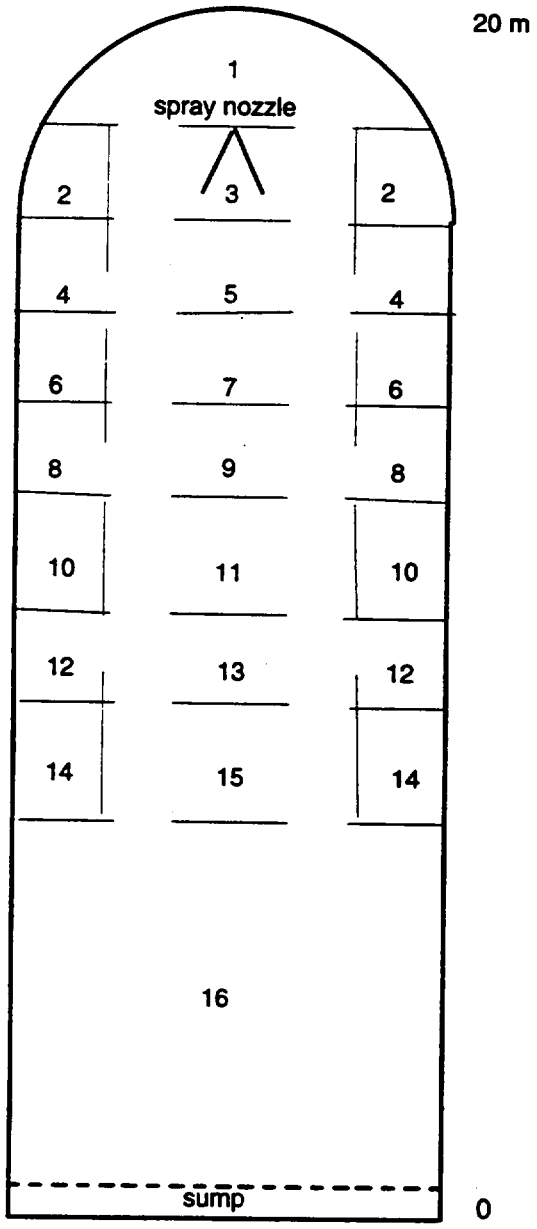

Figure 4.5 Containment vessel for spray testing, showing the 16-cell CONTAIN nodalization of the JAERI spray vessel for the test PHS-6 (single nozzle test).

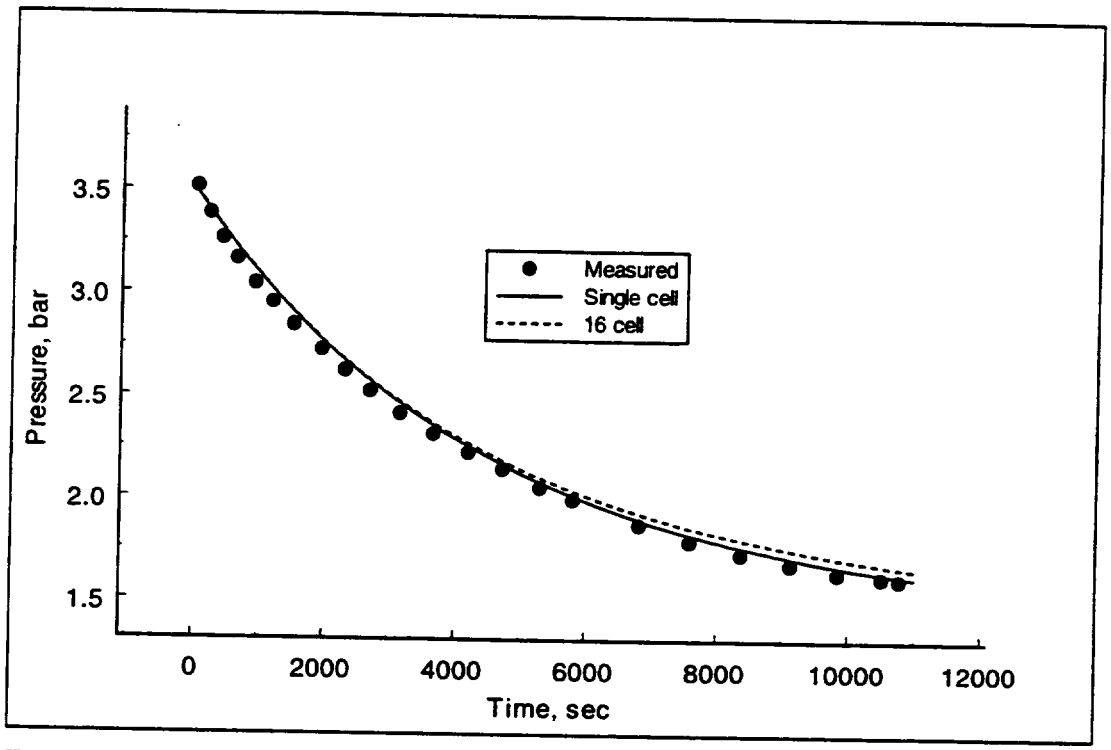

Figure 4.6 Comparison of measured and calculated pressures for a single nozzle test, showing the effect of vessel nodalization.

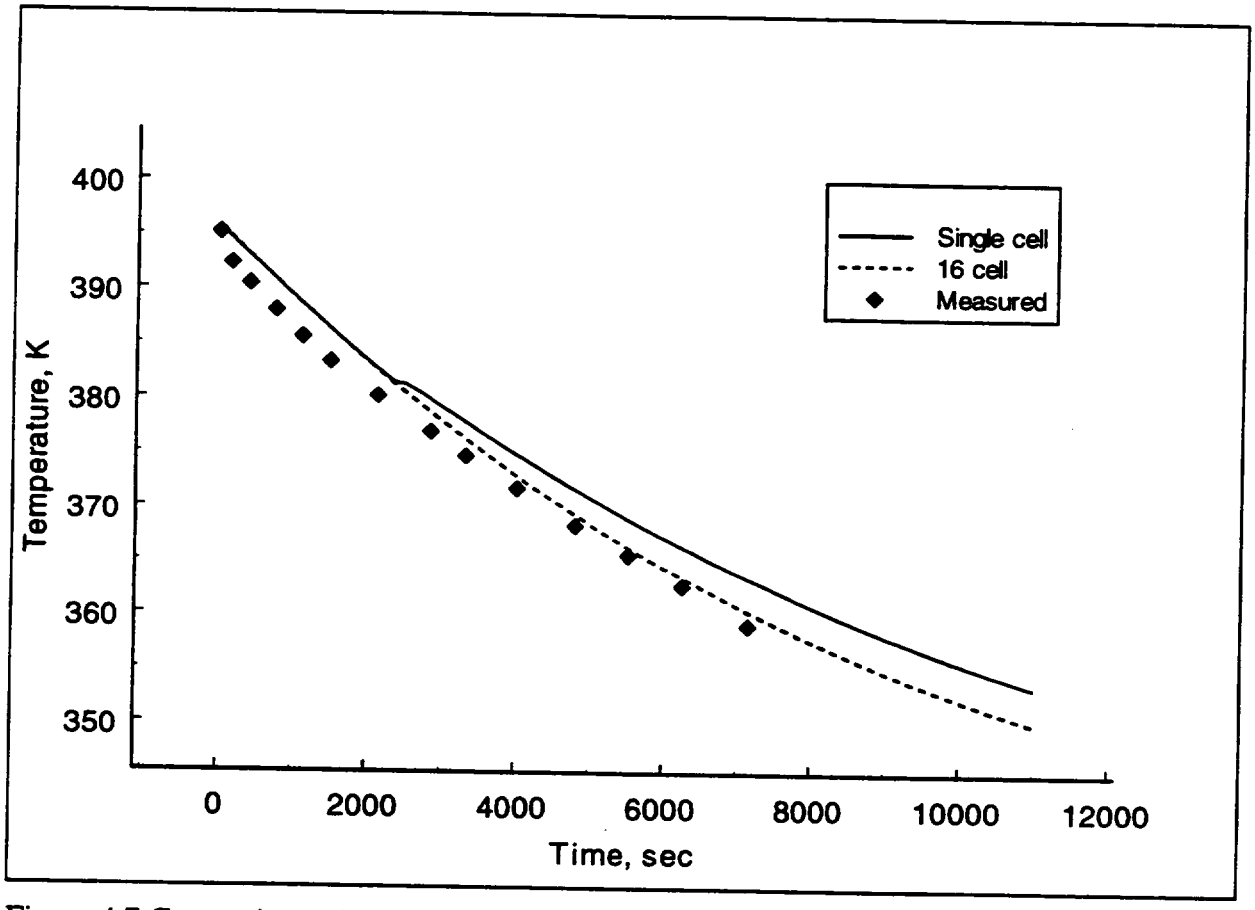

Figure 4.7 Comparison of measured and calculated temperature for a single nozzle tests, showing the effect of vessel nodalization.

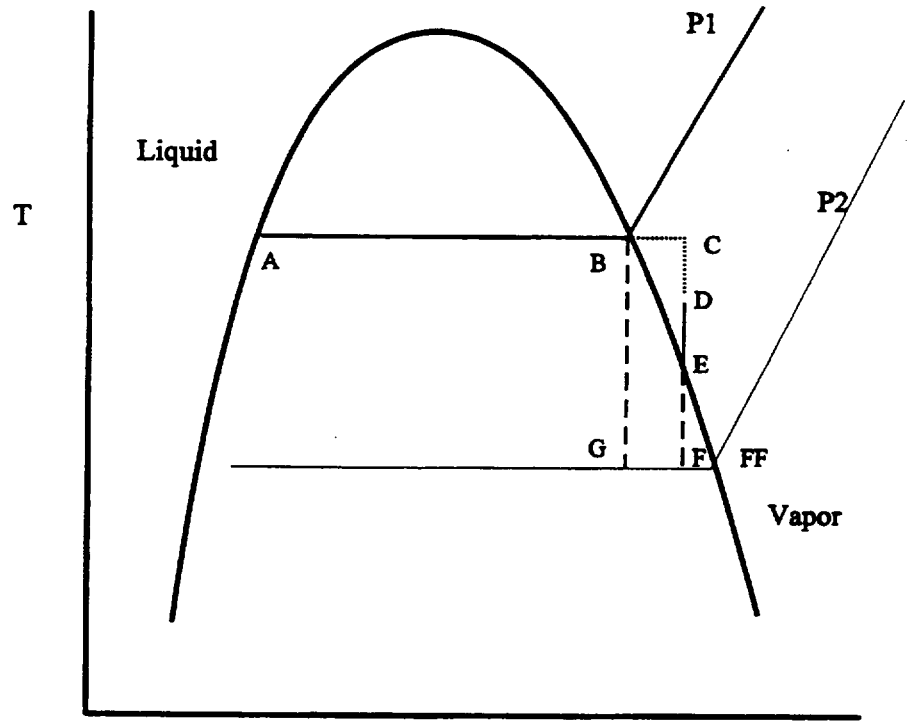

Figure 4.8 Sketch of the T-V diagram for water showing the effects of sprays on the thermodynamic state of the vapor space.

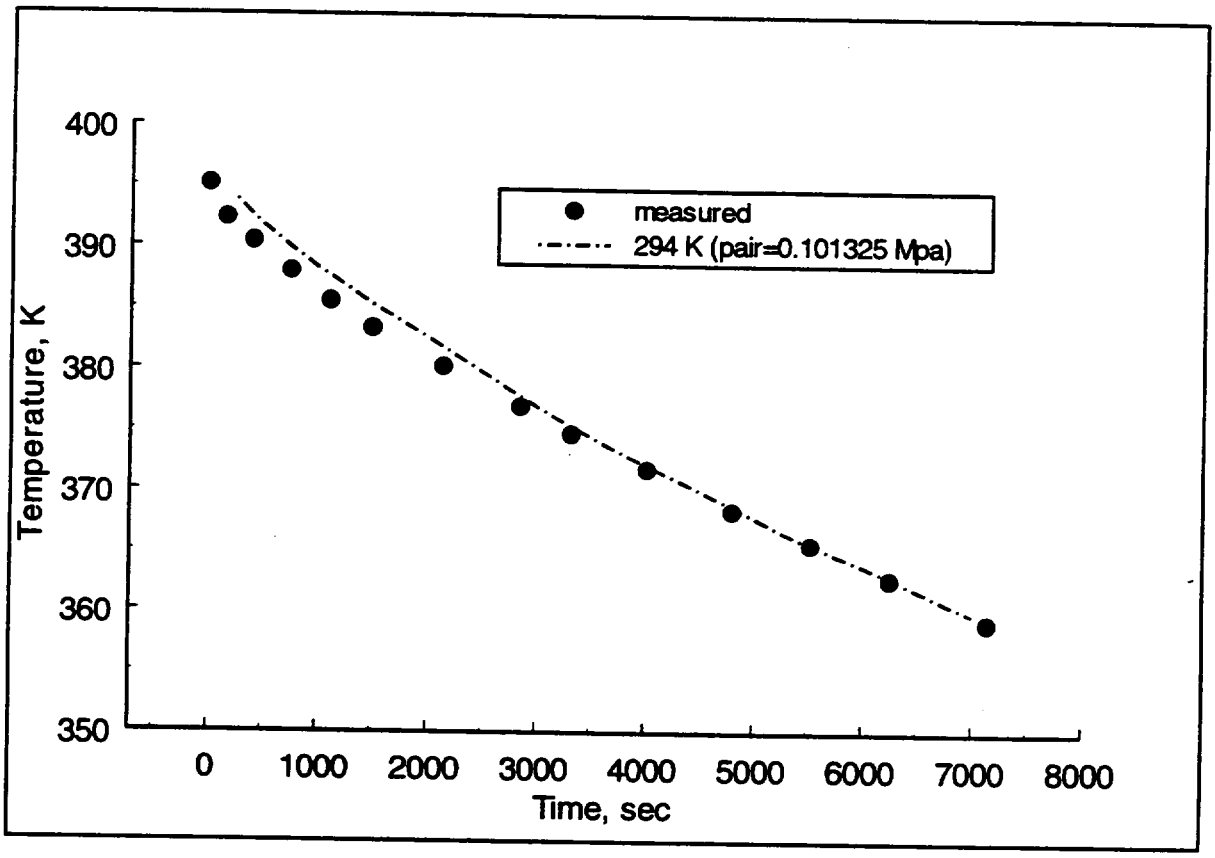

Figure 4.9 Comparison of measured and calculated temperatures for JAERI test PHS-6. The calculations are the saturation temperatures for measured total pressure, assuming steam injection into a well-mixed air volume initially at 294 K and standard pressure.

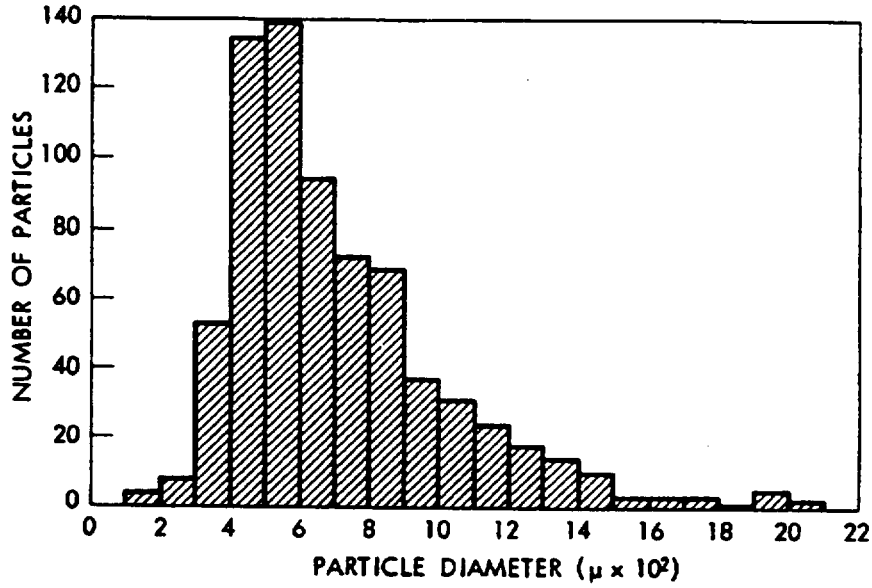

Figure 4.10 Drop size distribution from containment spray nozzle (50-psi pressure drop).

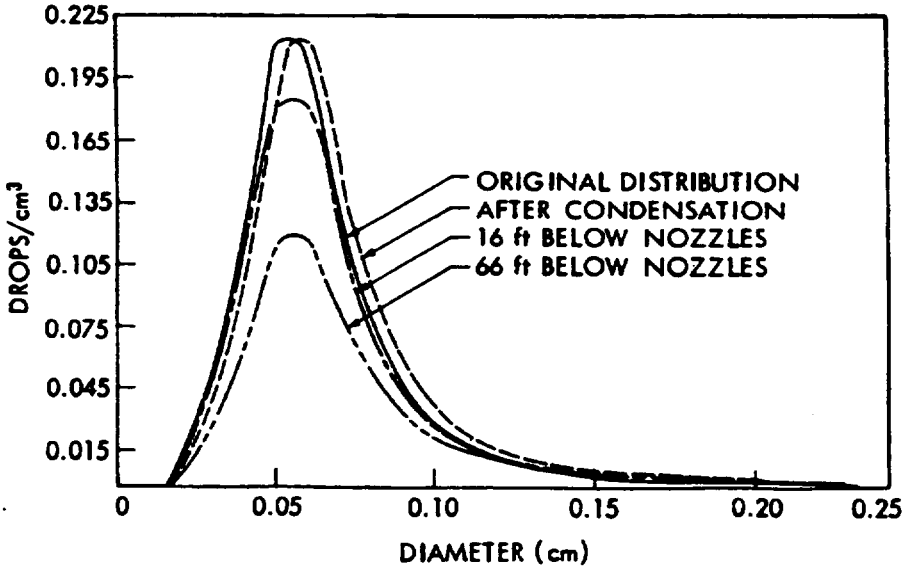

Figure 4.11 Drop size distribution after condensation and coalescence.

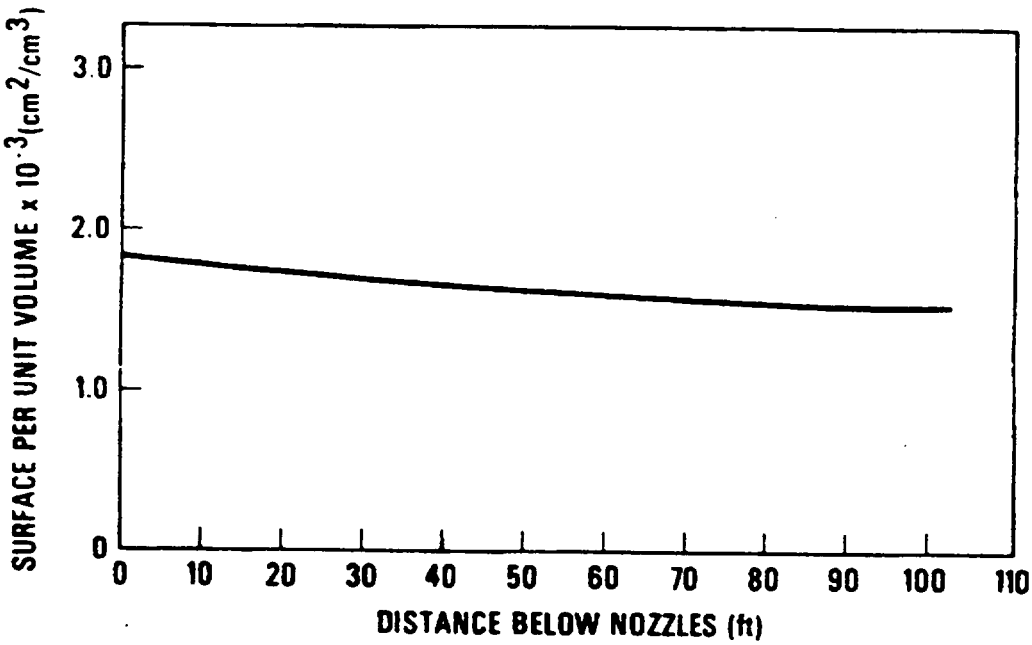

Figure 4.12 Regression analysis of temporal mass distribution for a SPRACO 1713A nozzle [BW74]

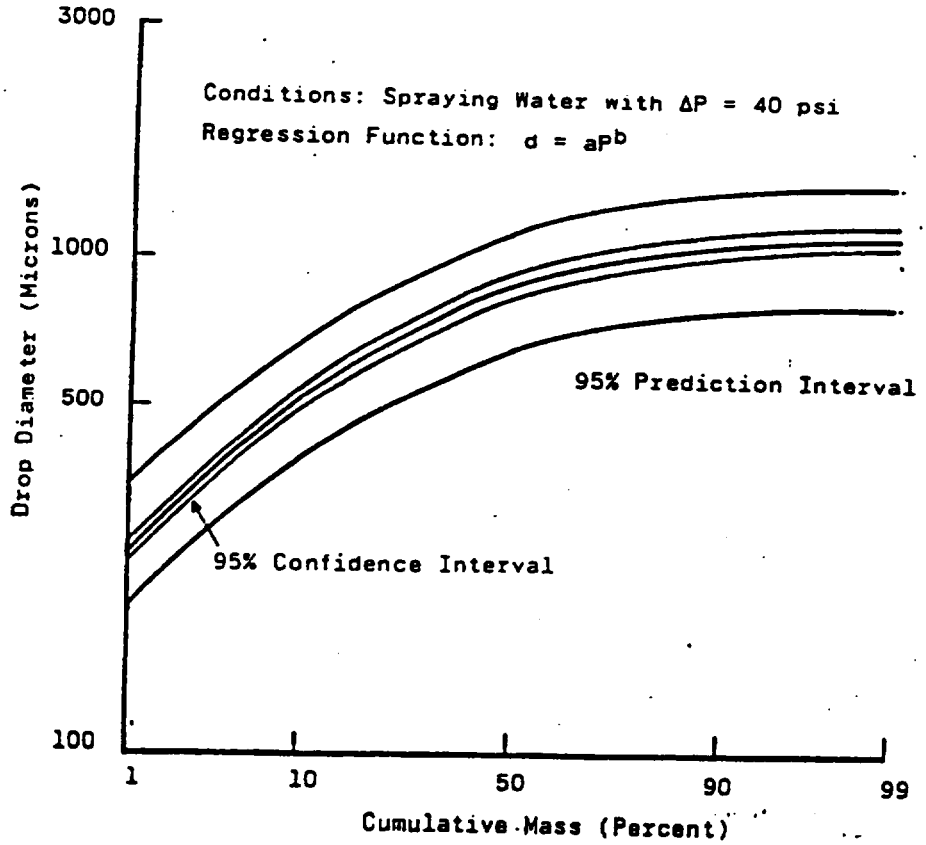

Figure 4.13 Regression analysis of temporal mass distribution for a SPRACO 1713A nozzle [BW74].

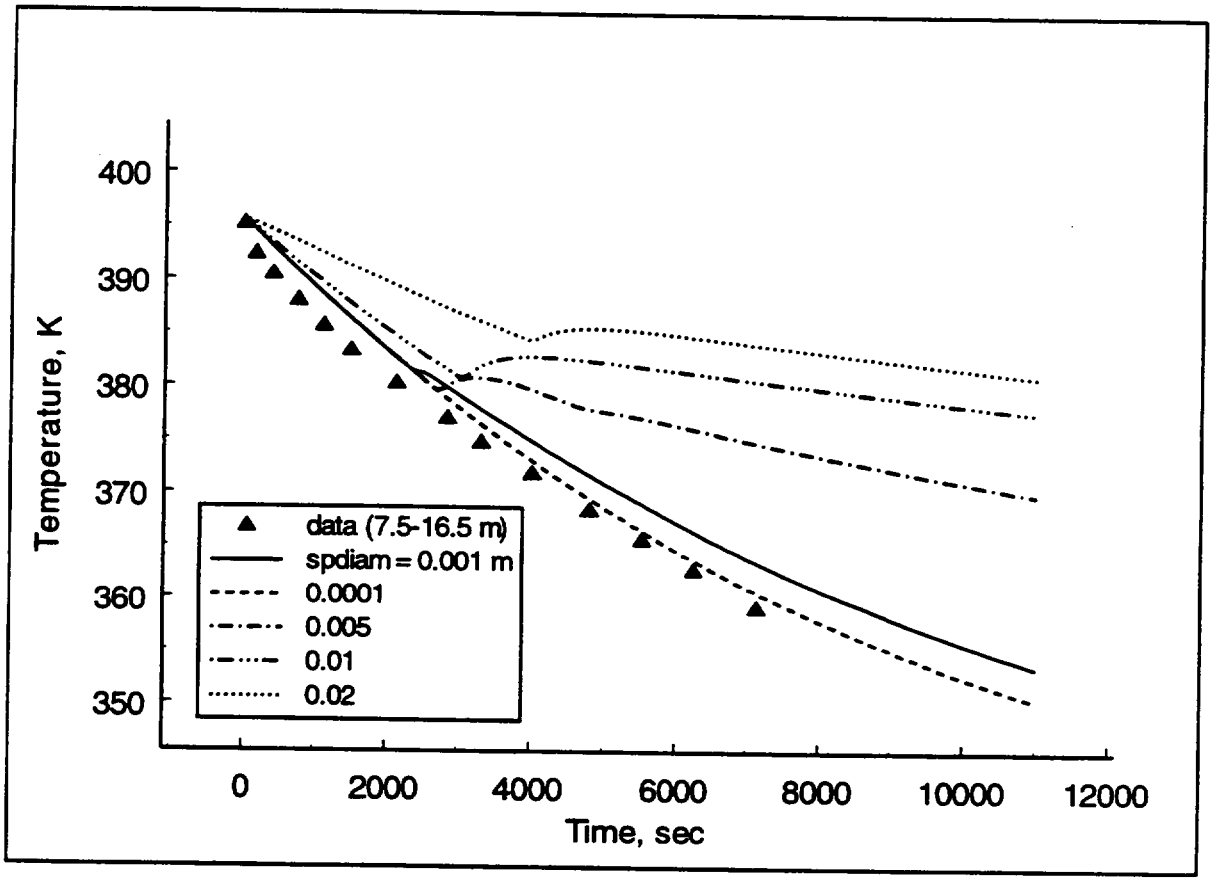

Figure 4.14 Temperature sensitivity of the vessel atmosphere during JAERI test PHS-6 (single nozzle test) to spray droplet size specified for the CONTAIN spray model.

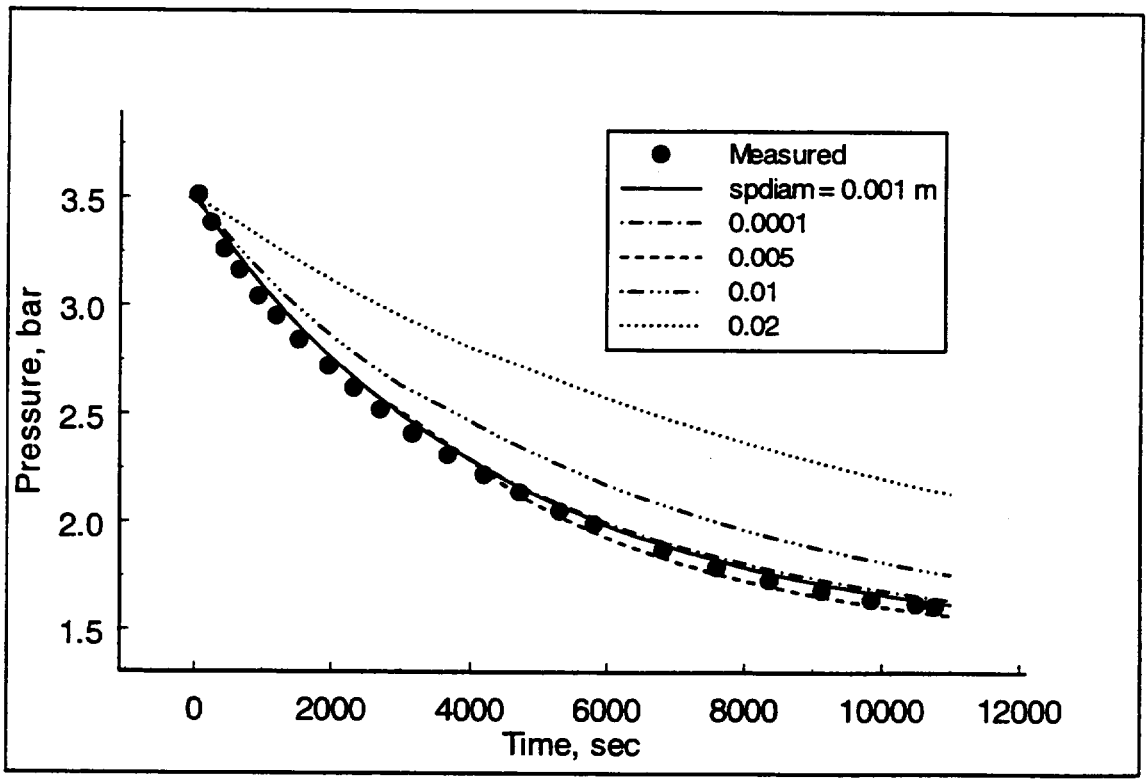

Figure 4.15 Pressure sensitivity during JAERI test PHS-6 (single nozzle test) to spray droplet size specified for the CONTAIN spray model.

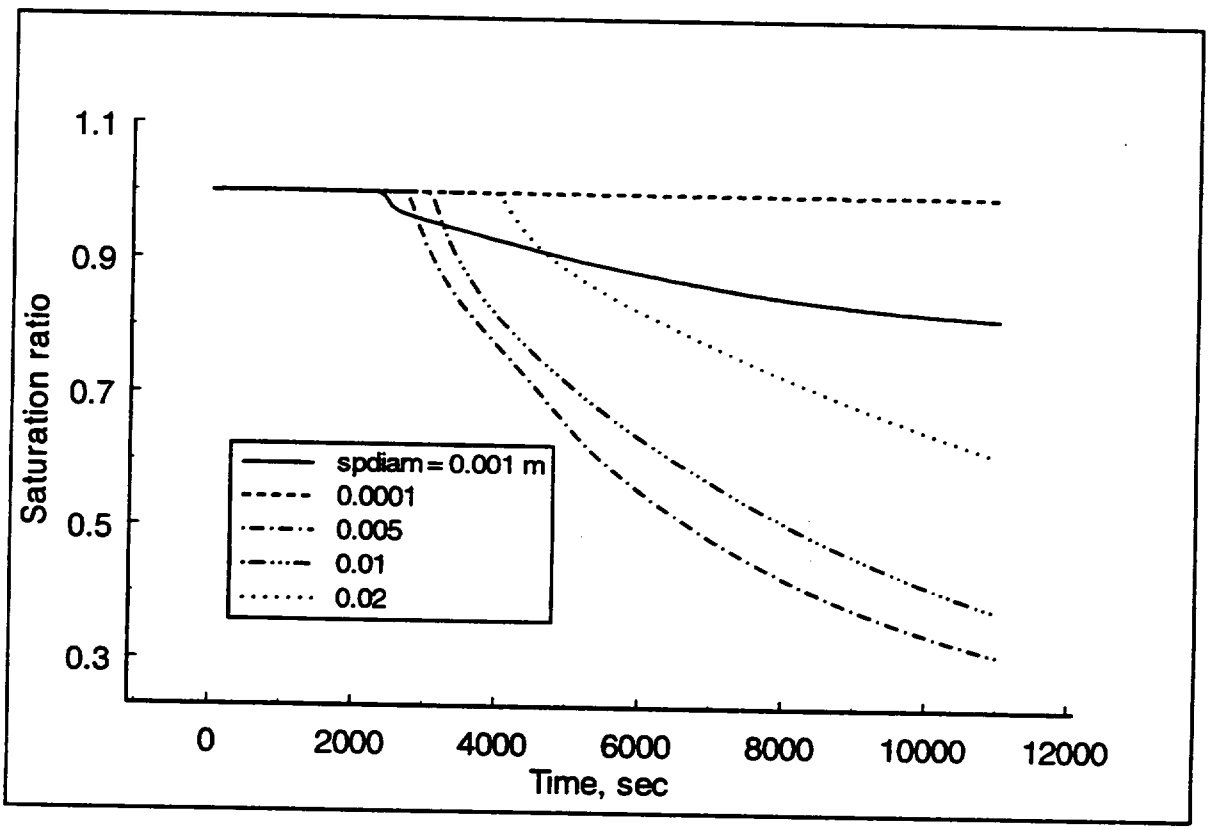

Figure 4.16 Saturation ratio sensitivity during JAERI test PHS-6 (single nozzle test) to spray droplet size specified in the CONTAIN spray model.

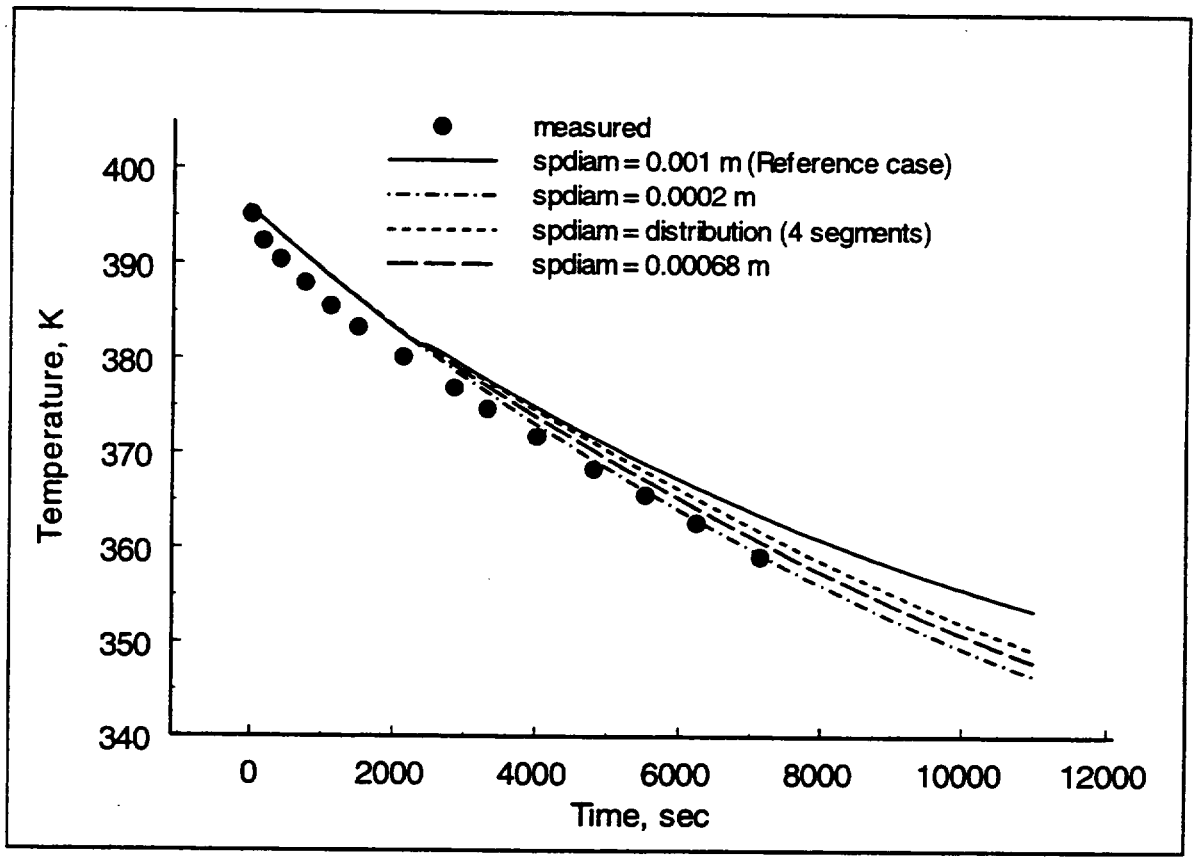

Figure 4.17 Comparison of measured and calculated gas mixture temperatures for JAERI test PHS-6, showing the effect of various assumptions regarding the injected spray droplet diameter, spdiam.

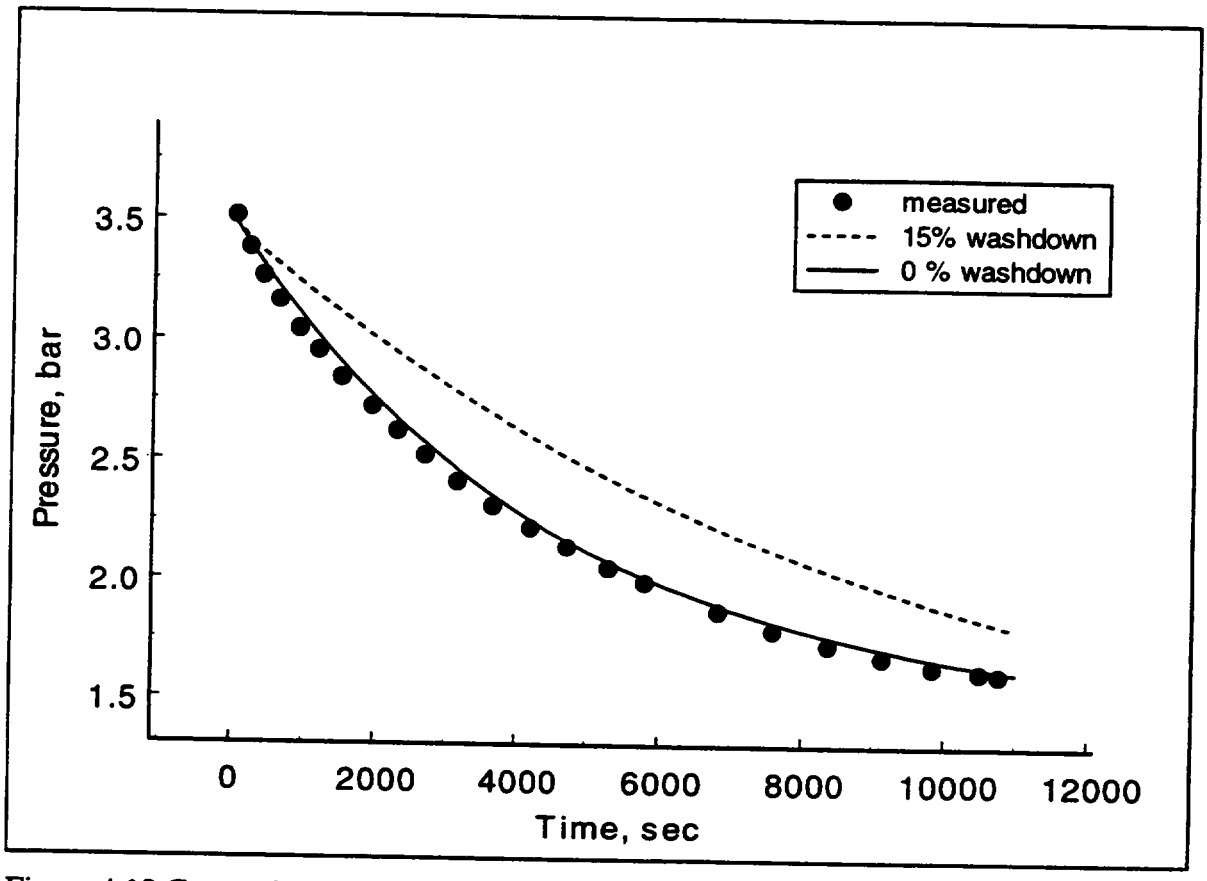

Figure 4.18 Comparison of measured and CONTAIN calculated pressure for a 0% and 15% spray washdown for JAERI test PHS-6.

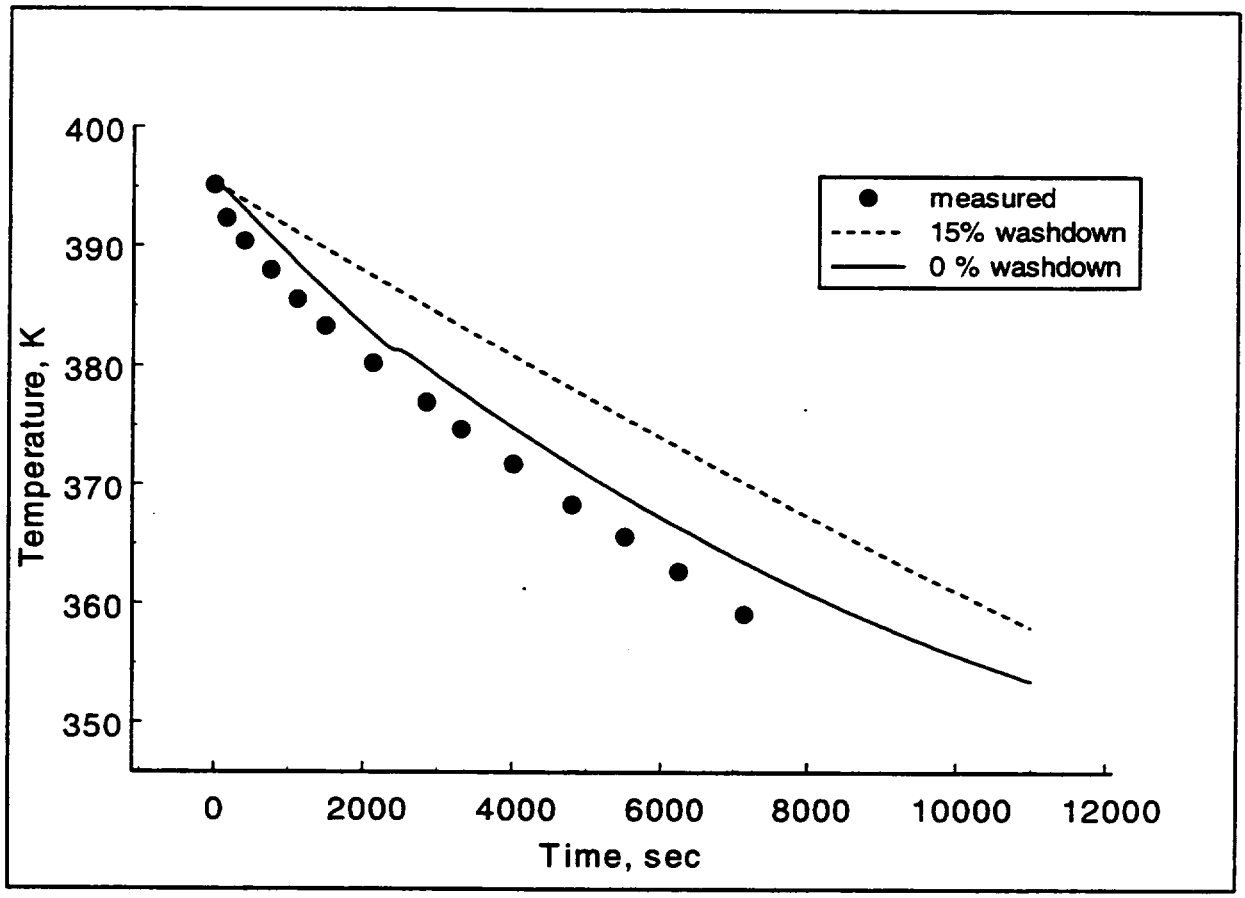

Figure 4.19 Comparison of measured and CONTAIN calculated gas temperature for a 0% and 15% spray washdown for JAERI test PHS-6.

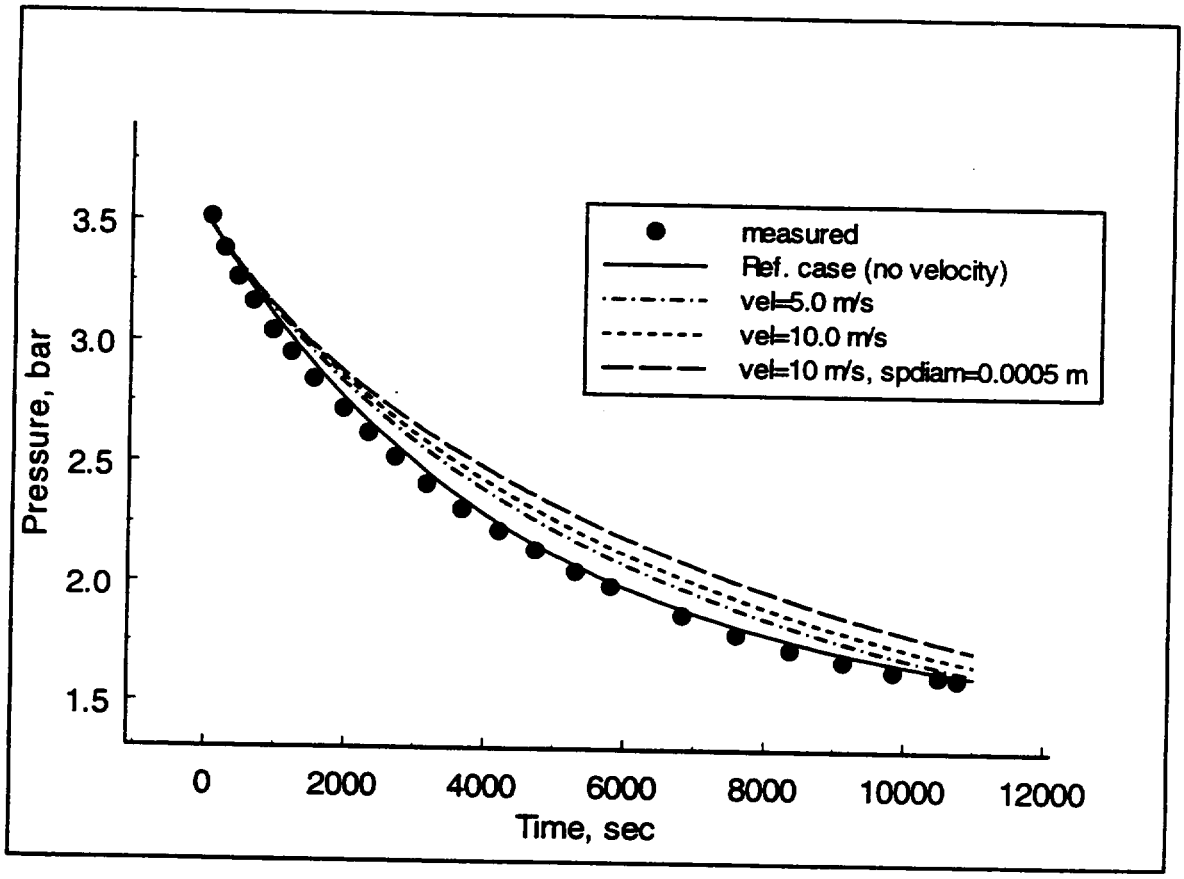

Figure 4.20 Comparison of JAERI PHS-6 measured and CONTAIN calculated pressure for various forced convective flow velocities along the vessel wall.

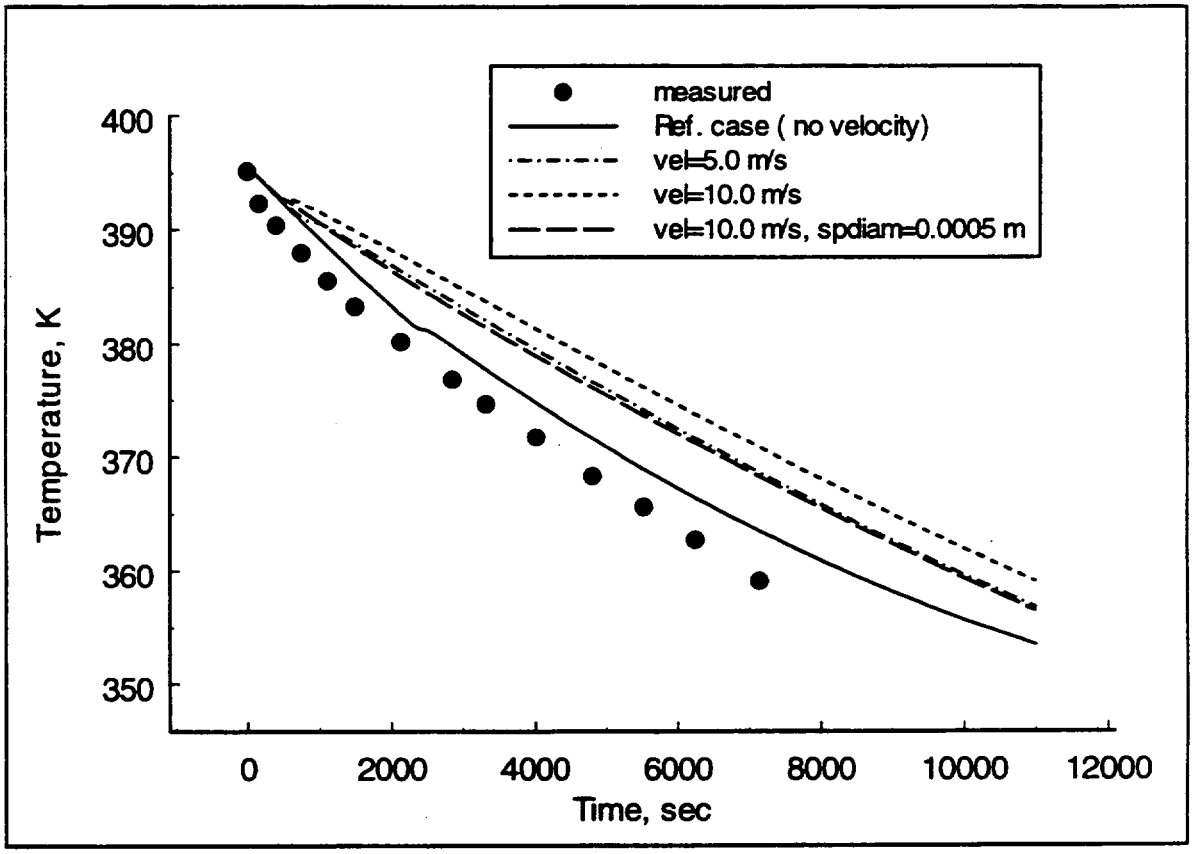

Figure 4.21 Comparison of JAERI PHS-6 measured and CONTAIN calculated gas temperature for various forced convective flow velocities along the vessel wall.

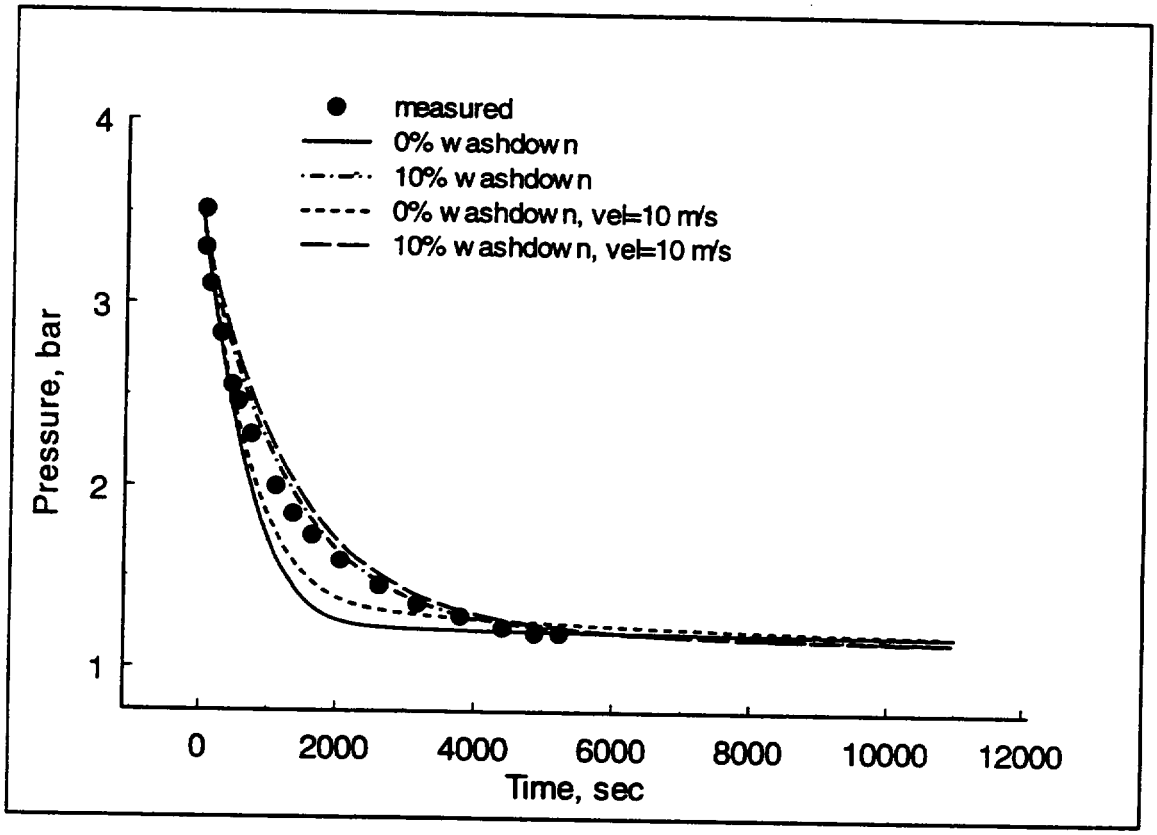

Figure 4.22 Comparison of measured and CONTAIN calculated pressures for JAERI test PHS-1.

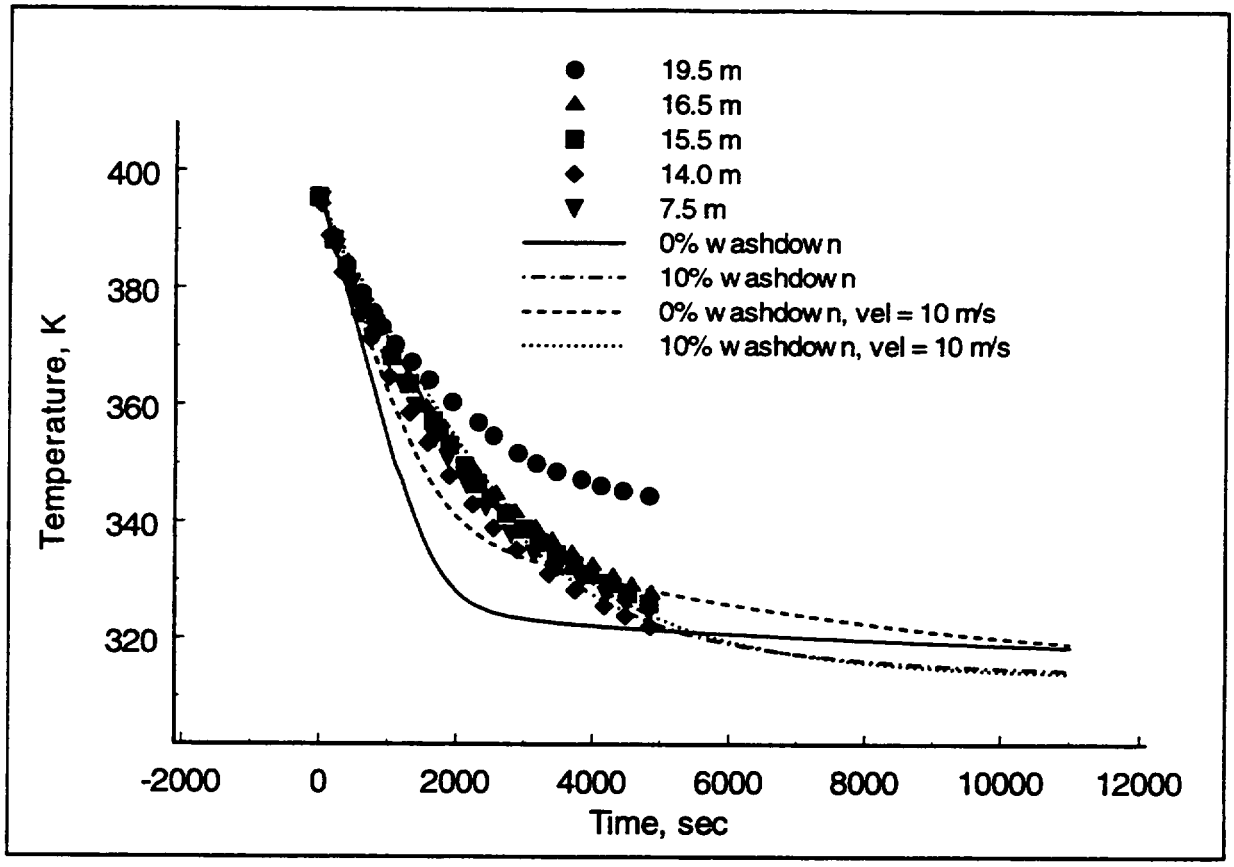

Figure 4.23 Comparison of measured and CONTAIN calculated temperatures for JAERI test PHS-1.

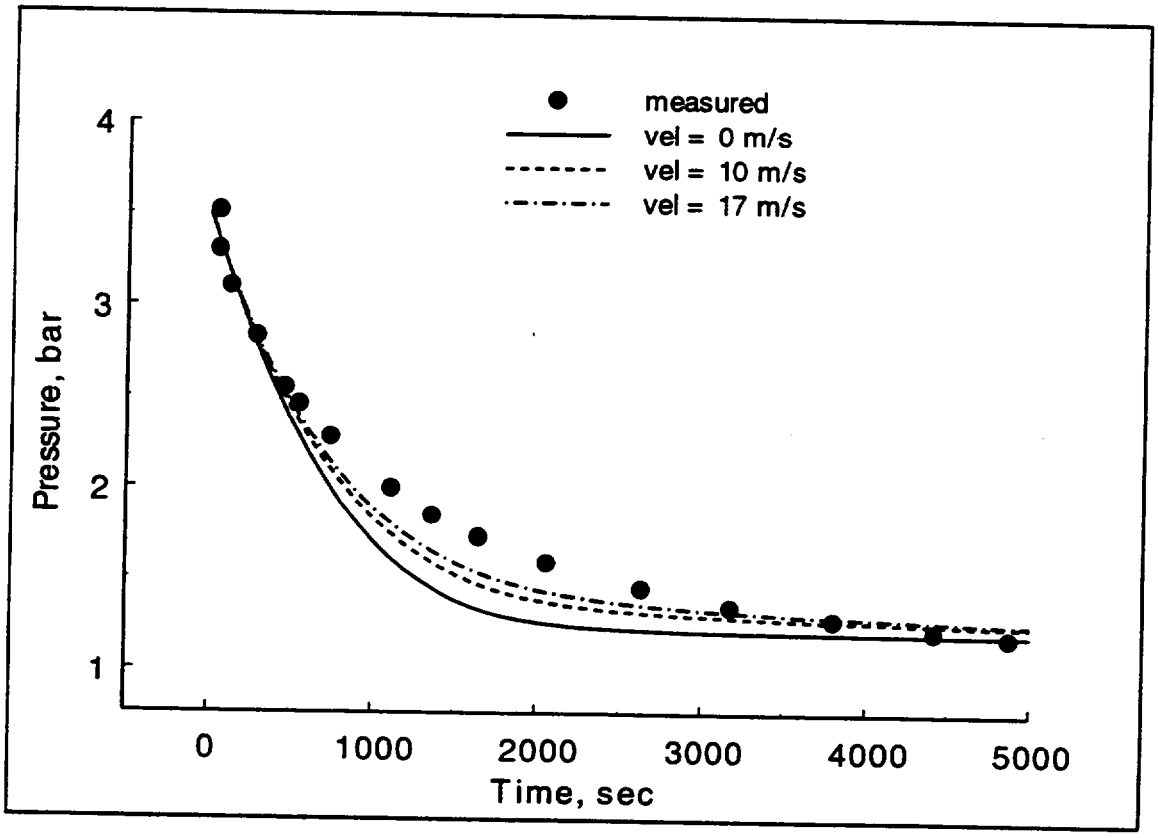

Figure 4.24 Effect of gas flows along the vessel surface on CONTAIN calculated pressures for JAERI test PHS-1.

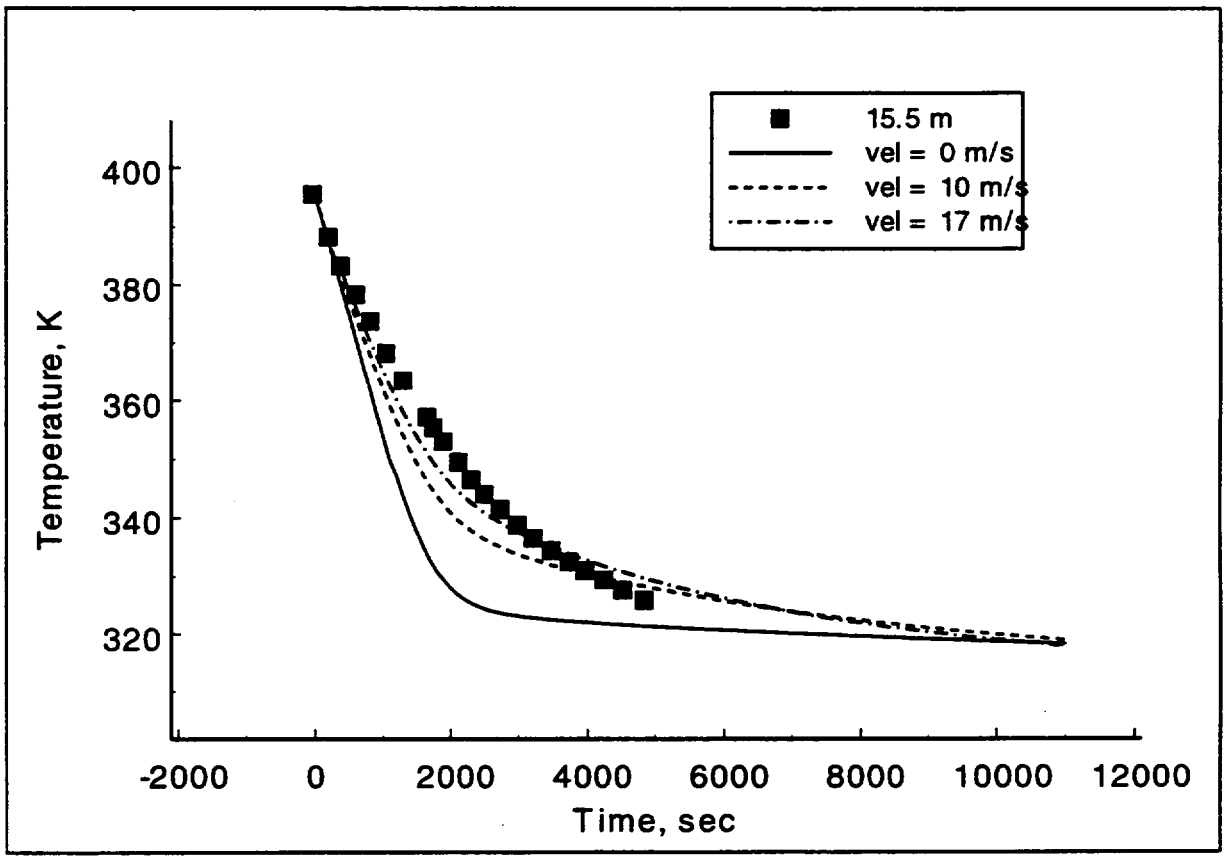

Figure 4.25 Effect of gas flows along the vessel surface on CONTAIN calculated temperatures for JAERI test PHS-1.

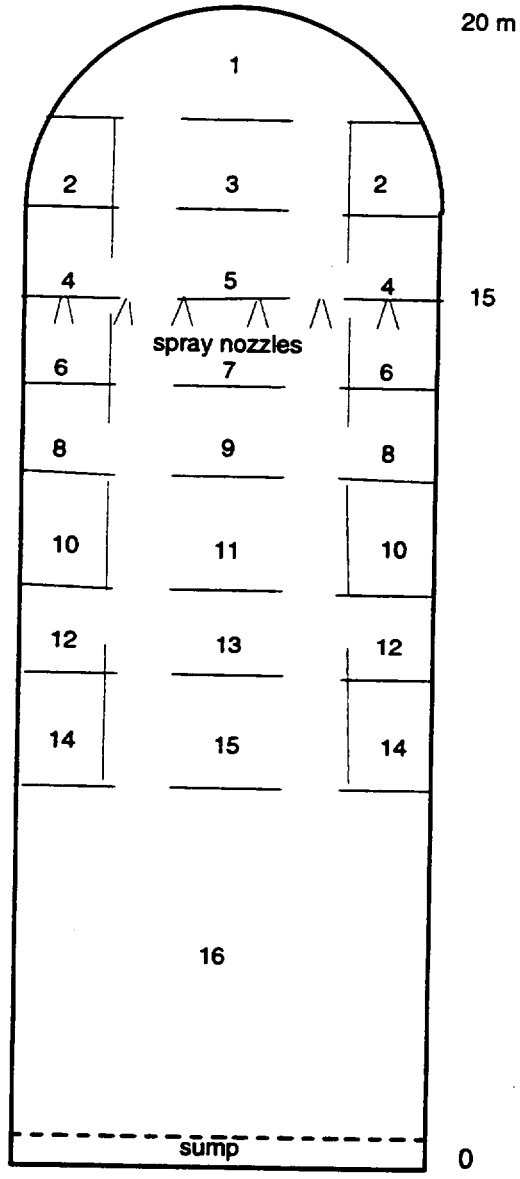

Figure 4.26 CONTAIN 16-cell nodalization of the JAERI spray vessel as configured for test PHS-1 (six spray nozzles).

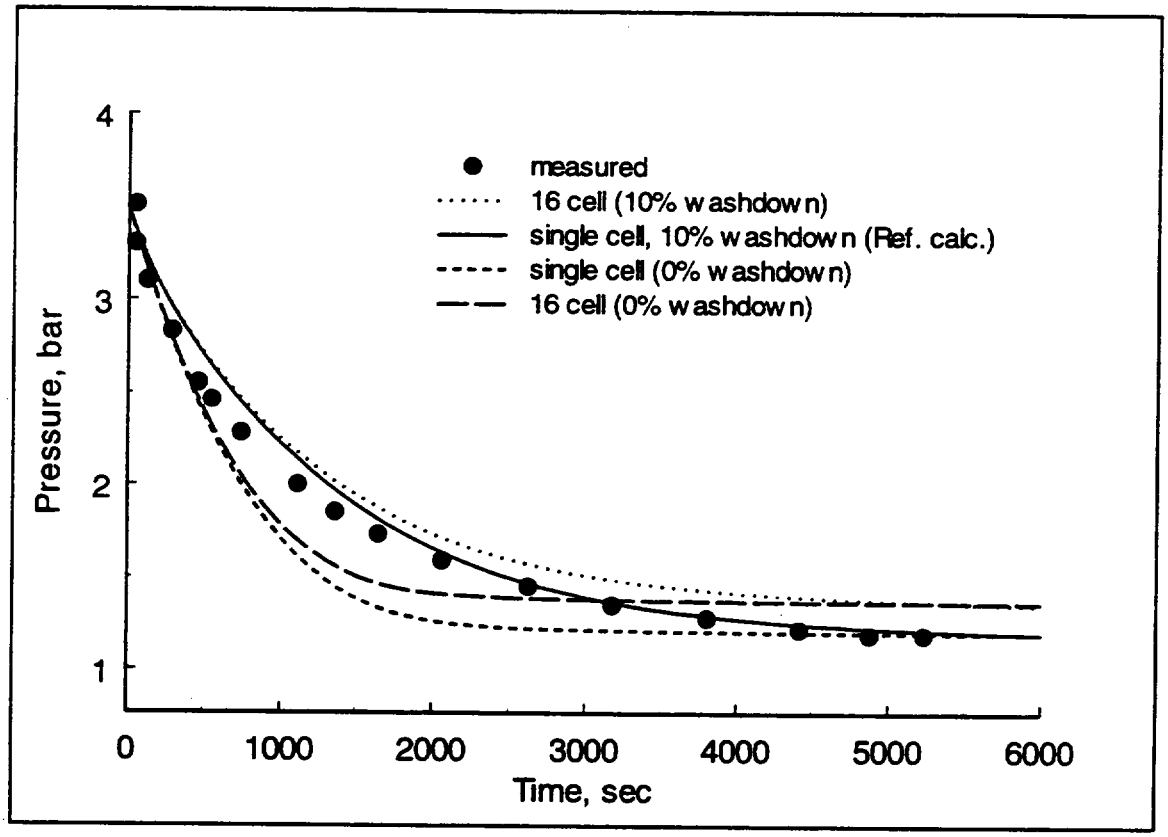

Figure 4.27 Comparison of measured and calculated pressures for JAERI test PHS-1, showing the effect of spray/wall interaction and vessel nodalization on the predictions.

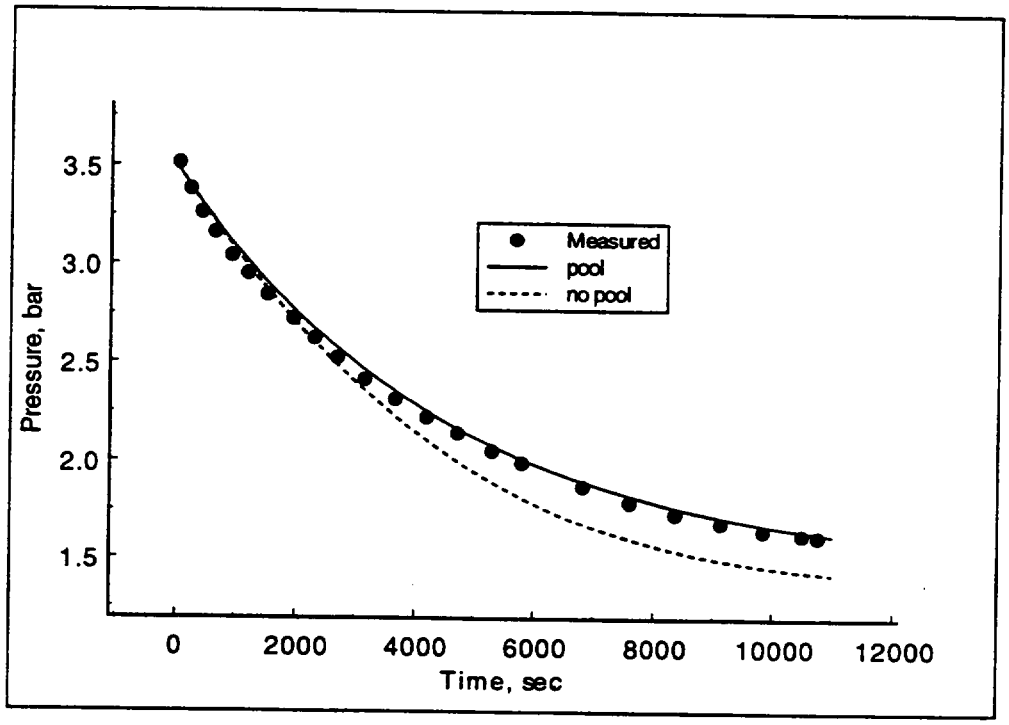

Figure 4.28 Comparison of measured and calculated vessel pressure for JAERI test PHS-6, showing the effect of pool mass and heat transfer on predicted pressure.

4.2 Integral Effects

4.2.1 HDR Tests

4.2.1.1 HDR Test V44 [ISP-16]

The sensitivity of the predicted maximum pressure for various assumptions regarding various modeling parameters (heat transfer, nodalization, and suspended liquid water) are summarized in Table 4.11 for test V44. Differential pressure calculations may be affected by assumptions with regard to suspended liquid water and the choice of input parameter describing the flow characteristics of pathways. These variations are quantified in a discussion on the sub-compartment analysis of test V44.

4.2.1.1.1 Maximum Pressure

Forced Convection.

Table 4.11 provides a comparison of the reference peak pressure obtained using a default method for estimating forced convective velocities along structure surfaces (case 1) with results for a case without forced velocities (case 2). The comparison indicates that both cases predict identical pressures. The reason for this is twofold. First, the coarse nodalization used in this geometrical model of the HDR facility, by default, uses a hydraulic area (= cell volume ** 2/3) that is too large, resulting in a low forced velocity prediction. Secondly, the default convection algorithm uses only the largest of the natural or forced convective components in a mixed convective process involving heat and mass transfer along a structure surface. In case 1, the forced convective component (Nusselt for heat transfer and Sherwood for mass transfer) is less than the respective natural convection components; therefore only the natural convective component is used to determine heat and mass transfer from the atmosphere. Hence, since both cases 1 and 2 are calculated only with a natural convection method, the pressure results are the same. However, even with a significant velocity for the breakroom (cell #1) and adjoining rooms (cell #2 and #3), the effect of forced convection on energy transfer is insignificant. In case 3, the cell velocities for the breakroom (cell #1), adjoining cells #2 (1701u) and #3 (1701o, 1704) are specified by input to be 24 m/s for up to 35 seconds and then reduced to follow the approximate decline in the injection rate. There, again, are two main reasons why the case 3 peak pressure is nearly identical to cases 1 and 2: 1) only a small fraction of the total heat sink capacity in the containment is contained in cells 1-3; and, 2) the steam fraction in these cells is so high during the blowdown that the condensation process is governed primarily by the thermal resistance of the water film on structures rather than the gas/steam diffusion layer that is determined by forced convective flows. Case 5 indicates the sensitivity of maximum pressure to surface resistance for cells #1- #3, where the maximum water film thickness is reduced by a factor of ten from the default thickness of 0.0005 meters and also the paint resistances is essentially eliminated by setting the paint conductance to a value of 10000 w/m^2-K.

However, if the forced convective processes are extended to other compartments, such as cell #4 and #5, encompassing more of the available heat sinks, the effect of forced convection on the heat and mass transfer process is significant, as shown for case 4. A reduction of calculated pressures so as to match better the measured pressure, requires an estimate of forced convective processes beyond the immediately adjoining rooms surrounding the breakroom.

Nodalization.

In case 6, reducing the 5-cell nodalization to a single cell model results in only a slight increase in the predicted pressure and produces, in this test, a more conservative pressure loading. However, reduced nodalization will substantially affect local temperature estimates, and these estimates may not follow along a conservative direction in some locations, as shown in Figure 4.29 for the extreme temperatures predicted in the location of the breakroom.

Structure heat transfer.

Cases 7 and 8 show the pressure variation to various structure modeling parameters. The multiplier on the heat and mass transfer indicates approximately the degree of condensation enhancement due to turbulent processes (turbulent forced convection) that is required to substantially affect the atmospheric energy balance. Case 9 shows the importance of steel structure energy transfers to the pressure predictions.

Atmospheric liquid water.

Cases 10 and 11 reflect on the methods for modeling liquid water suspended in the atmosphere during a blowdown, using the single cell nodalization. The reference case, as well as the single cell calculation, case 6, assume that condensed water in the atmosphere is suspended as aerosol particles which are rapidly removed from the atmosphere by settling and wall deposition. In this test, even if condensed blowdown water is allowed to remain dispersed (case 10), the variation on maximum pressure is small. The additional liquid water in the atmosphere adds to the heat capacity of the atmosphere, reducing slightly the maximum calculated pressure. When the water is modeled as aerosol particles, not only is the liquid water removed rapidly, but the water aerosols remaining in the atmosphere do not add to the atmosphere heat capacity - aerosol particles are modeled without heat capacity. Case 11, with water dropout at the end of a time step, is a case that is essentially identical to the single cell case with water aerosols, indicating that water aerosols are rapidly removed from the atmosphere with the CONTAIN aerosol settling and deposition modeling. The comparisons between the reference case (case1) and similar atmospheric assumptions regarding liquid water suspension in the atmosphere (cases 12 and 13) do not correlate as well (in terms of an explanation based on atmospheric heat capacity) as for the single cell examples. This is because in these latter cases an associated effect related to liquid water transport between cells complicates the comparisons.

Energy velocity method for blowdown heat and mass transfer.

Case 14 represents an attempt to simulate the condensation heat transfer using a energy velocity methodology that is similar to the Tagami method used in the CONTEMPT code.[1] This case is similar to case 4 in that an enhancement of condensation on structures, greater than that produced by natural convective processes, is simulated. However, in this case the Tagami method is used to determine the condensation heat transfer coefficient; this information is then used to adjust condensation through the HMTA modeling method by inputting a time dependent Nusselt number for each structure.

[1] The steps in this method are as follows: 1) determine the time dependent heat transfer coefficient h using the Tagami correlation; 2) estimate the corresponding Nusselt number Nu from the definition, Nu=(h*L)/k, where L is the structure characteristic length and k is the atmosphere mixture thermal conductivity; 3) input the Nusselt number time dependent values in a table entry (NUS-FORC) as described in the STRUC block input for the CONTAIN code [Mur97].

Table 4.11 ISP-16 peak pressure sensitivity calculations

Case #	Description	Predicted Peak Pressure, P_{max} ,bar	$\left[\frac{P_{calc}}{P_{measured}}\right]_{max}^{*}$	$\left[\frac{\Delta P_{calc} - \Delta P_{measured}}{\Delta P_{measured}}\right]_{max}^{**}$ %
1	Reference case (default velocities, water aerosol ...)	3.19	1.31	52
2	Vel=0 m/s	3.19	1.31	52
3	Vel=func(t) for cells 1-3	3.19	1.31	52
4	Vel=func(t) for cells 1-5	2.67	1.09	16
5	mindepth=0.00005 and hpaint=1.0e4 (cells 1-3)	3.11	1.27	47
6	Single-cell	3.32	1.36	61
7	Hmxmul=5 (steel only)	2.95	1.21	35
8	Hmxmul=5 (all struc.)	2.79	1.14	24
9	No steel sinks	3.7	1.52	87
10	Single-cell (dispersed liquid water)	3.23	1.32	55
11	Single-cell (dropout of dispersed liquid water)	3.31	1.36	60
12	dispersed liquid water	3.19	1.31	52
13	dispersed liquid water with dropout	3.26	1.34	57
14	Single-cell with an energy velocity methodology applied	2.49	1.02	3.5

* $P_{measured} = 2.44$ bar

** $\Delta P = P - P_{init} = P - 1.0$

4.2.1.1.2 Subcompartment Analysis

The CONTAIN code has been applied in the HDR blowdown tests (V44 and T31.5) to investigate the code's ability to predict maximum differential pressures generated between the break room and adjoining compartments. The analyses include a number of sensitivity studies to focus the effort on important phenomena and input that are not known a priori; and that can be determined only by comparison to experiments. The studies reported here are not exhaustive in this regard. Furthermore, these tests do not represent the most severe conditions that may arise during LOCA events, that is, under conditions where the maximum breakroom flows, and therefore differential pressures, are determined through estimates of critical two-phase flows through containment pathways. In spite of these shortcomings, however, the results are important since they do provide information regarding two-phase blowdowns and differential pressure estimation for prototypical breakroom geometries.

To aid the reader in the discussion of the sensitivity studies, a short background section is included here, and will be referred to in the following subsections.

Background

Differential pressure calculations obtained with CONTAIN are performed using the inertial flow model described in Reference Mur97. The simplified governing equation for gas flow rate from cells i to j is

$$W_{ij} = MIN\left(W_{iner,ij}, W_{cr,ij}\right)$$

where the inertia flow rate $W_{iner,ij}$ is calculated from the momentum equation given by

$$\frac{dW_{iner,ij}}{dt} = \left(\Delta P_{ij} - C_{FC} \frac{\left|W_{iner,ij}\right| W_{iner,ij}}{\rho_u \left(A_{ij}\right)^2} \right) \frac{A_{ij}}{L_{ij}}$$

, and the critical flow $W_{cr,ij}$ is given by

$$W_{cr,ij} = A_{ij} \nu_{ij} \sqrt{\gamma_u P_u \rho_u \eta_u}$$

In the above,

W = total mass flow rate of gases, coolant vapor, and homogeneous dispersed liquid coolant;

ΔP = differential pressure;

C_{FC} = irreversible flow loss coefficient;

ρ = flow path density;

A = flow path area;

L = inertia length;

γ = ratio of c_p/c_v for the gas/vapor mixture;

η = $\left[\frac{2}{1+\gamma}\right]^{\frac{\gamma+1}{\gamma-1}}$;

ν = vena contracta factor.

The subscripts i and j refer to the connecting cells and subscript u denotes the upstream cell, which, for flow from i to j corresponds to u=i. Inputs to the code are the flow path area, loss coefficient, and A/L. Table 4.12 gives the reference values used for these three quantities for the CONTAIN model of the V44 test. The A/L parameters are determined using the formula

$$\frac{A_{ij}}{L_{ij}} = \frac{A_{ij}}{\sqrt[3]{MIN(V_i, V_j)}}$$

, where V is the volume of a cell associated with the connecting pathway. The loss coefficients are estimates based on information supplied from Project HDR for single-phase pressure drops. The effective contraction coefficient, A_{flow}/A_{actual}, is assumed to be unity for each pathway in the reference calculation; that is, the contraction coefficient is enfolded in the value of the estimated loss coefficient.

Inertia Lengths.

Inertia lengths L_{ij} can be determined by a number of prescriptions. One method is to consider the length to be the approximate pathway length. For containment pathway geometries, consisting of doorways or other "orifice" type openings, this method would result in A/L values that are very high. Alternately, the method that has been used in the reference calculation (which also represents a slightly more conservative approach for maximum breakroom pressure and pressure

differentials), is based on the recognition that the effective inertia length for a cell extends some distance into a cell volume as the cell gases are accelerated through the pathway. Pressure differentials, for events similar to the test procedure and geometry, are relatively insensitive to reasonable uncertainties in the inertia lengths, and therefore the exact prescription for estimating these lengths is not very important. For example, when the inertia lengths (given in Table 4.12) are reduced by a factor of five, the pressure differentials predicted for test V44 are essentially unchanged.

Suspended liquid water.

In the CONTAIN flow equation, the flow path density will vary depending on whether suspended liquid water is assume to be homogeneously dispersed or treated as an aerosol, and additionally, on the assumption regarding water carryover from the compartment atmosphere to the exiting pathway. When homogeneously dispersed, and with a carryover fraction (carryover fraction = ratio of liquid water concentration in the pathway to water concentration in the volume) greater than zero, the flow path density will include the liquid water mass as well as air and water vapor in the density term ρ_u. However, when considered an aerosol, the suspended liquid will not be included in the flow path density, according to the CONTAIN model. For CONTAIN, it is assumed that the carryover fraction is always equal to one, so that the pathway flow density is the upstream volume density. In addition, the default model for homogeneously dispersed liquid water does not dropout liquid water in the atmosphere. To remove homogeneously dispersed liquid water, the "dropout" keyword must be used in the CONTAIN input. Shown in Figure 4.30 are the liquid water inventories for two modeling assumptions, condensed liquid suspended as a homogeneously dispersed water and liquid suspended as water aerosols. In the first few tenths of a second following the start of the blowdown, the injection water is steam and the suspended liquid amount is essentially zero, no matter if the modeling is dispersed liquid or aerosol. After this short period, the injection is two-phase and the suspended water amount increases significantly for the case with dispersed liquid water. In the case of the aerosol model, a significant amount of the liquid is removed from the atmosphere in the breakroom by settling and wall deposition. For the homogeneously dispersed modeling option, the injected water remains in the atmosphere, and since the flow path density is increased for this model option, the effective inertia of the fluid moving through pathways from the breakroom is increased substantially, approximately by a factor of 2-3. As a result, the pressure differential during the two-phase portion of the blowdown is increased compared to the suspended aerosol case, as shown in Figure 4.31. The first peak in the differential pressure profile, however, is unaffected since the that peak occurs during the dry steam injection when the suspended liquid water mass is very small.

The differential pressure profile with homogeneously dispersed liquid water is similar in shape to the measurement, except that the maximum value is under predicted by about 30000 Pa. This

discrepancy of approximately 40% is believed to be caused by 1) the coarse nodalization used for this test geometry, and 2) by using too low an estimate for pathway loss coefficients during the time when the pathway flow is two-phase flow, having a quality of about 0.4. Again, it should be noted that the CONTAIN water carryover fraction is 1.0 for either dispersed liquid water or aerosol modeling cases; that is, the pathway fluid density is equal to the fluid density in the upstream cell. This carryover fraction can not be modified by user input. The potential implications of this carryover percentage is discussed in relation to HDR test T31.5.

Loss Coefficients for Parallel Pathways.

In early versions of the CONTAIN code, only one pathway was allowed between connected compartments. As a result, multiple pathways connecting compartments required a collapsing method. For this method, a commonly used procedure for combining multiple paths in a steady state flow system was applied. With the more recent versions of the code, invoking an implicit flow solver, multiple flow pathways may be input directly using the engineering vent input, or a combination of "regular" and engineering vent inputs. Since the reference case was developed using the older method where pathways were collapsed, and since it could be anticipated that some collapsing may also be used to simplify other containment models. Hence, it is useful to investigate what effect such collapsing might have on the prediction of pressure differentials. A number of calculations were made comparing the collapsed and multiple pathway models, assuming reasonable variations in individual pathway loss coefficients (especially increasing the loss coefficients for pathways connecting the breakroom with cell #2). Shown in Figure 4.32 are the comparisons for the two cases (collapsed and multiple pathways) where the loss coefficient between the breakroom and cells #2 and #3, pathways #140, #143, and #145 in Figure 4.33, are assumed to be represented by a C_{FC} value of 1.5, rather than 1.0 used in the reference case. As noted, the two calculations do not overlap. This is because the steady state assumption on which the collapsing method is based is not entirely appropriate for the highly transient condition imposed on this code calculation. However, the difference is small and not considered an important feature of the sensitivity study. Still, the difference does suggest that the multiple pathway modeling method is a preferred approach.

Nodalization.

With the implicit flow solver, CONTAIN is a robust computational code which provides the opportunity for the user to include more detail into the description of the inter-connective modeling of containment compartments. How important is the added detail to differential pressure predictions is shown in Figure 4.34. In this comparison, the five-cell reference case is compared to a 33-cell model of the HDR facility. The loss coefficients C_{FC} in both models are taken as 1.0. From this comparison we see that nodalization (especially in the regions adjoining the breakroom) can make a significant difference in the differential pressure calculations. Specifically, there are three noted observations: first, the early rise and first maximum in the differential pressure is well predicted with the more detailed nodalization scheme; second, the

decline in differential pressure after this first maximum is reduced, also in better agreement with data; and third, that the second maximum is higher than the first maximum, which is also in better agreement with data than the results from the five-cell nodalization.

Two-phase Loss Coefficients.

The pathways between compartments are approximated as orifices, such that the steady state two-phase pressure drop across an orifice is given by

$$\frac{\Delta P_{correlation}}{\Delta P_g} = \Phi^2$$

where $\Delta P_{correlation}$ is the effective, or two-phase pressure drop, and ΔP_g is the single phase pressure drop for flow of gas at the total mass flow for the two-phase fluid. In the above equation the multiplier Φ^2 is correlated from the experimental data. As an approximation we consider a case where $\Phi^2 = fnc(S, \rho_u, \rho_g)$. Here S is the velocity slip ratio between phases and the densities are the upstream fluid and gas densities. The exact functional dependence for the transition from single to two-phase flow is not known, but at least we can attempt to correlate the bounds according to the transient density profiles by indicating the following;

$\Phi^2 \rightarrow 1$, as $\rho_u \rightarrow \rho_g$, and

$\Phi^2 \rightarrow$ constant, as $\rho_u / \rho_g \rightarrow$ constant

The first condition gives the single phase loss coefficient C_{FC} in the case where the upstream fluid and gas densities are the same; the second condition sets up a correlation for an effective two-phase CONTAIN loss coefficient dependent on the ratio of upstream density (including dispersed liquid) to the gas density, that is,

$$C_{FC}^{'} = C_{FC}\left(\frac{\rho_u}{\rho_g}\right)\Phi^2$$

Since we know that we can get a reasonably good fit to the differential pressure with C_{FC} during the single phase first maximum (33 cell nodalization), occurring during the single phase portion

of the blowdown, we set C_{FC} equal to one for the first condition. The limiting condition for the density ratios is inferred by the density ratios for this example, which is shown in Figure 4.35, and is relatively insensitive to assumptions regarding the value of C'_{FC}. This suggests that because the density ratios reach a limiting value, C'_{FC} must also reach a limiting value at approximately the same time in the test. For this test, we have correlated the differential pressure profile by using a value of $C'_{FC} = 1.5$, Figure 4.36. We see in the figure that the first maximum is over predicted since we are not allowed to include a function dependence for C_{FC} in the code input.

The initial over prediction of the pressure differential (first maximum), that has been observed here has been noted by others [Fir85] in their predictions. This analyses would suggest that it is related to a flow transition, where the upstream conditions are changing from single to two-phase. It should of course be noted that the agreement here, or the disagreement observed for the reference case, may also be partly the result of other causes; these causes may be related to unknown uncertainties in the injection rate and specific enthalpy – these uncertainties however are not considered here.

It should also be noted that the observed under prediction of maximum pressure differential for the reference calculation was also observed for the USNRC's pre-test prediction of test V44 using the CONTEMPT code. Other experimental investigations of subcompartment tests, Battelle-Frankfurt D-Series, using the USNRC code COMPARE have not indicated under prediction of pressure differentials; however, these tests were conducted with high quality steam injections, and are therefore representative only of single-phase blowdowns. As noted, in Figure 3.7, the HDR blowdown tests were run with injections that were very similar to prototypical blowdowns; that is, with low quality injections during the early portion of the blowdown period. This means that the conditions in the HDR test are expected to be similar to actual blowdown conditions in small compartments where high temperature/pressure water lines have ruptured. The potential for under predictions of pressure differentials under these types of conditions is therefore a matter for some consideration. Having said that, it is still not entirely clear whether these under predictions are solely the result of two-phase phenomena associated with the compartment thermal hydraulics and/or pathways or other causes yet to be investigated. With respect to one possibility, nodalization, we have provided some indication of its importance. The above discussion, however, points to an important consideration for subcompartment analyses, that is, the effect of dispersed liquid in the break compartment and flow pathways exiting the compartment.

Critical Flows.

Estimating critical flows for two-phase flow through pathways in containments is uncertain. In Figure 4.37, the calculated mass flux (G=W/A) by the CONTAIN critical flow equation is

compared to the mass flux calculated in the code for the reference case and a similar case with dispersed liquid. This plot shows that critical flow is not reached in the CONTAIN calculation using the single phase critical flow equation, although it is approached. Other methods for estimating critical flow for two-phase conditions can also be investigated and compared to the single-phase critical flow equation used in CONTAIN. For example, shown in Table 4.13 are critical flow estimates for various two-phase flow assumptions and limits. In each case, we see that the V44 test was apparently not in the critical flow regime. The critical flow approximation used in the CONTAIN code is therefore not applied for this test. That is, the limiting mass flow rate as calculated in CONTAIN is not used to determine the flow exiting the breakroom. This is unfortunate since we can anticipate that accident injections into a room the size of the HDR breakroom would either be choked or, for a orifice-like pathway, approaching a limiting flow rate. At this time, there is no known containment experiments that represent conditions where critical flow models based either on single flow models, such as CONTAIN, or other models (homogeneous versus Moody, or equilibrium versus non-equilibrium) may be assessed.

Table 4.12 Pathway parameters from breakroom to adjoining rooms for the reference calculation				
Pathway		Area, m^2	Area/Length, m	C_{FC}
from cell	to cell			
1	2	3.196	0.905	1.028
1	3	2.593	0.396	0.87
1	4	0.283	0.04	1.6
1	5	2.138	0.32	1.12

Table 4.13 Critical mass flux predictions for HDR test V44 at 2 seconds		
Method	Critical mass flux, kg/s-m^2	Predicted mass flux, kg/s-m^2
CONTAIN single-phase equation	270 (reference calc. - water aerosols) 440 (dispersed liquid water) 440 (dispersed liquid water, detailed nodalization, Cfc=1.5 in breakroom pathways)	155 340 300
Moody steam/water flow	560 (dispersed liquid)	340
Moody steam/water flow X 0.6	336 (dispersed liquid)	340
Homogeneous-equilibrium	390 (dispersed liquid)	340

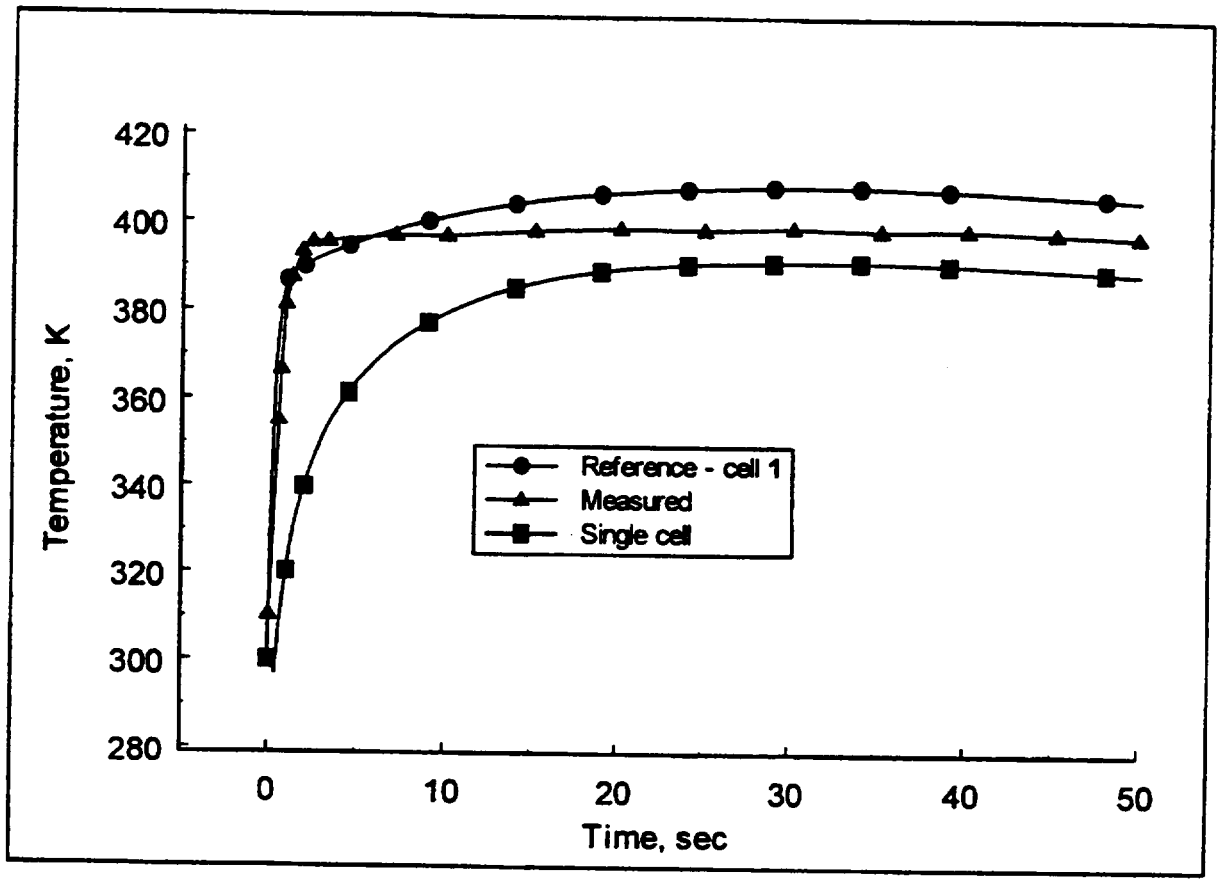

Figure 4.29 Comparison of measured and calculated local temperature for the breakroom in HDR test V44 (ISP16).

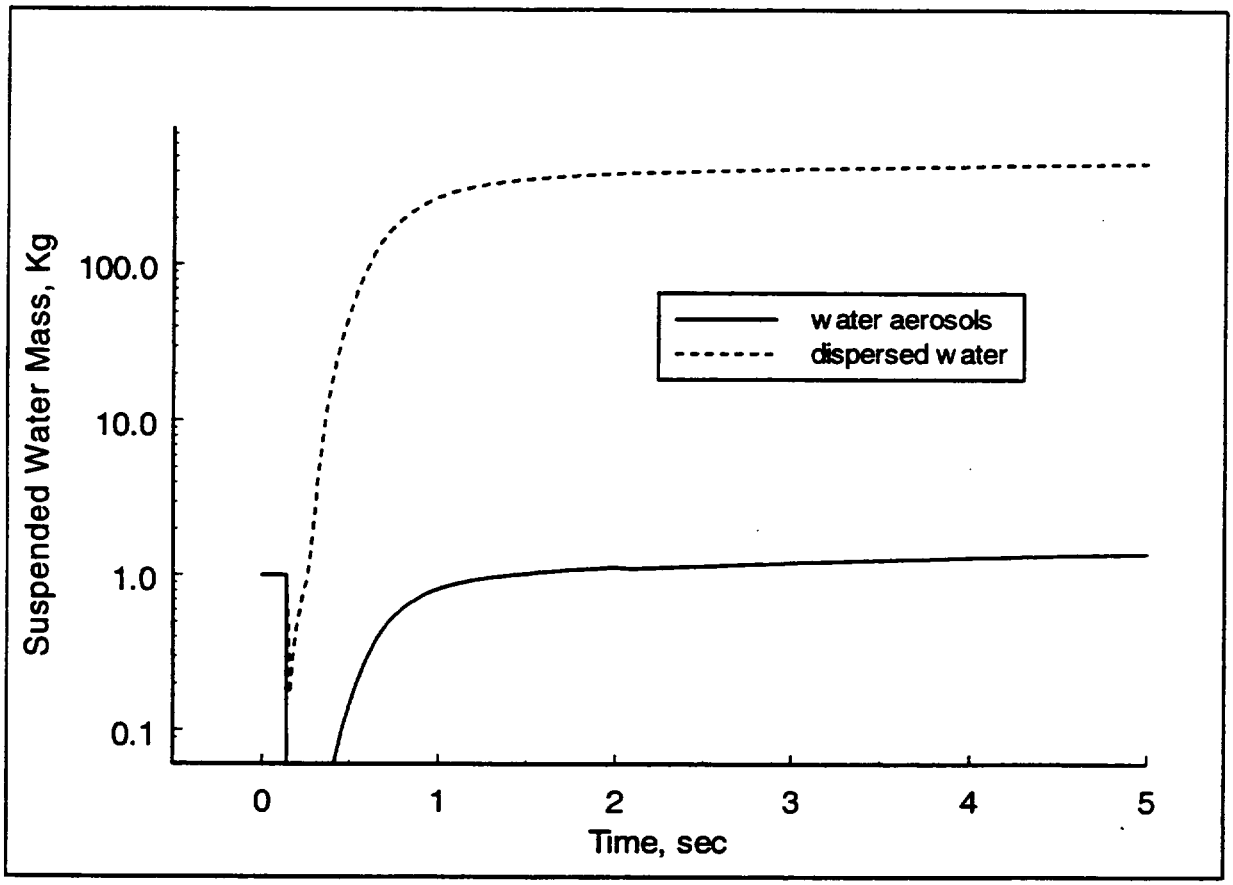

Figure 4.30 Calculations of suspended water mass in the breakroom of the HDR facility for test V44. The water aerosols curve represents a modeling choice used in the CONTAIN reference calculation, while the dispersed water curve shows the suspended water mass if water aerosol modeling is not selected (default option).

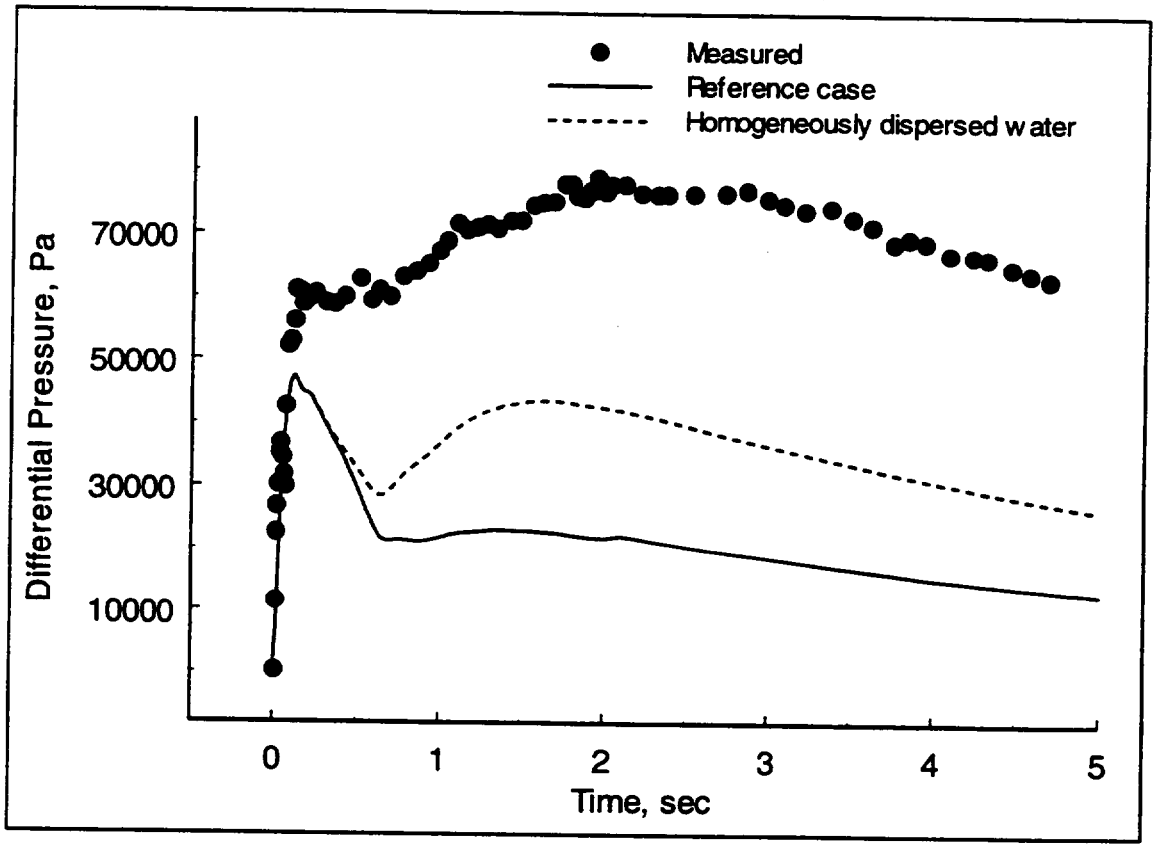

Figure 4.31 Comparisons of measured and calculated differential pressure profiles between the HDR breakroom and adjoining room, 1704. Calculations are based on the five-cell HDR facility model.

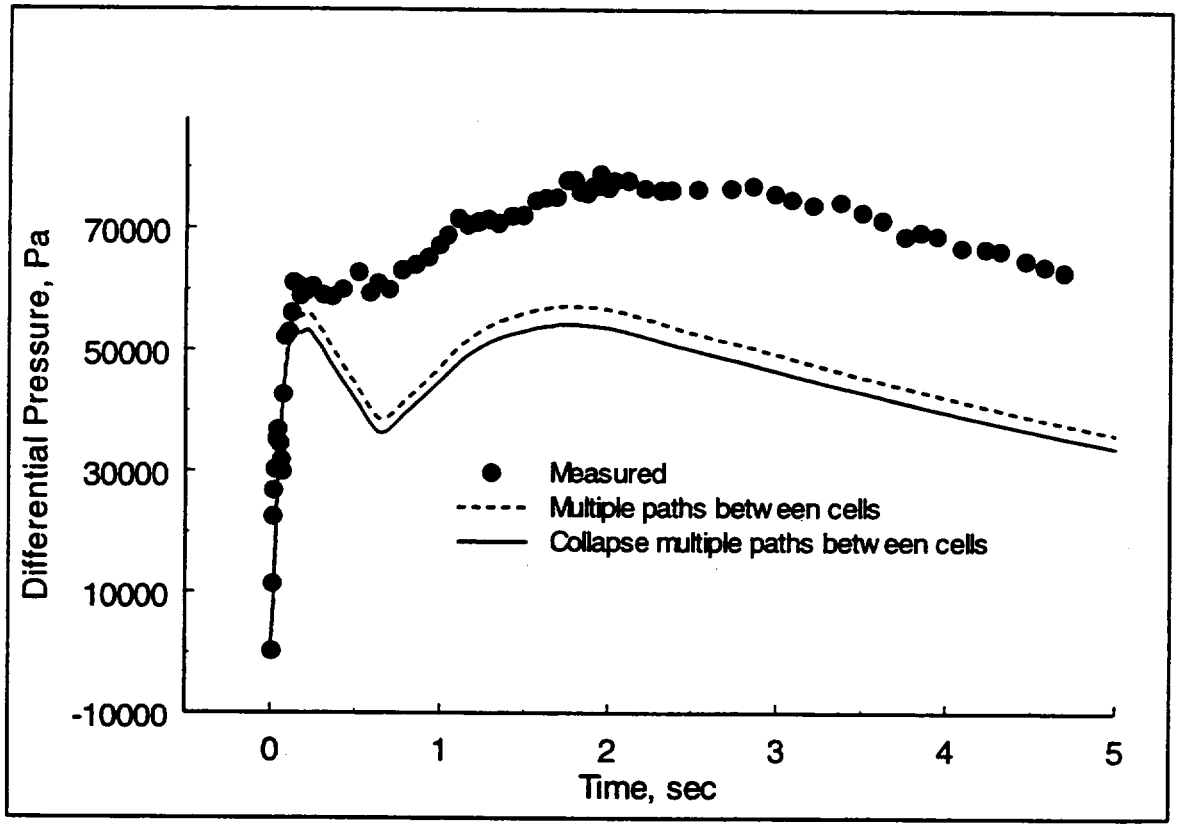

Figure 4.32 Comparison of measured and calculated differential pressure profiles between the breakroom and adjoining room, 1704. The calculations assume that the CONTAIN loss coefficient C_{FC} between the breakroom and cell#2 is equal to 1.5, compared to $C_{FC} = 1$ for the reference case.

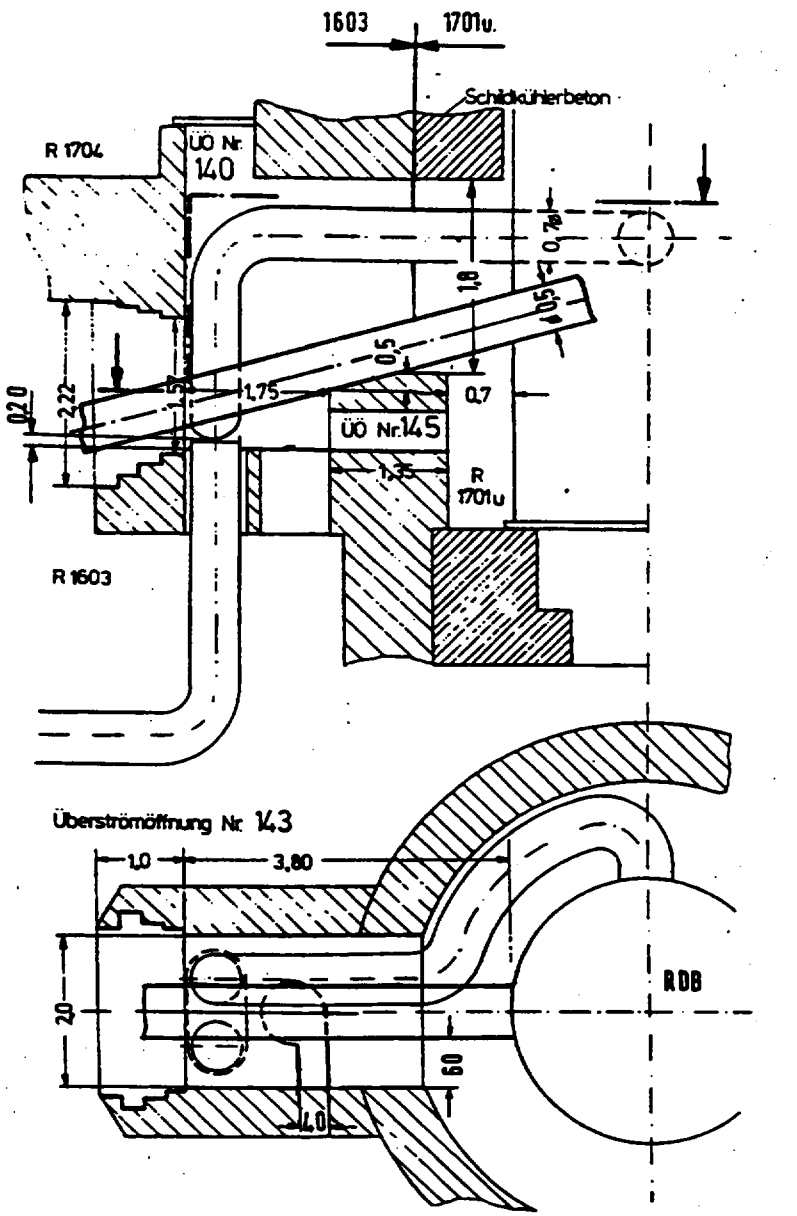

Figure 4.33 Flow path geometry connecting HDR compartments 1603 (breakroom) and the adjoining compartment 1701u. In the five-cell HDR model, these rooms are denoted as cells #1 and #2, respectively.

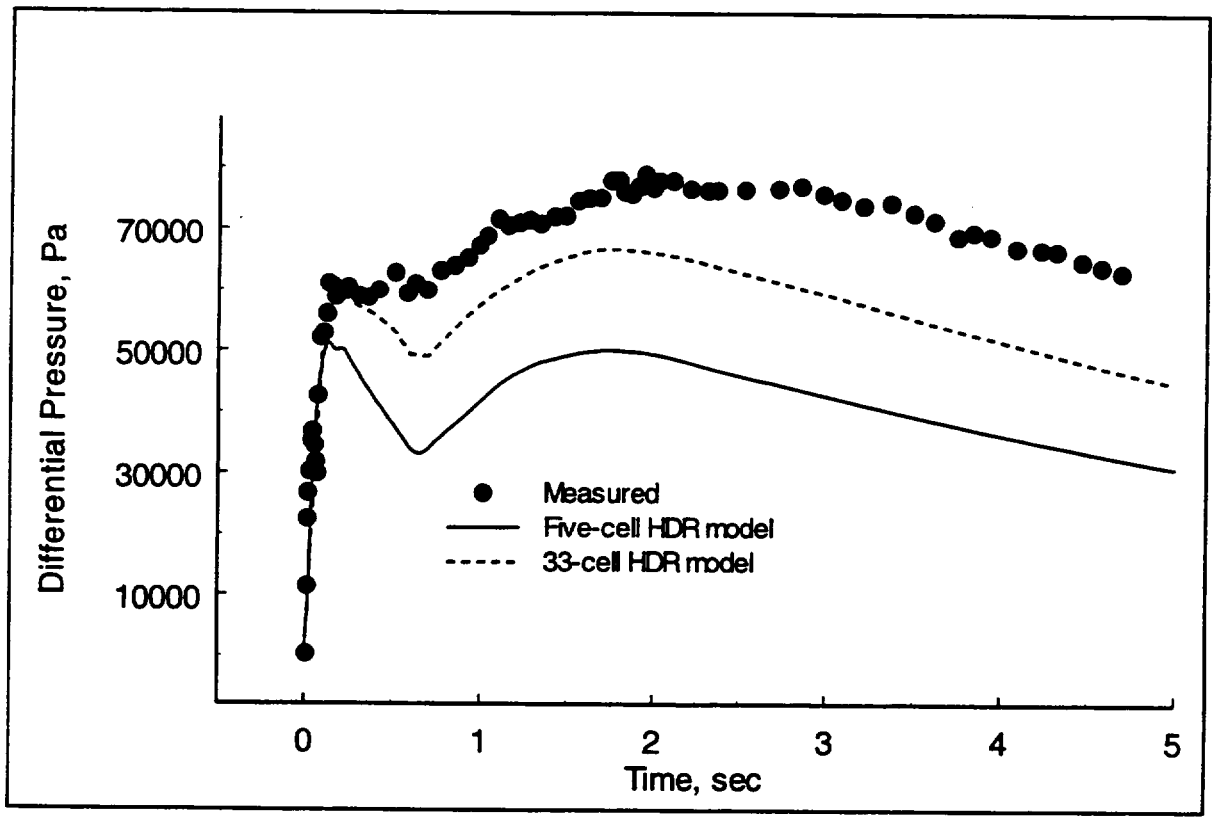

Figure 4.34 Comparison of measured and calculated differential pressure profile between the breakroom and adjoining room, 1704. The calculations show the effect of nodalization on the predicted differential pressure - all loss coefficients are equal to 1, and the liquid water in the atmosphere is modeled as dispersed liquid.

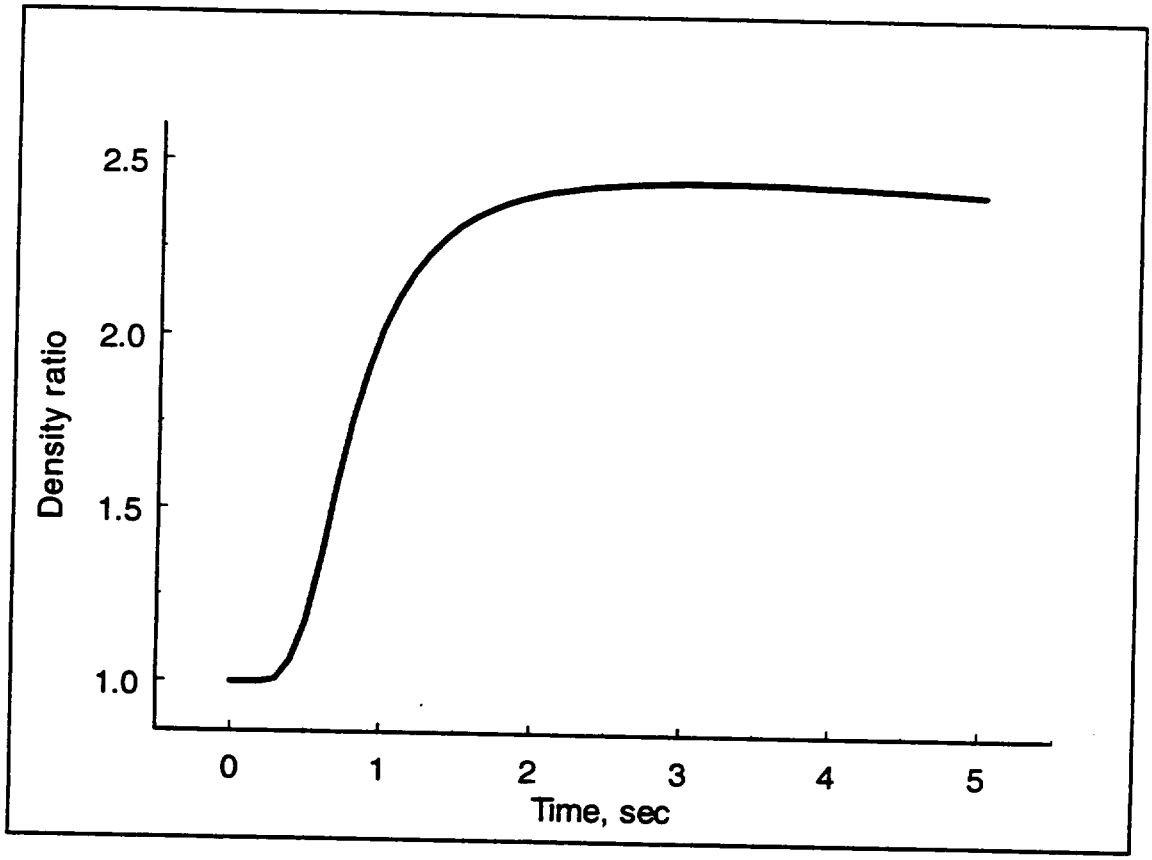

Figure 4.35 Calculated density ratio, ρ_u / ρ_g, for HDR test V44 assuming that the liquid water in the atmosphere is dispersed liquid.

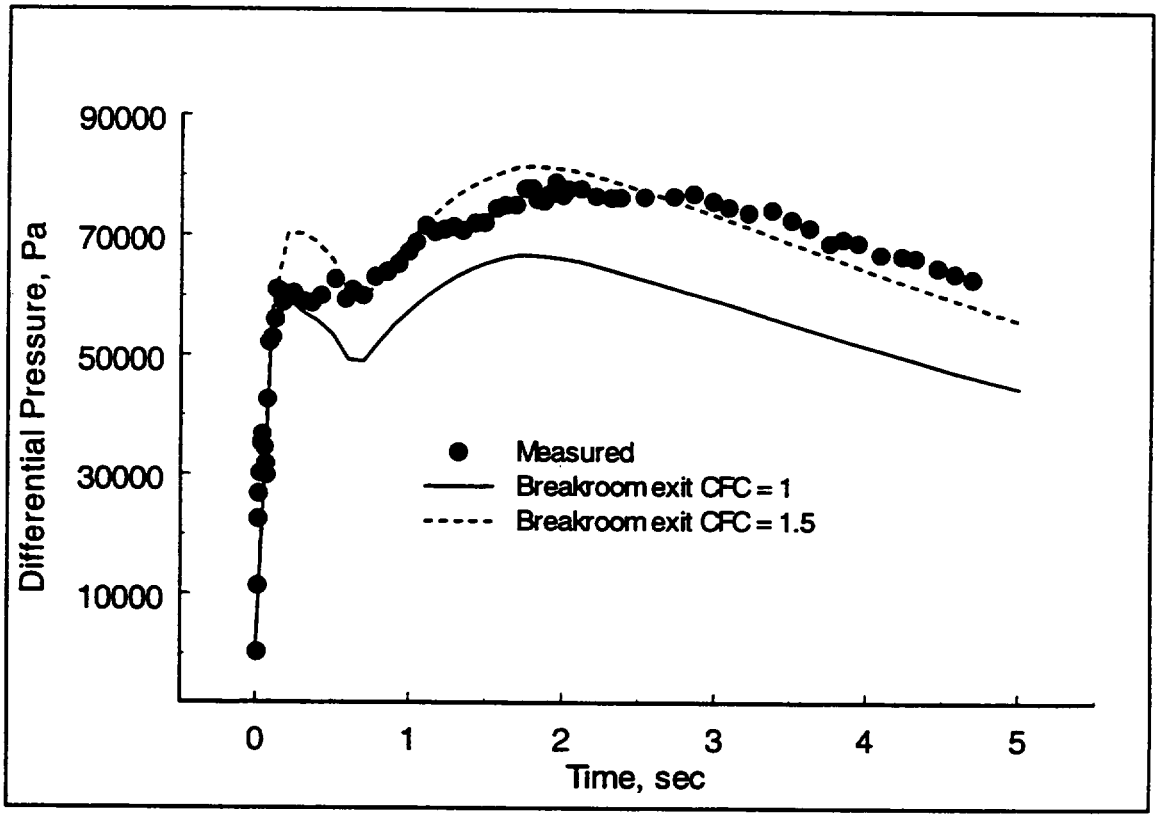

Figure 4.36 Comparison of measured and calculated differential pressure profiles between the breakroom and adjoining room, 1704, for HDR test V44. CONTAIN calculations are for a 33-cell model of the containment.

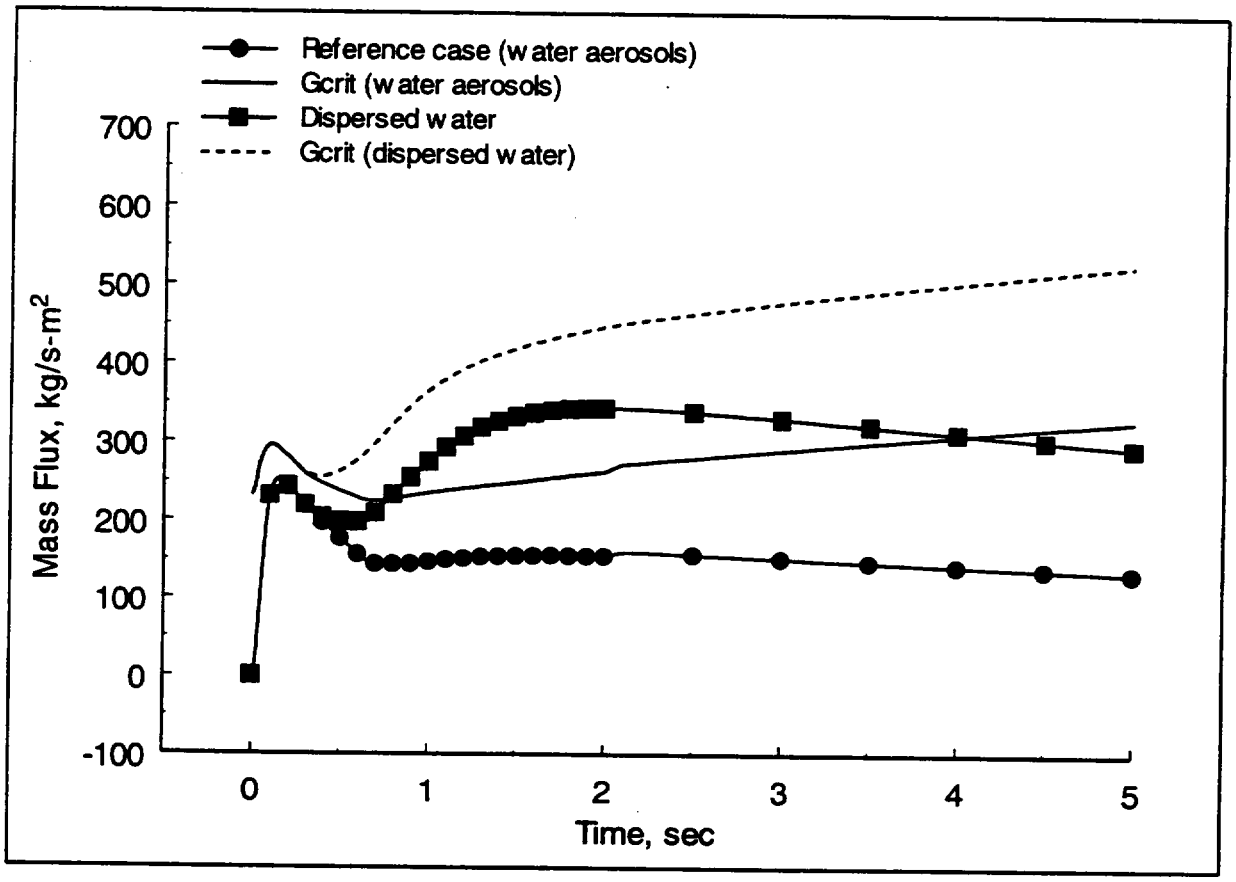

Figure 4.37 Comparison of CONTAIN calculated mass flux for the pathway between the breakroom and adjoining room, 1704. The calculations are made using the reference input for HDR test V44. The notation, Gcrit, denotes the single phase critical mass flux calculated in the CONTAIN code.

4.2.1.2 HDR Test T31.5 [ISP23]

4.2.1.2.1 Maximum Pressure

A summary of sensitivity cases, for dependence on forced convection and dispersed liquid water modeling, showing the effect on maximum pressure is presented in Table 4.14.

Forced convection.

In this test, for the forced convective study, higher velocities (48 versus 24m/s) are specified than in test V44. This is reasonable in the sense that the reference model input for this test consisted of more cells in the vicinity of the breakroom, and therefore allowed estimates of convection velocities into those regions near the breakroom but not too far distance (two levels below and two levels above the breakroom; that is, levels 1500 to 1900 -- see Figure 3.38). Figure 4.38 shows the pathway velocities for regions near the breakroom, compartment 1704, and the estimated forced convective velocity (dash line in the figure) input into the code. The effect of using forced convection in this case on the pressure predictions is more evident for this analysis than in the previous V44 analysis. For example, a noticeable reduction in the peak pressure resulting from forced convection is obtained for test T31.5, as shown in Figure 4.39; whereas, no reduction was observed for V44 (Table 4.11, case 1 versus 3) when forced convection was used in the limited region of the breakroom and the two adjoining cells.

Atmospheric liquid water.

As in the sensitivity cases run for test V44, the effect of dispersed liquid water in the atmosphere was also investigated for this test. The reference calculation used water aerosols to model condensed water in the atmosphere. Because of the manner in which CONTAIN treats aerosols (i.e., as having no inertia in a flow path or heat capacity), the use of aerosols is essentially equivalent to a dropout model, provided that evaporation of the aerosols is not important, the water aerosols deposit rapidly (as occurs in this test), and the effects of transport are relatively unimportant. As noted in the ISP-16 (V44) sensitivity analysis, dropping out the water tends to increase the containment pressure slightly. This effect is also illustrated in Figure 4.39, where the case labeled "dispersed liquid water" represents a calculation with dispersed liquid water in the atmosphere. As can be seen from the comparison between the pressure plots for the reference and dispersed water cases, pressures calculated with water aerosols (reference case) tend to be slightly higher.

4.2.1.2.2 Subcompartment Analysis

A comparison of pressure differentials for tests V44 and T31.5 are shown in Figure 4.40. Two points need to be made in regard to this figure: first, although the blowdown injection rate and enthalpy is nearly identical, the absolute pressure differential is significantly reduced for T31.5; and secondly, and perhaps more importantly, the differential profiles of the two tests are significantly different. The CONTAIN code has been used to investigate these variations. First, however, we note that there are some geometric differences between the two tests. The breakroom volumes are 280 and 793 m^3 for test V44 and T31.5, respectively; and, the total exit pathway areas from the breakrooms are 8.2 m^2 for test V44, and 5.7 m^2 for test T31.5. The most significant geometric difference is the volume size, where the breakroom for test T31.5 is approximately three times larger than for test V44.

Atmospheric liquid water.

When liquid water is allowed to remain in the atmosphere, the fluid inertia is increased over an atmosphere containing just air and water vapor and, like what was observed in test V44, this effect is to increase the pressure differentials. The effect is shown for this test in Figure 4.41. What is interesting with this test is that the calculation without dispersed liquid water, that is, when liquid water is modeled as aerosols, gives better agreement with measurements. The loss coefficients for the breakroom exit are set as $C_{FC} = 1$ in each case represented, which would be representative of single phase flows through unobstructed pathways. Clearly, the pressure differentials calculated by using aerosols to represent the suspended liquid water are lower than those calculated by retaining the liquid water in the atmosphere field and apparently represent the better estimate of maximum pressure differential during the two-phase injection period. Had we used the prescription of V44, with dispersed liquid water and $C_{FC} = 1.5$ for pathways exiting the breakroom (to account for the increased resistance with two-phase flow), the maximum pressure differential during the two-phase blowdown period would have been predicted to be approximately twice the measured value (breakroom to room 1708). This comparison between two rather similar blowdown tests indicates that the variation in the differential pressure maximums and profile may be caused by differences in 1) the details of pathway exits from the breakrooms, or 2) water carryover from the breakrooms to the pathways. We have noted some variation in pathways between the two tests, but the differences do not appear significant. The variations in the differential profiles would suggest that a more reasonable explanation involves the water carryover fraction, thereby affecting the pathway flow density and loss coefficient. If the difference is in water carryover, we note here a very sensitive parameter for which we do not have a predictive model in the code. The limiting or maximal approach however appears to be indicated with an assumed dispersed liquid model and an adjustment in the loss coefficient to account for the added resistance associated with two-phase flow.

Table 4.14 ISP-23 peak pressure sensitivity calculations				
Case #	Description	Predicted Peak Pressure, P_{max}, bar	$\left[\frac{P_{calc}}{P_{measured}}\right]^{*}_{max}$	$\left[\frac{\Delta P_{calc} - \Delta P_{measured}}{\Delta P_{measured}}\right]^{**}_{max}$
1	Reference case (default velocities, water aerosol ...)	2.95	1.18	30
2	Forced convective velocity input	2.79	1.12	19
3	Dispersed liquid water	2.91	1.16	27

* $P_{measured} = 2.5$ bar

** $\Delta P_{measured} = P - P_{init} = P - 1.0$ bar

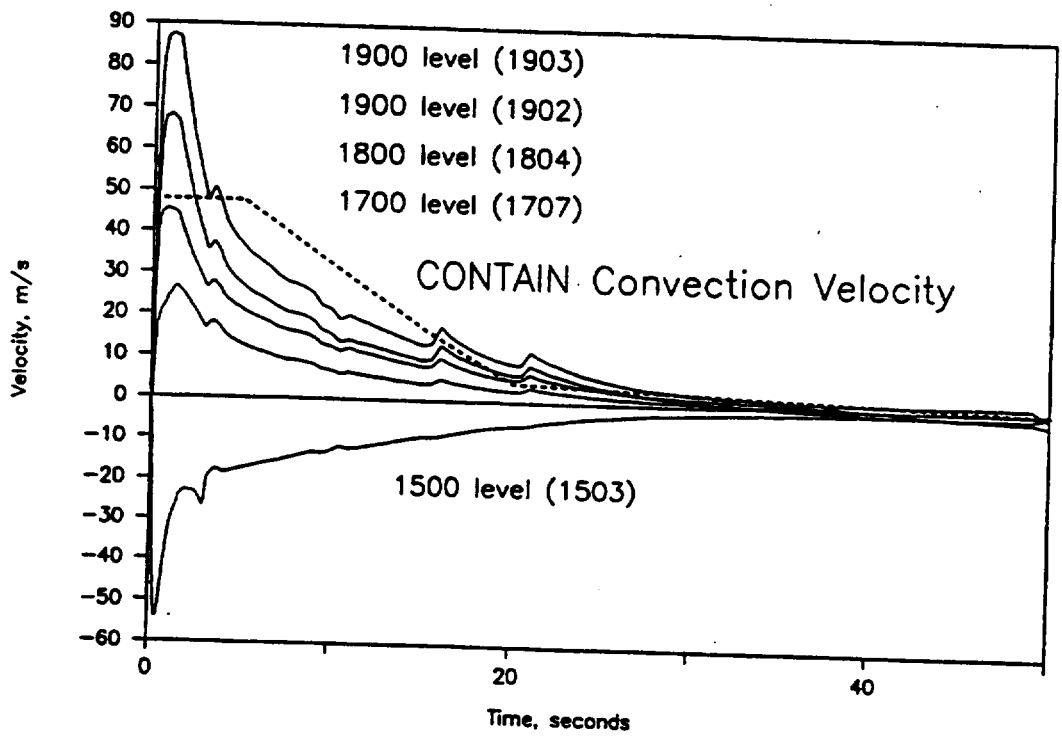

Figure 4.38 Representative pathway velocities calculated in the CONTAIN code for HDR test T31.5. The dashed line denotes the forced convective velocity profile used for levels 1500 to 1900.

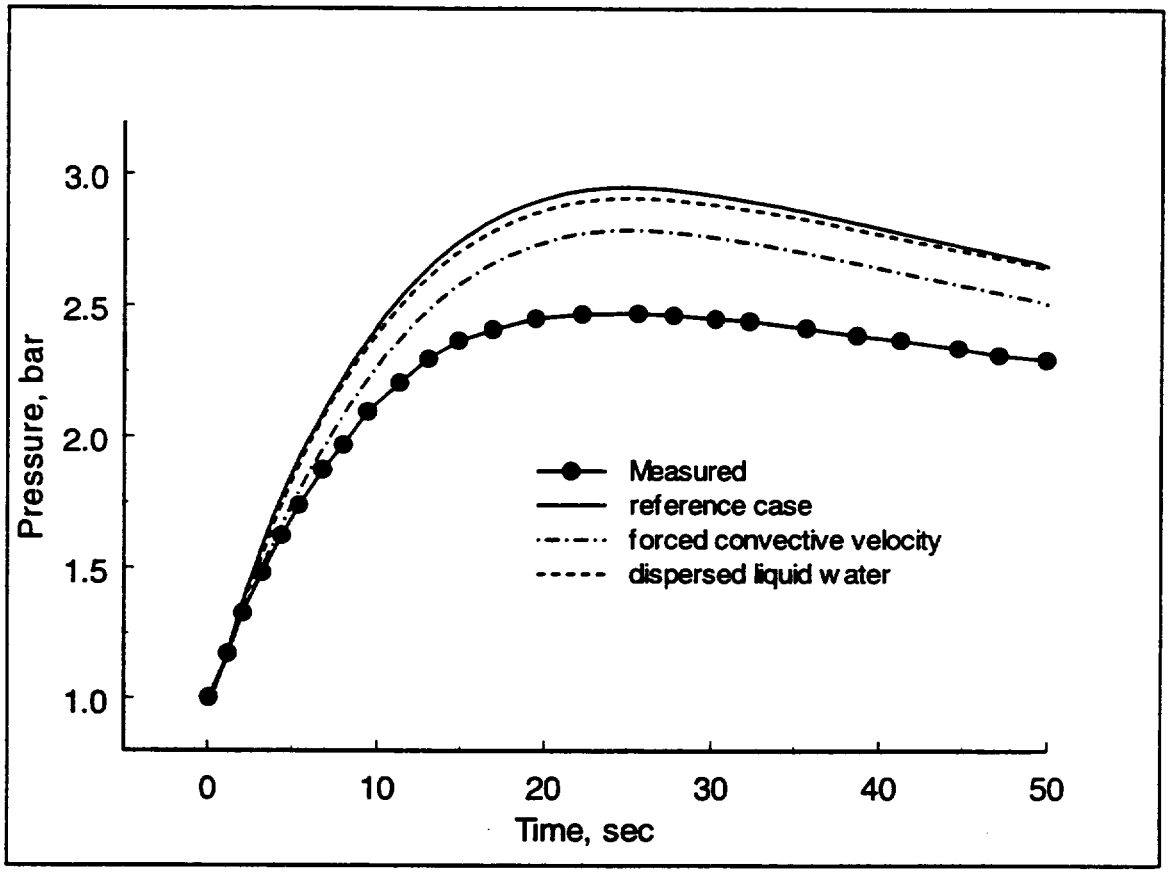

Figure 4.39 Comparison of measured and calculated CONTAIN pressure predictions for HDR test T31.5.

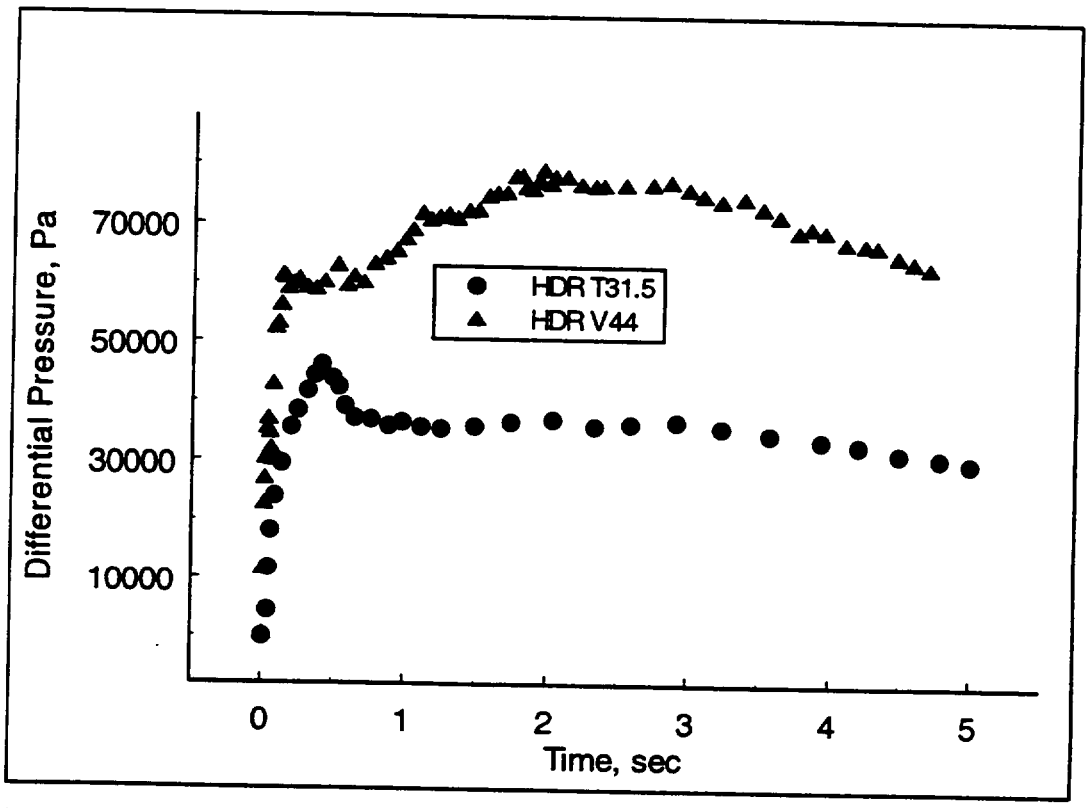

Figure 4.40 Comparison of measured differential pressure profiles between breakroom and adjoining room for HDR test V44 and T31.5.

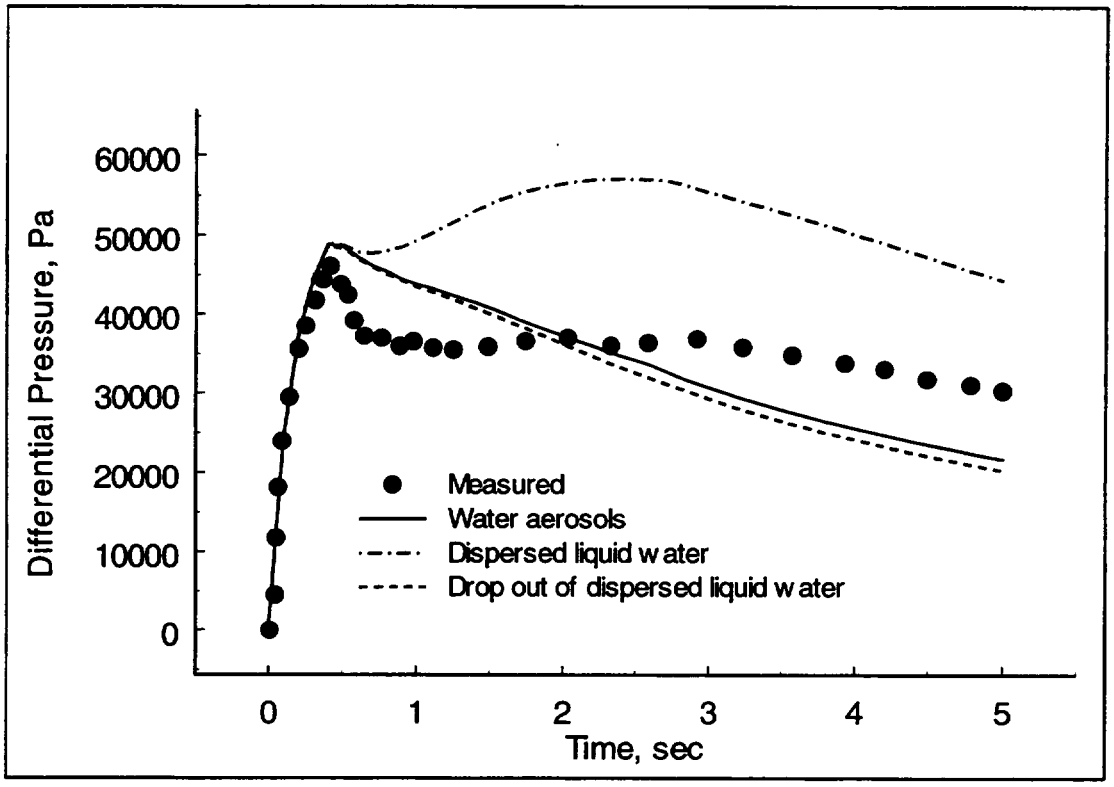

Figure 4.41 Comparison of measured and calculated differential pressure profiles between the breakroom and adjoining room, 1708, for HDR test T31.5. The CONTAIN calculation with aerosols represents the reference calculation.

4.2.1.3 HDR Test T31.5 (Project HDR Benchmark)

Nodalization.

A single cell nodalization of the HDR containment was used to calculate the T31.5 test for the extended time period of the benchmark exercise. Figures 4.42, 4.43, and 4.44 show comparisons for pressure, local temperatures, and hydrogen concentrations, respectively. The pressure for the single cell is over predicted during the first 10 minutes of the test significantly more than in the case of the multi-cell calculation. This is partly caused by the reduced steam concentration predicted for the single cell during this period, which results in an under prediction of the condensation rate. The trend however is reversed at about 10 minutes when the effect of overmixing tends to bring more steam into contact with lower structures in the single cell as contrasted to the multi-cell calculation that correctly predicts stratification in the facility. The temperatures plotted in Figure 4.43 show one of the consequences of using a single cell to model a containment where the injection location is elevated. In this case the temperatures in the upper containment are significantly under predicted, while the lower containment temperatures are over predicted. The sensitivity of hydrogen concentrations to nodalization is also significant since the peak hydrogen concentration is under predicted by about 30%. The improvement in the multi-cell calculation is clearly shown in this sensitivity case. This is of interest in postulated beyond design basis accidents where many of the scenario characteristics are similar to this case.

Stratification modeling.

Degree of nodalization is an input choice that the code user can make to enable the prediction of stratification in a containment. Most lumped parameter codes, even when using multi-cell inputs, tend to over mix gases. This problem has been described in Mur96, and noted in other ISP final reports [Kar89, Kar93]. However, the problem of over mixing is not entirely caused by the lumped parameter approach; rather, the problem is the result of the manner that the flow equations are approximated under various flow conditions. In CONTAIN, a remedy for this artificial mixing has been found (hybrid flow solver) that works well for most scenarios considered for containment analyses - conditions where the stratifications develop quickly into stable quasi-steady stratifications. Test T31.5 is one such case. The reference calculation was made using the new hybrid flow solver. We can also invoke the old method of solving the transport of gases between cells by using the keyword MSTABLE in the FLOW block of the CONTAIN input. Shown in Figure 4.45 are the upper and lower containment temperatures calculated using the keyword MSTABLE. The variation in the temperatures calculated by this method compared to the reference case (Figure 3.43) is noticeable but not what could be considered significant. This general agreement between the two temperature calculations are the result of the strong blowdown effect that was responsible for the initial temperature profile in the containment. The severity of the blowdown partly offsets the stratification effect established by the late time buoyancy-driven flows.

In the case of the late time hydrogen injection, an event following a significant time lapse from the blowdown period, stratification is sensitive to whether the modeling is by the hybrid flow solver or the "old" method. This is indicated by a comparison of the results shown in Figure 4.46, calculated with the MSTABLE keyword, and results obtained for the reference input that used the hybrid flow solver, Figure 3.44. In the "old" method of calculating gas transport, the over mixing in the lower containment is clearly shown, and the under prediction of peak hydrogen concentration is demonstrated. It is important therefore to note that the CONTAIN 2.0 code has been updated with an improved method (i.e., the hybrid flow solver) for calculating stable stratifications, and that this improvement is able to treat the types of stratifications expected in many postulated beyond design basis accidents. This is demonstrated by a comparison of the reference and sensitivity calculations using the MSTABLE keyword for HDR Test T31.5.

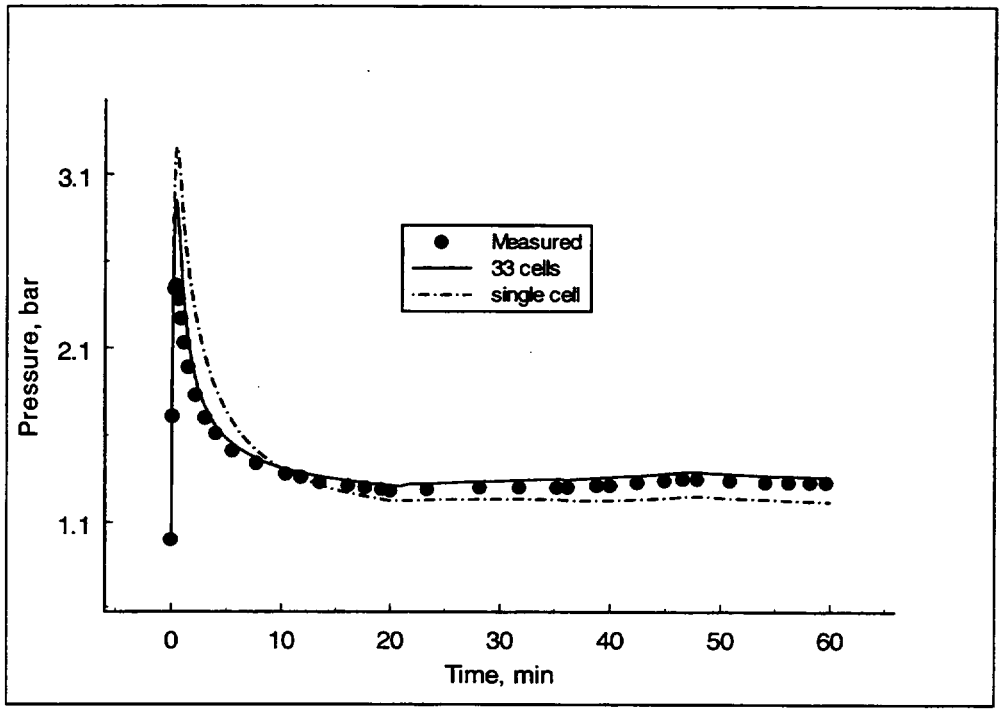

Figure 4.42 Comparison of measured and calculated pressure for T31.5, showing the effect that nodalization has on the results.

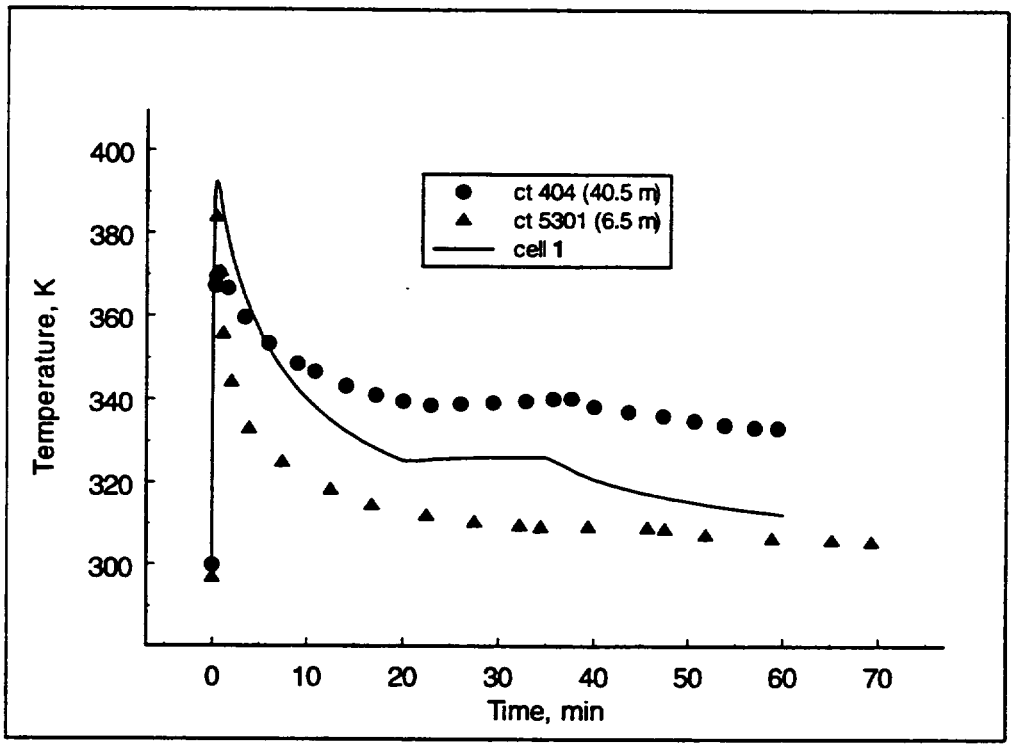

Figure 4.43 Comparison of measured and calculated temperature in the upper and lower containment for T31.5, showing the effect that nodalization has on the results.

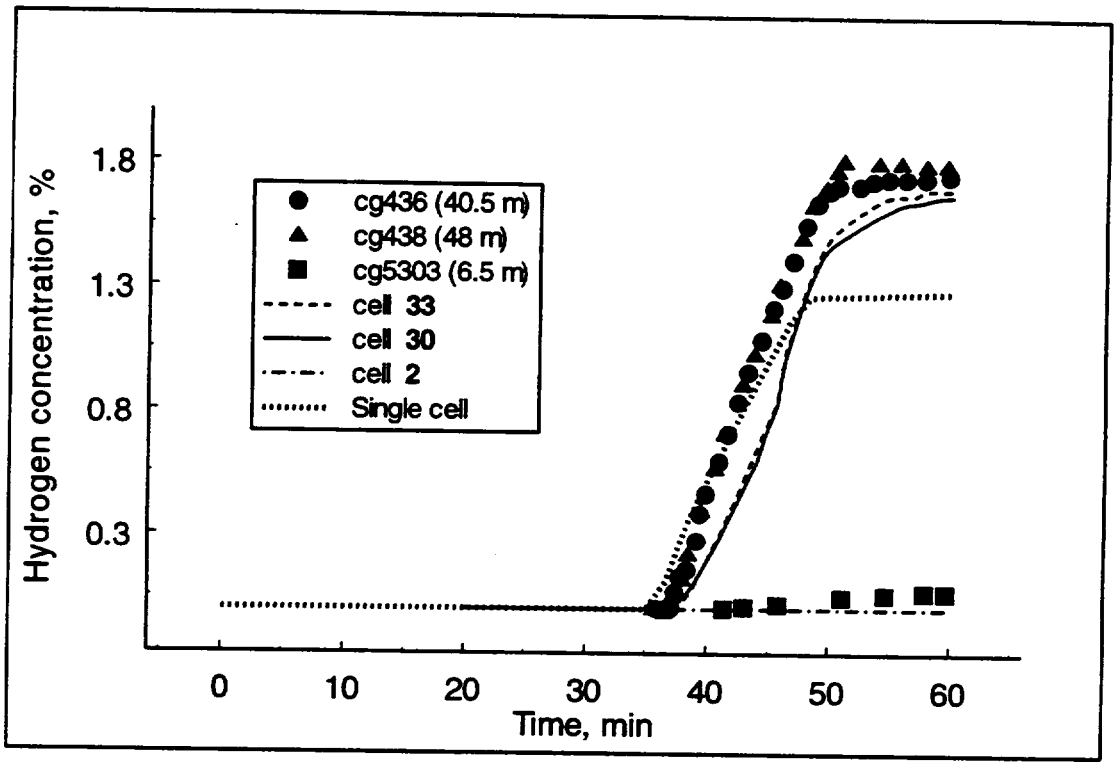

Figure 4.44 Comparison of measured and calculated hydrogen concentration in the upper and lower containment for T31.5, showing the effect that nodalization has on the results.

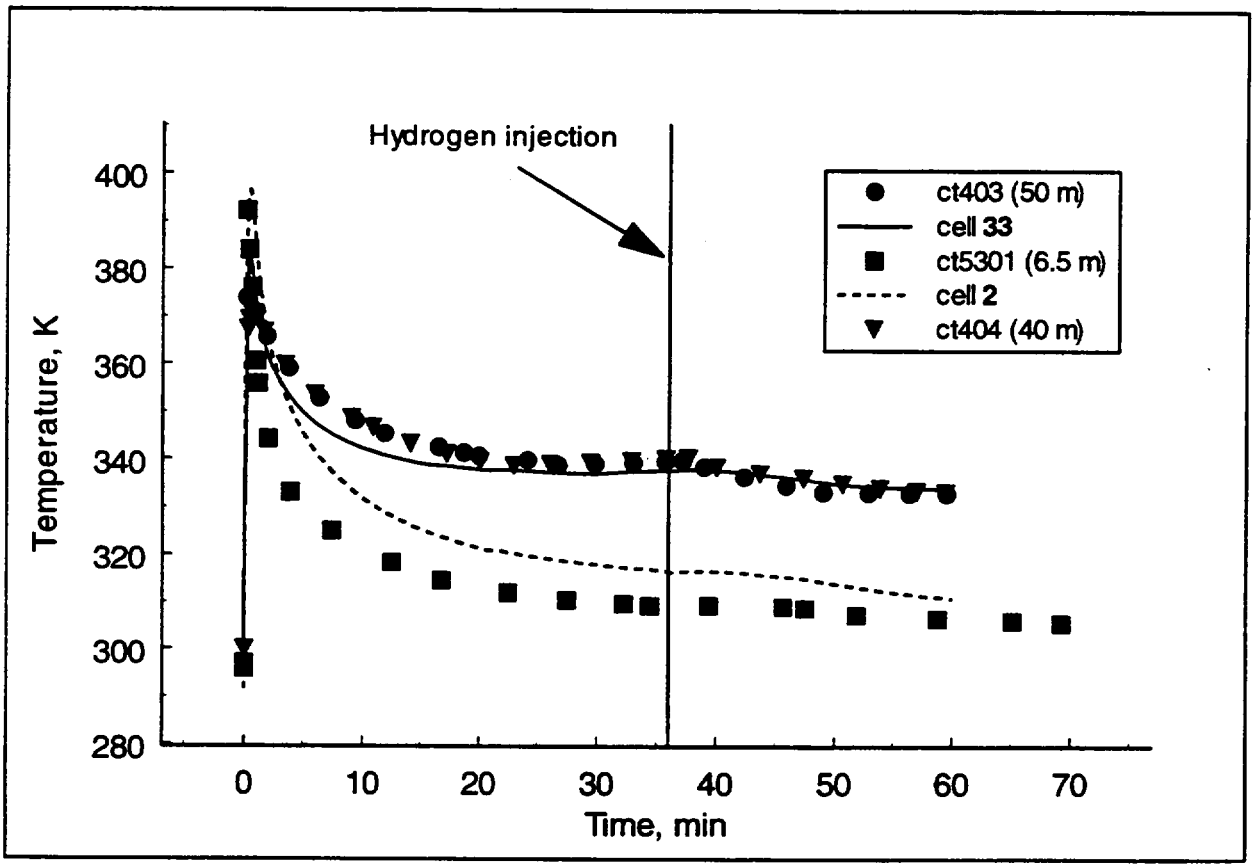

Figure 4.45 Comparison of measured and calculated upper and lower containment temperatures for the T31.5 benchmark exercise, using the "old" flow solver method for calculating gas mixing.

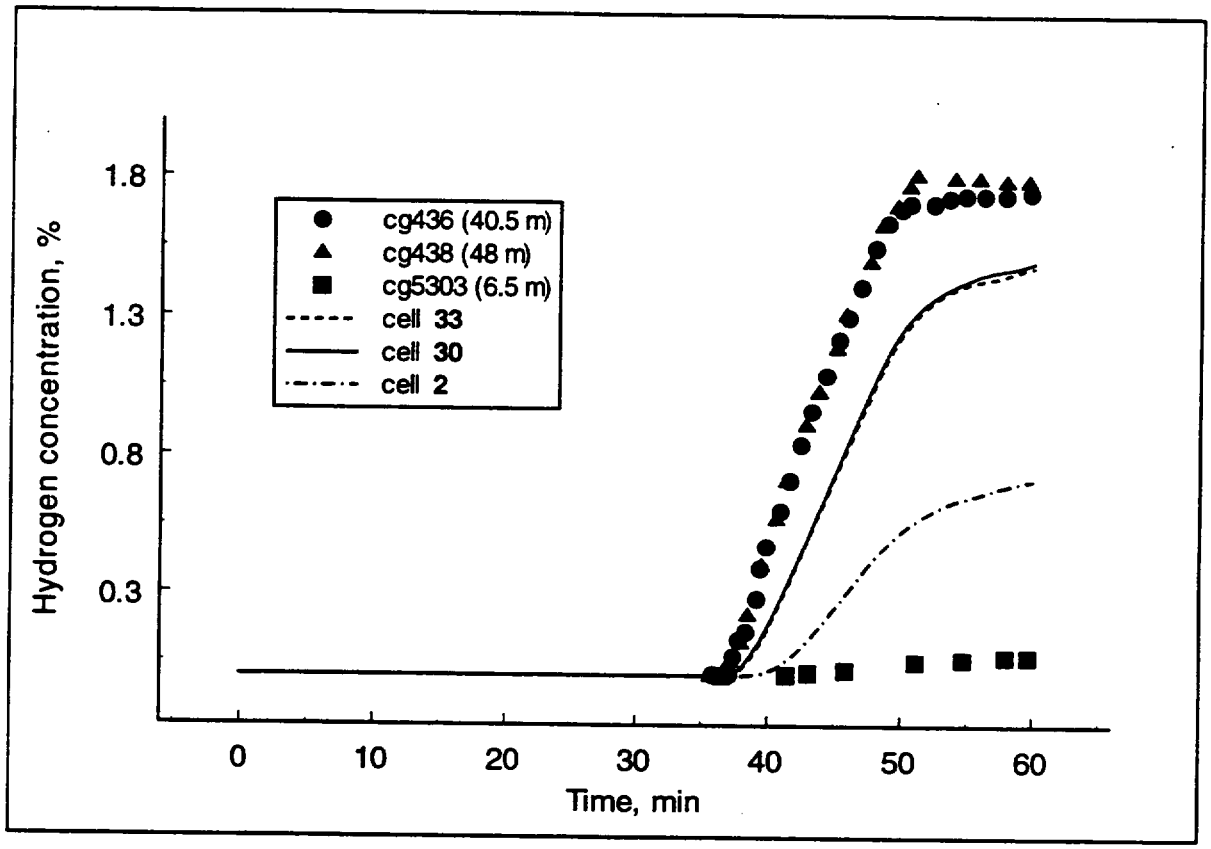

Figure 4.46 Comparison of measured and calculated hydrogen concentration in the upper and lower containment for the T31.5 benchmark exercise using the "old" flow solver method for calculating gas mixing.

4.2.1.4 HDR Test E11.2 [ISP29]

The original nodalization of the HDR facility used for the E11.2 test simulation was a 47 cell input deck (including an environment cell). This deck was used for the E11.2 pre-test calculations, which are documented in Val92. Those results revealed in a Project HDR benchmark exercise that the containment pressure at the end of pre-heat portion of the test was being over predicted by about a factor of two. To investigate this apparent erroneous calculation, a reduced nodalization was adopted in order to perform a series of sensitivity calculations; these sensitivities included parameter variations affecting condensation heat transfer coefficients, annular gap heat transfer, instrument cooling water, and external steam injection rates. Results of the sensitivity calculations were presented at a PHDR Working Group Meeting in 1990 and documented in Reference Til92. One of the conclusions from those sensitivity calculations is that the cause of the over prediction in pressure was an incorrect specification of the steam injection mass rates; it was determined that the steam injection rate was about 30% too high. Within a year after that presentation, Project HDR had confirmed that there had indeed been an error in the measured steam injection rates for the entire E series, and that the error in the steam injection rate was about 30% too high. This account is recalled here for two reasons: first, it demonstrates the importance and usefulness of sensitivity calculations to resolve thermal hydraulic issues; and second, it gives some additional historical background on the development and use of the 15 cell input deck used for the E11.2 reference calculation.

Experimental uncertainties.

One of the main lingering concerns with the E11.2 reference calculation with respect to DBAs is the over prediction of containment pressure at the end of the preheat portion of the test. Such over predictions of the pressure in this experiment are known to be a problem for codes that do a reasonably good job of predicting stratification observed in the test. Over predictions have been reported for a number of other codes besides CONTAIN, including finite-difference codes. It has been suggested [Kar93] that possible causes for this apparent discrepancy include uncertainties in the test boundary conditions, material properties, and the containment geometric specifications. The boundary condition uncertainty arises primarily from two sources: instrumentation cooling line energy extraction and the steam mass injection rate. Material property uncertainty arises from the condition of the HDR concrete, with its thermal conductivity varying as water is absorbed into the concrete during the prolonged preheat period. The uncertainty related to the geometric specifications involves a possible pathway for steam to access additional heat sink areas through an approximately 3.5 cm wide air gap between the concrete and the steel containment shell. This gap was originally filled with rigid insulation but may have opened up as

a result of shaker tests conducted in the facility.[2]

These uncertainties have been investigated in the sensitivity calculations as summarized in Table 4.15 and shown graphically in Figure 4.47 and 4.48. Each uncertainty has the potential to substantially affect the containment pressure. Resolution of one or more of these uncertainties could clearly result in a more accurate pressure prediction. At this point, however, there is not enough information to suggest how these uncertainties can be resolved.

Nodalization.

Since the reference calculation was calculated using a rather coarse nodalization of the HDR facility (i.e., the 15-cell scheme), it was considered useful to re-calculate the test using a more detailed nodalization. As indicated in Mur96, there is a rather delicate balance of gravity forces generated during the pre-heating and hydrogen injection periods when the source injection is on one leg of a circulation loop that surrounds the reactor vessel region (RDB), shown in Figure 4.49. Changing the injection elevation slightly, or the configuration of cells around this loop, can affect the distribution of steam in the upper containment. Depending on how this loop region is nodalized, the circulation can be either relatively strong or weak. If the circulation is weak, then steam injected into the containment will concentrate in the upper containment, and remain for relatively long periods since the upper containment has only a small amount of long term (concrete) heat sinks. However, if the circulation is stronger, steam injected into the containment will be transported around the loop (whose bottom is at level 1600, ~ 10 meters). Since there are significant amounts of long term heat sinks along this loop path, more steam will be condensed in this case than otherwise. This effect is demonstrated by comparing the steam concentrations for both a 15 and 47-cell nodalization and measurements, Figure 4.50. The 15 cell nodalization is set up with small variations to favor circulation in the loop [Mur96]. As a result, the steam concentration in the upper containment is less for this nodalization. In both cases, the lower containment steam concentration is small since this region is below the main circulation loop for either nodalization. Shown in Figure 4.51 is the pressure calculations for both the 15 and 47-cell nodalizations of the HDR facility. The 47 cell nodalization is similar to the 48-cell input used for the E11.4 reference calculation, except that cells 1 and 2 are combined as one cell. It is concluded from this sensitivity that at least some of the pressure over prediction in the E11.2 test is due to our inability to calculate accurately the loop circulation during the pre-heat period.

A number of lessons should be apparent from the E11 series of tests for both the experimentalist and analyst. From the experimental standpoint, uncertainties for energy sources and sinks need to be reduced for prolonged injections in containments; this includes the measured injection

---

[2] Huttermann, B., and Schwinges, B., "GRS Technical Note: Supplements and Corrections to HDR System Description and External Steam Supply for E11 Test Series," Cologne, April 1997.

rates, instrumentation effects on the fluid being measured, material properties, and pathways for access of containment steam to all heat sinks. For the analyst, main circulation loops that can bring steam in contact with long term heat sinks can be an important modeling concern, and depending on the configuration, that may be difficult to model correctly for prolonged periods. The prediction of prolonged injections are therefore a challenge since small uncertainties in circulation patterns for rapid blowdowns may become more important for the containment thermal hydraulics for long time periods. This realization may be important for investigations of equipment qualification and issues involving hydrogen mitigation and management.[3]

Stratification modeling.

Shown in Figure 4.52 are the comparisons of measured and calculated pressure for E11.2, showing the difference in pressure prediction between the default (hybrid) and old flow solver (metastable condition) methods of calculating gas transport within the facility. As noted previously, the metastable condition can be invoked in the code by including the keyword MSTABLE in the FLOW block input. Because the metastable condition increases mixing by buoyancy-driven transport, steam injected at the mid-elevation will be transported to lower regions of the containment where most of the long-term heat sinks are located, and in those regions the steam will condense at a higher rate than if retained in the upper containment. Even with this tendency to over mix, the late time over prediction of pressure is evident, indicating that some additional cause or causes for the over prediction are likely.

[3] It should be noted that the HDR facility with such a large aspect ratio (height/diameter) in conjunction with the procedure (injection location) for the E11.2 test greatly emphasizes the importance of circulation loop mixing within the containment. Most US containments have smaller aspect ratios. Moreover, the internal configurations of compartments in these containments, and likely injection locations, would place less emphasis on circulation loops as a mixing process than noted for the E11.2 test.

Table 4.15 Comparison of Measured and Calculated Containment Pressure at the End of the Preheat Portion of the E11.2 test.

Case #	Description	Pressure, bar
---	Measured	2.03
1	Reference case, Section 3	2.47
2	Concrete thermal conductivity increased by 30%	2.30
3	Upper bound for instrumentation cooling line energy extraction	2.31
4	Addition of gap heat sinks from level 1500 to the upper containment	2.15
5	Steam injection mass rate decreased by 20%. (This is approximately twice the uncertainty that would be realized in most containment experiments.)	2.00
6	Combination of cases 2 and 3	2.17

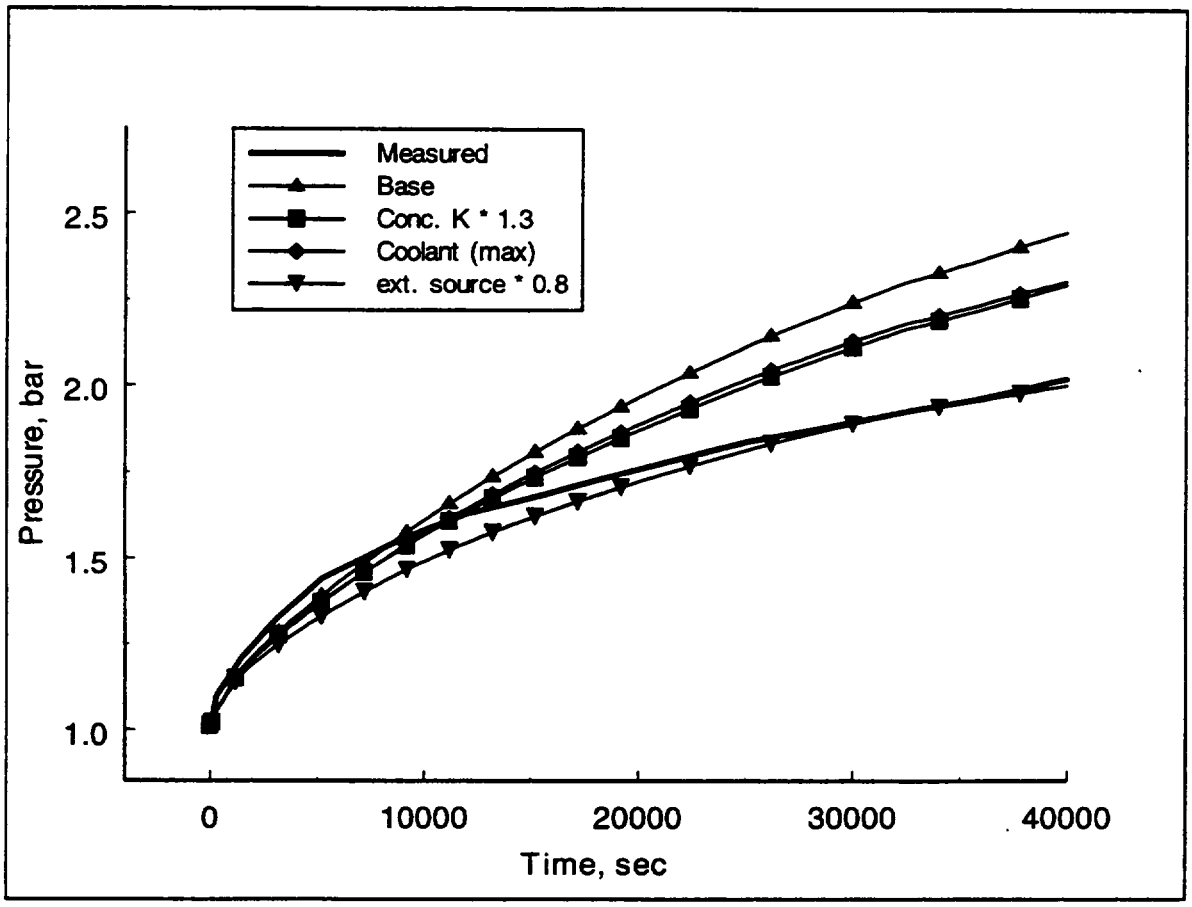

Figure 4.47 Comparison of measured and calculated containment pressure for E11.2 during the pre-heating portion of the test. The various parameter variations denoted in the legend are described in Table 4.15.

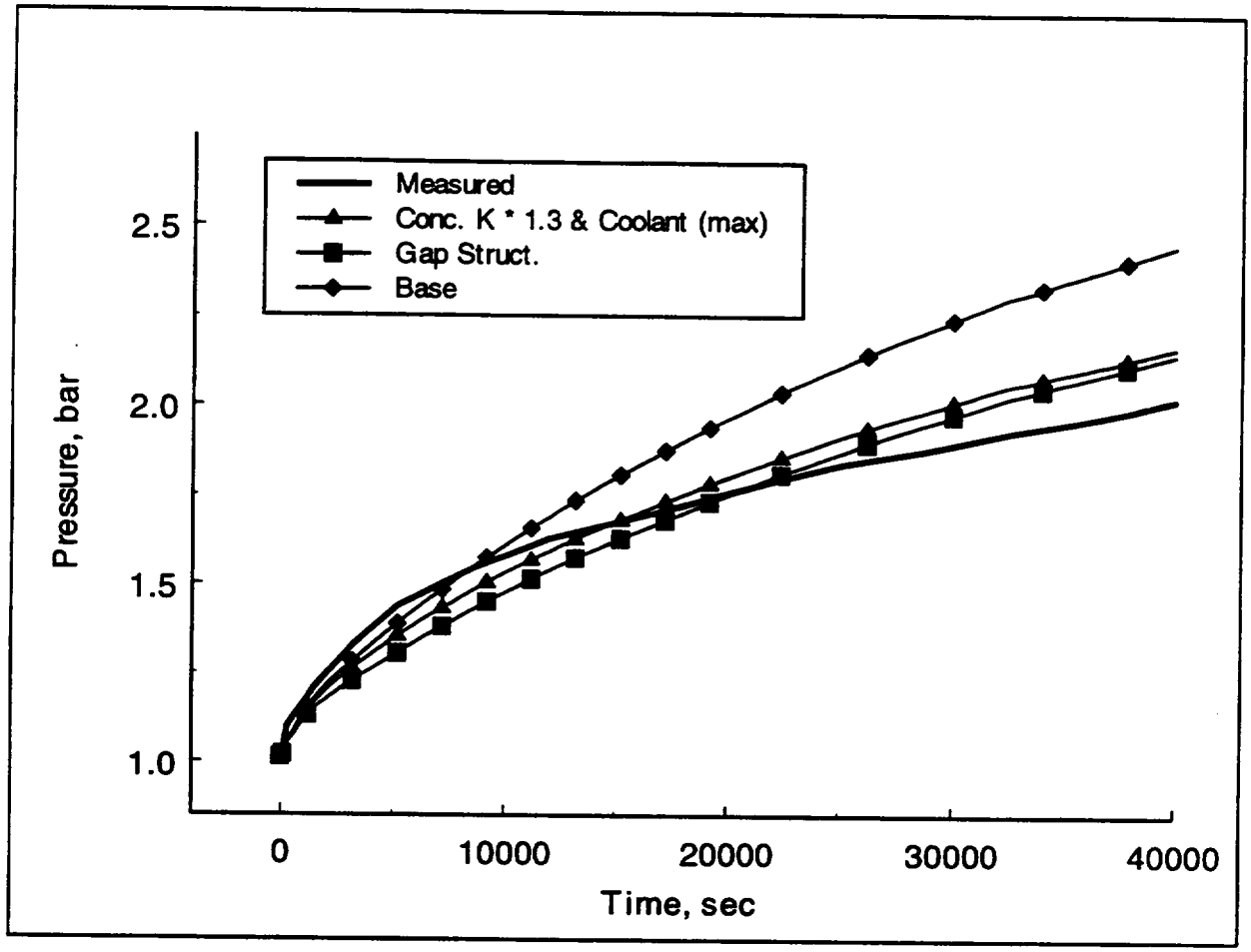

Figure 4.48 Comparison of measured and calculated containment pressure for E11.2 during the pre-heating portion of the test. The various parameter variations denoted in the legend are described in Table 4.15. A combination case is represented for a scenario were the concrete thermal conductivity and coolant line energy extraction are increase relative to the reference or base case.

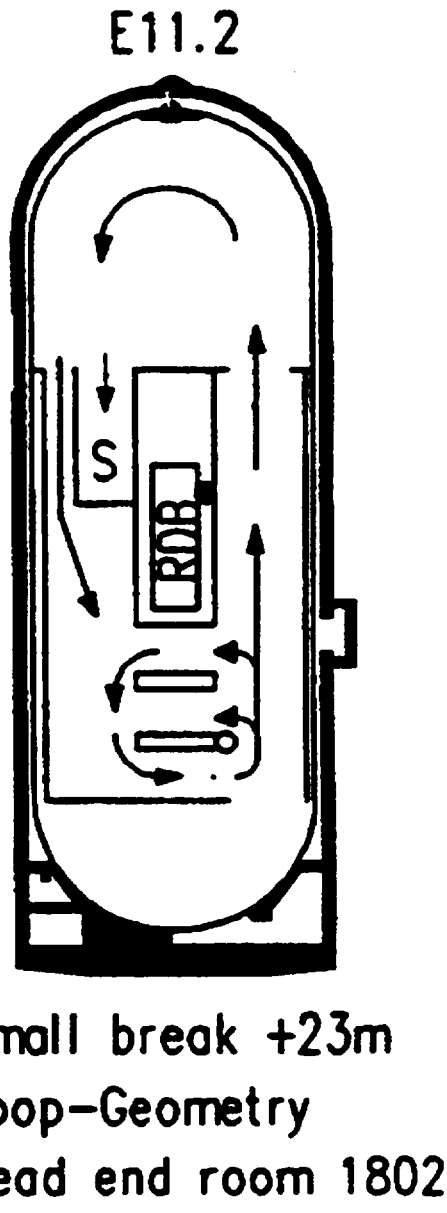

Figure 4.49 Sketch of the HDR facility for the E11.2 test showing some of the circulation currents expected for the test. ■ position of break and injection; o second position of late time break; S dead-ended compartment.

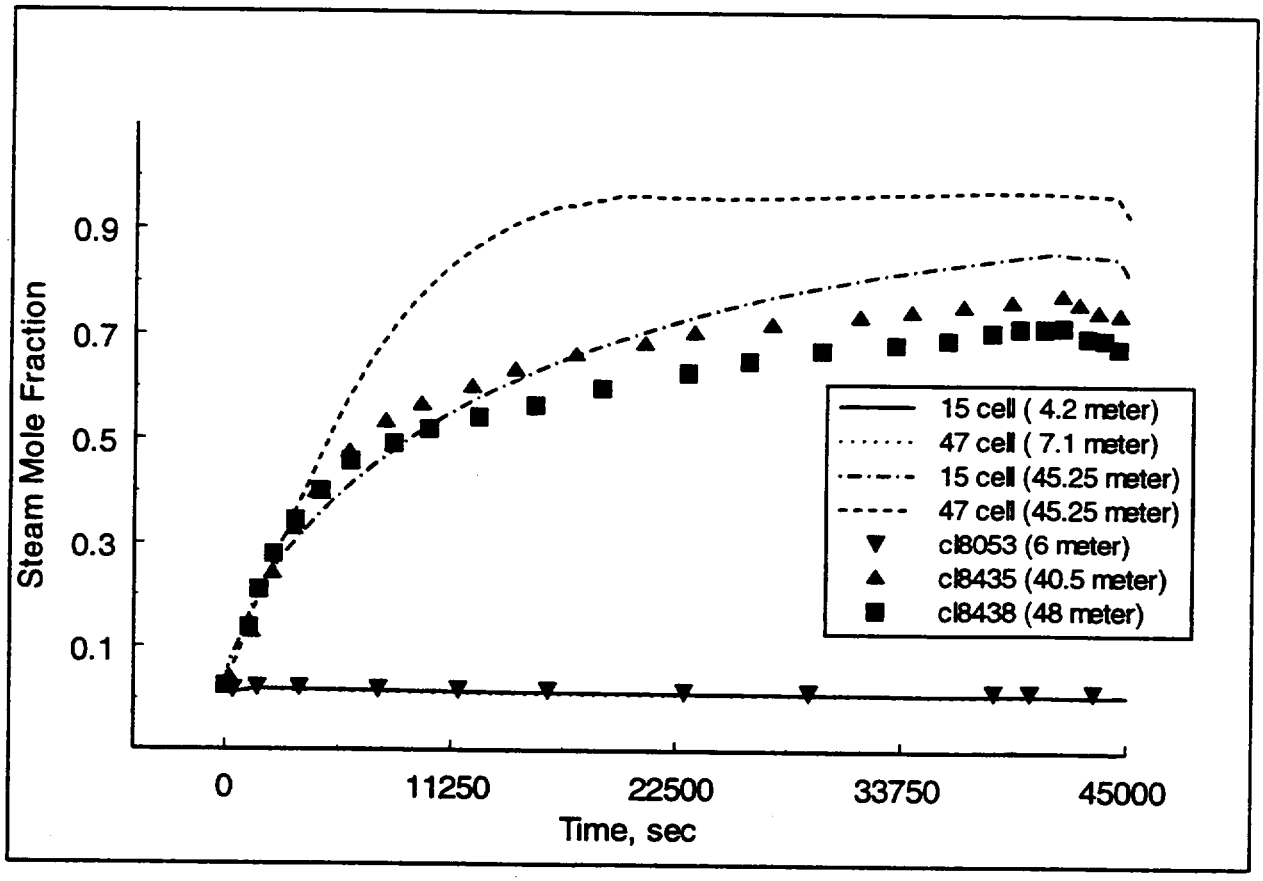

Figure 4.50 Comparison of measured and calculated steam mole fractions for HDR test E11.2. Calculations are made using a 15-cell (reference input) and 47-cell nodalization of the HDR test facility.

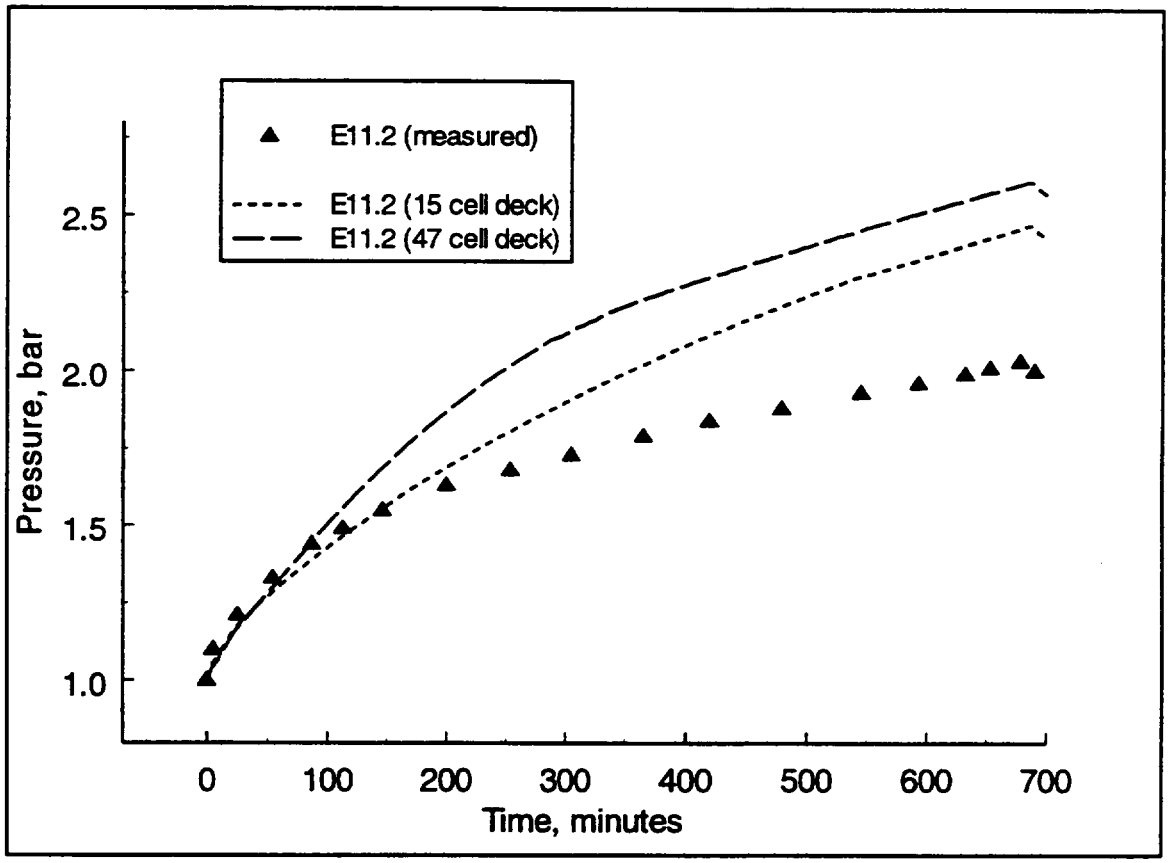

Figure 4.51 Comparison of measured and calculated containment pressure during the pre-heat period for test E11.2. Calculations are made using a 15-cell (reference input) and 47-cell nodalization of the HDR test facility.

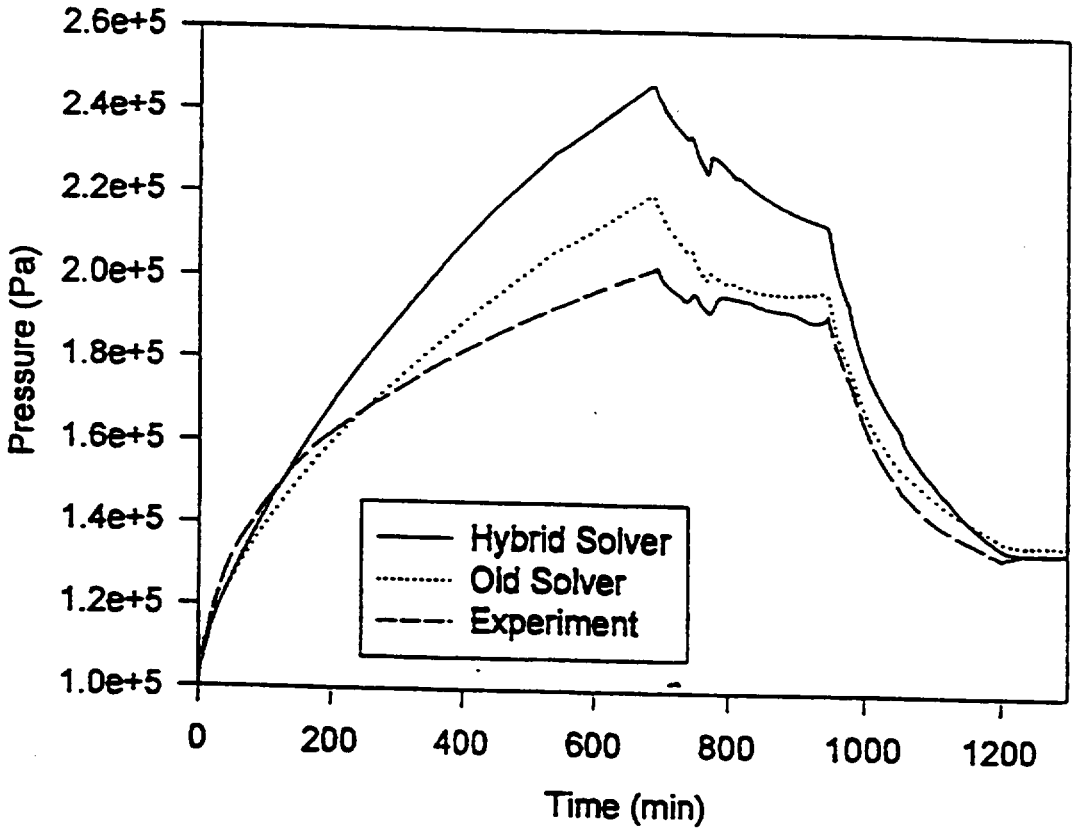

Figure 4.52 Comparison of measured and calculated gas pressures for HDR test E11.2, showing the variations between the calculations with the old (metastable) and hybrid gravitational head formulations.

4.2.1.5 HDR Test E11.4 (Project HDR Benchmark)

Nodalization.

The reference calculation for the E11.4 test was run using a 48-cell nodalization of the HDR facility. This nodalization was identical to the 47-cell nodalization used for the E11.2 pre-test calculation, except that one additional cell is added to the lower containment region near the source location to better model this area. The 15-cell nodalization used in the E11.2 reference calculation had a very coarse nodalization of the lower containment, since this region was removed from the mid-elevated injection location. To see the effect of nodalization on pressure, the 15 and 48 cell nodalizations are compared in Figure 4.53. During the early portion of the test, the 15-cell nodalization run under predicts pressure; this appears to be caused mainly by the coarse nodalization near the injection location. The geometric model in this region enables too much steam to be in contact with heat sinks which, in reality, by-passes a significant portion of the total region. Later in the transient the 15 cell nodalization run over predicts pressures. This late time behavior is partly the result of the early over estimation of heat transfer in the lower containment, where at later times a reduced heat transfer rate in the lower containment results in delayed over prediction in the containment pressure. The more detailed nodalization afforded by the 48-cell (base) nodalization improves the early and late time distribution of steam condensation in the containment, and therefore, is seen to be a better prediction of both early and late time pressurization (prior to steam injection cut-off).

Experimental boundary condition.

The initial conditions for long-term heat sinks (concrete) in the HDR facility are not specified for the test, that is, the surface and interior temperatures are not given. What is provided are the gas temperatures in various rooms in the facility [Val92]. The reference calculation was setup using a constant initial temperature for concrete structures, 293.15 K. Initial gas temperatures are higher than the assumed temperature for structures, as shown in Figure 7.3-15 of Val92. These gas temperatures should provide an upper bound on the structure's initial temperatures. The run designated as "Case3d" in Figure 4.53 used the gas temperatures as the initial temperatures for the concrete structures. This sensitivity case gives an over prediction of pressure, and demonstrates that while the initial temperature of the concrete can affect the calculated pressures, the effect is probably not severe, given the extreme temperature variation used in this example.

Material Properties.

In the E11.2 reference calculation, the thermal conductivity of HDR concrete, as specified in Reference Val92, at low humidity, was used in the calculation. Previously, in the E11.2 sensitivity calculations, the concrete thermal conductivity was increased by 30% to account for water absorption. In the E11.4 reference calculation, the CONTAIN concrete thermal properties were used. Shown in Figure 4.54 are the comparisons between the HDR specification for

concrete thermal conductivity and the CONTAIN default values; the default values are seen to be higher than the HDR specification, and a better approximation of properties under high humidity conditions (thermal conductivity assumed to be approximately 30% higher during high humidity conditions). In performing the E11.2 sensitivities, the issue concerning loop circulation not being accurately calculated by the code, masked somewhat any conclusions regarding thermal property sensitivity. However, in the case of E11.4, the loop circulation concern is minimized due to the change in the injection location. Shown in Figure 4.55 therefore are comparisons of measured and calculated pressures, indicating that the HDR low humidity thermal conductivity specification for concrete results in an over prediction of containment pressures for the E11.4 test, and that the better agreement with gas pressure measurement is obtained using the CONTAIN default concrete properties.

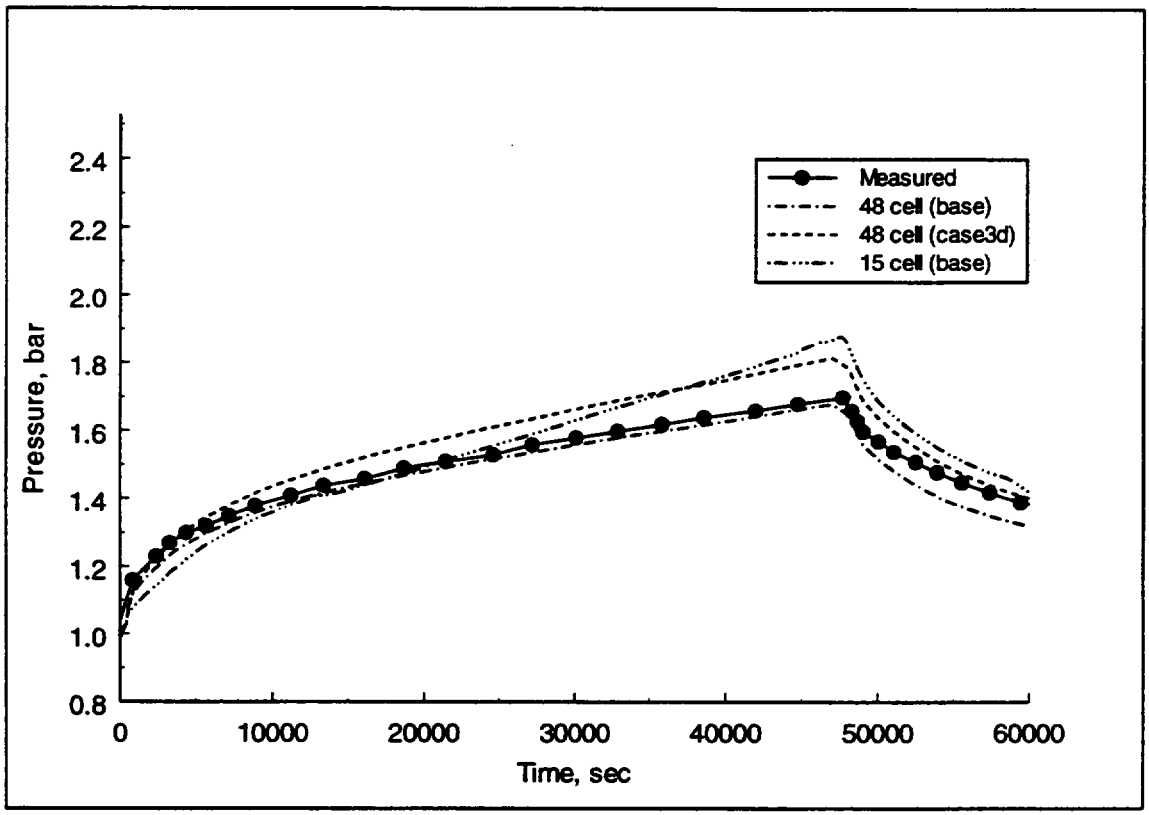

Figure 4.53 Comparison of CONTAIN and measured pressures for HDR test E11.4. Sensitivity runs are provided for nodalization (15 vs. 48 cells) and heat sink initial temperature. Case3d is a sensitivity run where the facility initial conditions for gas temperature are used to initialize both the gas and heat sink temperatures. Initializing the heat sink temperatures to the gas temperatures tends to overestimate sink energy prior to injection and therefore results in a slight increase in predicted pressure.

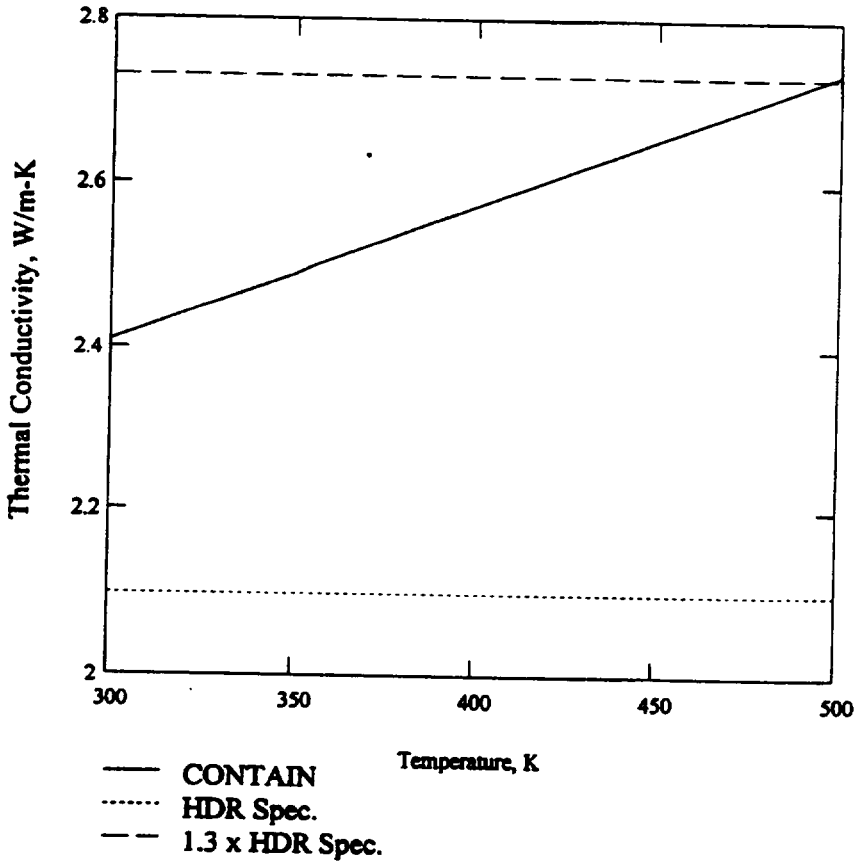

Figure 4.54 Comparison of concrete thermal conductivity for the CONTAIN default properties, HDR specification at low humidity, and a 30% increase over the HDR specification.

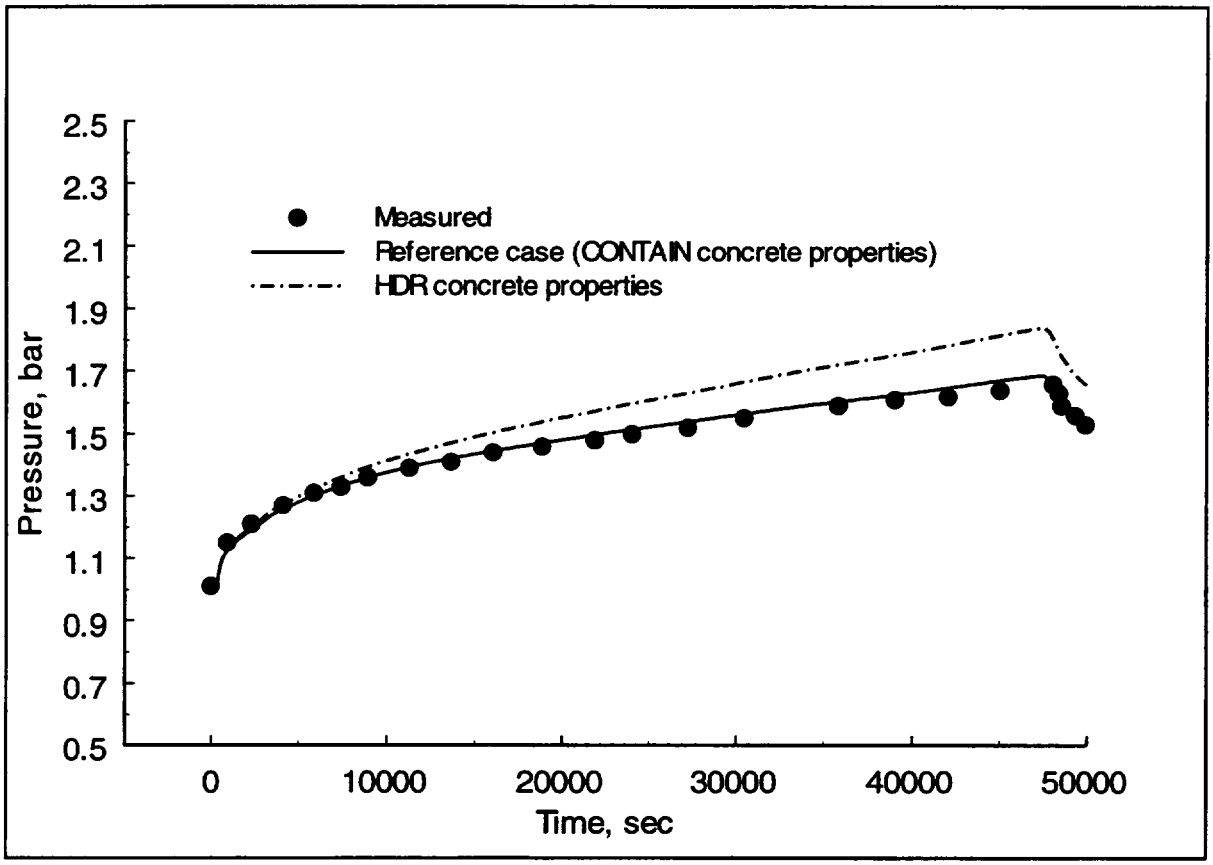

Figure 4.55 Comparison of measured and calculated containment gas pressures for HDR test E11.4, showing the effect of concrete thermal conductivity on calculations.

4.2.2 CVTR Test #3

Most containment analyses for the CVTR test #3 as reported in the literature have been performed using a single-cell representation of the containment. The CONTEMPT code has been utilized for many of these analyses, and therefore, the reported results for these single-cell calculations also include the effects of specific limitations of the CONTEMPT code models as well as the user's judgement in selecting various input parameters. Some of the modeling and user imposed uncertainties common to past CVTR analyses include: (1) the use of the Uchida correlation for determining condensation heat transfer; (2) the presence of an air gap resistance for the containment shell; (3) the role of condensate film resistance and advection; (4) the role of thermal radiation; and (5) the presence of a paint resistance on structural surfaces. In addition to these heat and mass transfer modeling limitations, there are other uncertainties involving the specification of heat sink areas, such as the miscellaneous steel and internal concrete wall areas[Sch70]. Some of these uncertainties are investigated in this section using a single cell model of the CVTR facility. Additionally, the 15-cell CVTR reference deck is scrutinized in more detail in this section with respect to possible causes of the discrepancies between predictions and experiment, regarding the pressure and local temperatures. The multi-cell representation of the CVTR facility, of course, addresses another limitation of previous single cell calculations; that is, the inability to treat the significant stratification that develops in the test facility with an elevated steam injection. This scrutiny has resulted in a third set of results based on a refinement of the 15-cell deck, namely, a 19-cell CVTR deck, that is more suited to treating the motion of the steam stratification boundary in the lower containment of CVTR. This stratification boundary initially forms just below operating deck but then is pushed into the lower containment as a result of pressurization effects during the blowdown.

Experiment and user uncertainties investigated with a single cell model.

A pressure comparison for the 15-cell and single cell calculation of CVTR test #3 is shown in Figure 4.56. The single cell calculation uses the same input as the reference 15-cell calculation except for the consolidation of 15 cells into one. The temperature comparisons are given in Figure 4.57. The pressure predictions from the single-cell calculation tend to follow closely the multi-cell prediction during the blowdown period and are only slightly higher. However, during the relaxation period when heat transfer to structures dominates the pressure response, the single cell calculation under predicts both the measured pressure and the calculated pressure with the multi-cell model. During the blowdown, the "average" temperature predicted with the single cell model is shown to be similar to the measured temperature in the upper containment. Comparing the single with the multi-cell temperature calculations (shown in Figure 3.68), the single cell temperature calculation is shown to predict a lower maximum temperature for the containment during the blowdown. During the post-blowdown period, when heat transfer becomes more important, the single cell calculation under predicts both the measured and the multi-cell predicted maximum temperature in the containment (upper containment region).

Although we have noted differences between single and multi-cell results, the single cell model is useful for addressing many limitations and input uncertainties noted in previous CONTEMPT code applications. For this reason, a single cell sensitivity study is summarized in Table 4.16. In this study the single cell input for generating the results in Figures 4.56 and 4.57 is modified slightly to better simulate typical single cell CVTR computations. Those modification are minor but are noted to be 1) reduce the film thickness from 0.0001 to 0.00005 meters, and 2) eliminate the paint resistance on structures. The effect of these changes, the most significant being the elimination of paint resistance, is to decrease the maximum pressure from 2.67 to 2.63 bars, and to decrease the maximum temperature from 394 to 392 degrees Kelvin; see case 1s in Table 4.16. The reduced film thickness reflects on the more typical simulations that utilize the Uchida correlation for condensation heat transfer. (Condensation measurements on which the Uchida correlation are based were obtained using a small-scale test cell where the condensate film thicknesses would be significantly smaller than in the large-scale containment facilities.) Paint resistance modeling is an item typically not addressed in most reported single cell calculations; therefore, we deal with the sensitivity of results to this item at the beginning of the study.

The single-cell sensitivity calculations are interesting in that they indicate how sensitive the pressure prediction is to the estimated amount of miscellaneous steel (i.e., an increase of 50% steel inventory to account for upper bound uncertainty) in the containment and the method chosen for modeling steel structures, and how sensitive temperature predictions are to the injected steam enthalpy. For each case, pressure and temperature entries are given for calculations performed with and without thermal radiation modeled. Thermal radiation between the containment atmosphere and the structural surfaces is not modeled in the CONTEMPT code. Case 2s represents a containment input model that is similar to the CONTEMPT model used by authors of other articles on CVTR DBA analyses [Car81, Kro78]. In particular, the peak pressure and temperature predicted for case 2s, without thermal radiation, are nearly identical to the results reported in Reference Car81 for the CONTEMPT run (#5) that used the Uchida correlation with a condensation efficiency of 0.92 (Table 4 of Car81 gives pressure maximum = 2.86 bar and temperature maximum = 418 K). Therefore, case 2s agrees very well with a CONTEMPT calculation of CVTR test #3 with those parameters.

Case 3s, in which the air gap between the containment steel shell and the adjoining concrete has been implemented, shows that this gap is not very important for estimating peak pressures. There is of course much uncertainty with regard to gap modeling since the actual gap thickness itself is a very uncertain number.

Case 4s demonstrates that the use of the upper bound estimate of concrete surface area for CVTR does not affect the predicted peak pressure. The difference in concrete area between the reference calculation and case 4s is approximately 584 m^2, which is approximately a 30% increase in the total concrete area used for the reference calculation.

Cases 5s and 6s are interesting cases since they show how sensitive the predicted gas temperature

is to the injected steam enthalpy. The peak temperatures calculated in cases 1s and 2s indicate a fair amount of superheat -- approximately 20 and 30 K. The amount of energy in the atmosphere corresponding to this amount of superheating is relatively small compared to the total atmospheric energy (including latent heat); therefore, slight variations in steam enthalpy could have a significant affect on atmospheric temperature, at least until the saturation temperature is reached. For the single cell calculation, case 1s, the injected steam specific enthalpy is 2779.6 kJ/kg; the uncertainty range for specific enthalpy was given in the CVTR final report [Sch70] as 2791 - 2735 kJ/kg. Cases 5s and 6s use a steam specific enthalpy of 2700 kJ/kg, a 2.8% reduction from that used for case 1s. As shown in Table 4.16, the predicted maximum gas temperature is reduced substantially with this change in the injected steam enthalpy.

The CVTR structural steel, in Reference Sch70, is given in terms of the structural area and thickness (fixed volume). In the reference calculation, internal steel is modeled assuming that both sides of a structural member is exposed to the atmosphere, in which case an adiabatic boundary condition is applied to the half thickness and the structural area is doubled. This is one interpretation for such a specification. However, an alternative modeling approach would be to consider that only one surface is exposed, as in the case of a pipe structure, such that the actual specified area and thickness is used with an adiabatic boundary condition applied to the back surface of the structure. Case 7s shows the effect of this modeling approach on pressure and temperature. In this case, thicker steel slabs are used to describe the heat sinks and therefore the transient energy transfers from the atmosphere to steel are reduced somewhat and pressure and temperature increase slightly. As with case 2s, the maximum pressure and temperature calculated for this case also agrees fairly well with the results reported in Car81.

Table 4.16 Matrix of Single-Cell Calculations for CVTR Test #3			
Case #	Description	Max. Pressure, bar	Max. Temperature, K
----	Measured	2.27	389
1s	Single cell reference case*	2.63 (2.67)**	392 (402)**
2s	Case 1 with no misc. steel (used nominal steel inventory)	2.93 (2.98)	407 (416)
3s	Case 1 with containment shell air gap included (3/8 inch gap assumed)	2.66 (2.7)	394 (404)
4s	Case 1 with maximum concrete area	2.58 (2.63)	389 (399)
5s	Case 1 with steam enthalpy reduced by 2.8%	2.55 (2.55)	380 (380)
6s	Case 2 with steam enthalpy reduced by 2.8%	2.8 (2.82)	385 (390)
7s	Case 1 with steel structure thickness doubled, mass remains the same	2.78 (2.83)	399 (409)

* The input for this case is the 15-cell reference input reduced to a single cell with the following modifications: 1) film thickness is reduced from 0.0001 to 0.00005 meters, and the paint heat transfer coefficient is increased from the default 2000 to100000 W/m^2-K.

** ( ) denotes cases calculated without modeling thermal radiation from atmosphere to structures

Experiment and modeling uncertainties investigated with the 15 cell model.

The second set of results discussed in this section involve the sensitivity calculations that were made with the 15-cell CONTAIN input deck. The cases studied and the results of these sensitivity calculations are summarized in Table 4.17. The reference case presented in Section 3 shows that 15-cell model reproduces the temperature stratification profile with good accuracy shortly after the initial injection period (for times > 170 seconds), when the containment atmosphere becomes saturated. During the injection period, however, the reference calculation shows substantial superheating so that all the local temperatures are over predicted. When local saturation temperatures for the reference case were evaluated and compared to the measured temperatures during the blowdown, they were observed to be in good agreement with the measurements. This agreement plus other indicators such as the continuity in the temperature derivatives with time following the injection and the small measured temperature differences between the atmosphere and wall surfaces; all suggest that the local temperatures measured in the test were close to saturation. The single-cell sensitivity cases discussed above indicate that the over prediction of temperatures is the result of a small over prediction in atmosphere energy during and shortly after the blowdown period. Since the long term conditions are predicted fairly well, the 15-cell sensitivity cases focus only on the relatively small adjustments that could account for the over predicted atmosphere energy during and just after the blowdown.

In the reference case shown in Figure 3.68, the maximum calculated temperature corresponds to about 25 K of superheat, with the saturation temperature being approximately equal to the maximum measured temperature of 389 K. Likewise, in the lower regions of the containment the calculated maximum local temperatures in this region correspond to approximately 30 K of superheat. The existence of such superheated conditions is clearly not supported by the data. The reasons for this superheat are not necessarily the same in the upper and lower containment. With respect to the upper containment, the injected steam must enter relatively cold piping in the containment and flow through a 10-foot stand-pipe diffuser before being released into the containment atmosphere; some amount of heat loss to the containment delivery piping must be assumed, and this heat transfer would result in some reduction in the steam enthalpy. It is doubtful that such effects are reflected in the enthalpy uncertainties presented in the CVTR final report [Sch70]. In addition, the reference case uses an injected steam specific enthalpy of 2779.6 kJ/kg, which is on the high end of the uncertainty band for the measured enthalpy. Case 2m in Table 4.17 shows that the maximum predicted temperature is very sensitive to this injection enthalpy and that taking an injected steam specific enthalpy value near the lower end of the enthalpy uncertainty band substantially improves the agreement of the predicted maximum temperature with the data. Further, case 3m shows that modeling of liquid water in the atmosphere without dropout or aerosols has essentially no impact on the total energy balance or calculated local temperatures.

Even with a reduction in the injected steam enthalpy, problems with the predictions were still apparent. First, although not shown explicitly here, the lower containment region was still found to be superheated, and the heat transfer measurements in the upper containment indicated that the wall heat transfer was being under predicted. To address these concerns, two additional sensitivities were investigated. First, it was hypothesized that drain down (liquid water carryover) into the lower containment may affect the lower containment superheat, as drain down water comes into direct contact with the atmosphere. Second, in the upper containment, where high jet velocities were measured[4], forced convection along the containment wall was assumed to enhance convection heat and mass transfer, substantially increasing transfers above the levels invoked by the default modeling in the reference deck. The liquid water carryover hypothesis was also suggested previously as a possible reason for the discrepancies between the predicted and measured temperatures in the lower containment for ISP23 and ISP29.

Cases 4m through 8m were run to investigate these modeling hypotheses. To model the effect of liquid water carryover on lower containment thermal hydraulics, an engineered-system spray model was added to the lower containment cells using the condensation pool in the bottom containment as the water source. The enhanced heat and mass transfer due to forced convection was simulated with a forced convective velocity input table for wall structures, using as a basis, the velocity measurements in the experiment. The results of cases 4m - 8m in Table 4.17 indicate that the combination of water carryover, reduced steam enthalpy, and forced convective heat and mass transfer leads to a very good overall prediction of the containment pressure and local temperature stratification at the end of the blowdown when the maximums are recorded. As an example of the good agreement with measurements for both the injection and relaxation periods, the gas temperature profiles from case 4m are shown in Figure 4.58; in this case, the calculated temperatures, assuming liquid water carryover and reduced steam enthalpy, give much better agreement with measurements than the calculations shown in Figure 3.68.

[4] With respect to the upper containment heat transfer, the CVTR was instrumented with air velocity measurement devices near the location of the two wall heat transfer instrumentation plugs. The former devices were reported to have measured convective currents ranging from 4.5 to 9 m/s along the containment wall above the operating deck.

Table 4.17 Summary of Containment Loads Sensitivity Results for CVTR Test #3 *				
Case #	Description	Maximum Pressure, bar	Maximum Temperature, K	Max. Basement Temperature, K
----	Measured	2.27	389	325
15-cell:				
1m	Reference case	2.52	415	355
2m	Steam enthalpy reduced by 2.8%	2.47	390	347
3m	Case 2m with no dropout	2.47	390	347
4m	Case 2m with sprays in cells 1 -4 (with a 2.5 kg/s spray flow rate in each cell)	2.45	390	325
5m	Case 4m with forced convection above deck, 4 m/s	2.34	388	322
6m	Case 4m with forced convection velocity doubled for cell 12	2.34	388	322
7m	Case 5m with reference case steam enthalpy	2.43	410	322
8m	Case 5m with reference case steam enthalpy; velocity above deck = 8 m/s	2.35	406	323
19-cell:				
9m	Similar to Case 1m (reference case)	2.54	413	346
10m	Case 9m with forced convection	2.36	401	343

* includes atmospheric thermal radiation

Nodalization and HMTA modeling of forced convection uncertainties.

The third set of results discussed in this section involves a refinement of the 15-cell model. Close inspection of the 15-cell calculations showed that the stratification behavior in the lower containment was not being adequately modeled. The expected behavior is the simple downward motion, from pressurization effects, of the steam stratification interface separating the steam-rich and steam-poor regions of the containment. It is well known that the accurate rendition of one-dimensional advection of a sharp stratification interface through a stationary mesh, without substantial numerical diffusion, requires extremely fine nodes. The three nodes used in the vertical direction in the lower containment in the 15-cell model, while consistent with the nodalization of other CONTAIN decks created for the study of stratification effects, were not adequate to capture the motion of the stratification interface when large pressurization effects and therefore substantial motion of the interface is present. Another problem appeared to be the generation of substantial horizontal temperature gradients in the lower containment, beyond what one would expect on the basis of the distribution of heat sinks. The latter appeared to be the result of a heat-transfer-coupled flow instability that created highly non-uniform (tortuous-path) downward flow distributions in the lower containment in response to the pressurizing effect of the blowdown in the upper containment.

The 19-cell model shown in Figure 4.59 was created to minimize these problems. Four new cells (16, 17, 18, and 19) were introduced into the lower containment with the intent of reducing the numerical diffusion discussed above. In addition, to reduce horizontal temperature and concentration gradients, the gas flow paths between cells 3 and 4; 5 and 6; 16 and 17; and 18 and 19 were split into an upper and a lower path to promote countercurrent flow of gas within a node layer (such flow is a natural consequence of horizontal buoyancy gradients). Heat sinks in the old cells 3 through 6 were in addition split between the old and new cells. These changes appear to have adequately addressed the problems discussed above with the 15-cell model.

Only two cases were run with the 19-cell model: the equivalent of the 15-cell reference case, and a forced convection sensitivity case. The forced convection case was set up to simulate the wash of the jets from the diffuser against the containment shell, using the default forced convection model, but with appropriate values for cell hydraulic areas. To accomplish this, the blowdown steam was injected equally into cells 7 and 9, and constant (outward) volumetric flow boundary conditions were imposed during the blowdown at the junctions between cells 7 and 8; 7 and 10; 9 and 10; and 9 and 12. (The second and last junctions were introduced specifically for this purpose.) The volumetric flow rates were adjusted to match the forced convection enhancement in heat transfer over the natural convection values, observed in the heat plugs located in cell 8 and cell 12. The enhancement was taken to be a factor of 2 in cell 8, a factor of 3 in cell 10, and a factor of 4 in cell 12. The enhancement in other cells is controlled by the velocity distributions set up in the upper containment by the imposed volumetric flow boundary conditions; the

velocities drop off rapidly with distance from the junctions at which these flow boundary conditions were applied. Note that at the midpoint of the blowdown (80 seconds) the average upward gas velocity at the junction between cells 10 and 12 was found to be 10 m/s.

The pressures in the 19-cell reference case and the forced convection case are compared with experiment in Figure 4.60. Figure 4.60 shows that forced convection modeling reduces the discrepancies in predicted and measured peak pressure by one-half, compared to the reference case. The gas temperatures for the 19-cell reference case are shown in Figure 4.61, and those for the forced convection case are shown in Figure 4.62. One can conclude from this figure that forced convection modeling can account for about one-third of the discrepancy in peak temperature in the reference case. (This is not obvious from Table 4.17, since the sensitivity to forced convection was examined in combination with other parameter changes.) Also, the peak temperatures in the lower containment are now in better agreement with experiment, compared to the 15-cell reference case shown in Figure 3.68. This reflects better control of numerical diffusion, as well as the improved ability in the 19-cell model to resolve temperatures with the finer nodalization. However, the predicted lower containment temperatures are still appreciably superheated. It appears that good agreement with the peak temperatures in the lower containment requires a mechanism such as drain-down, which has not been evaluated in the 19-cell calculations.

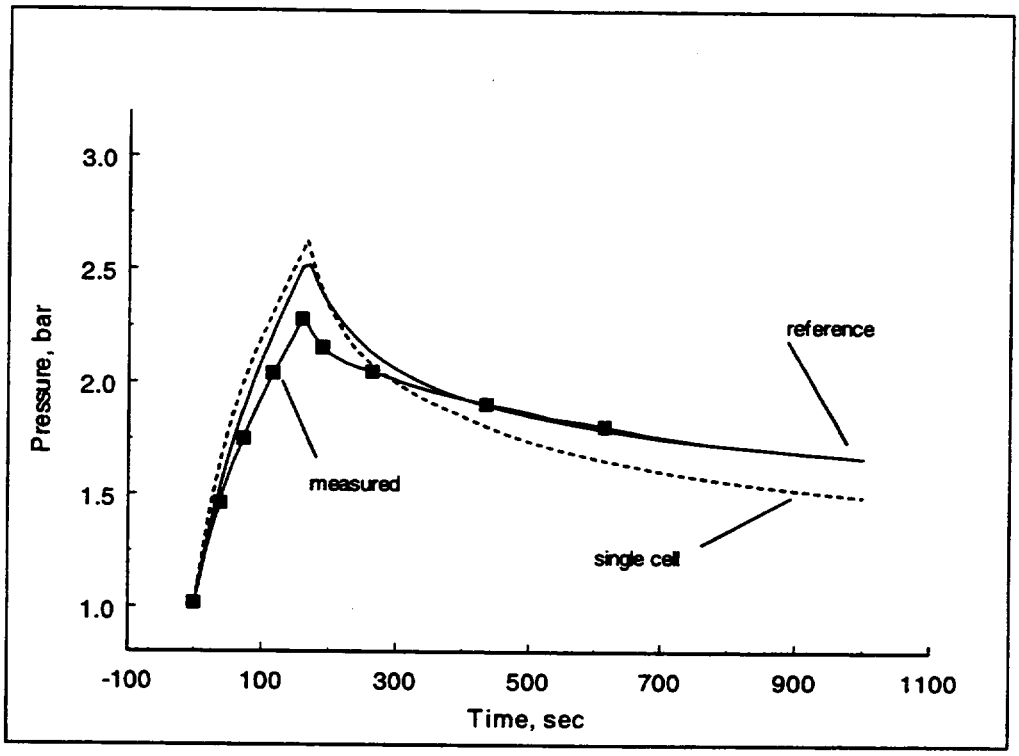

Figure 4.56 Comparison of measured and predicted pressure for the CVTR test #3.

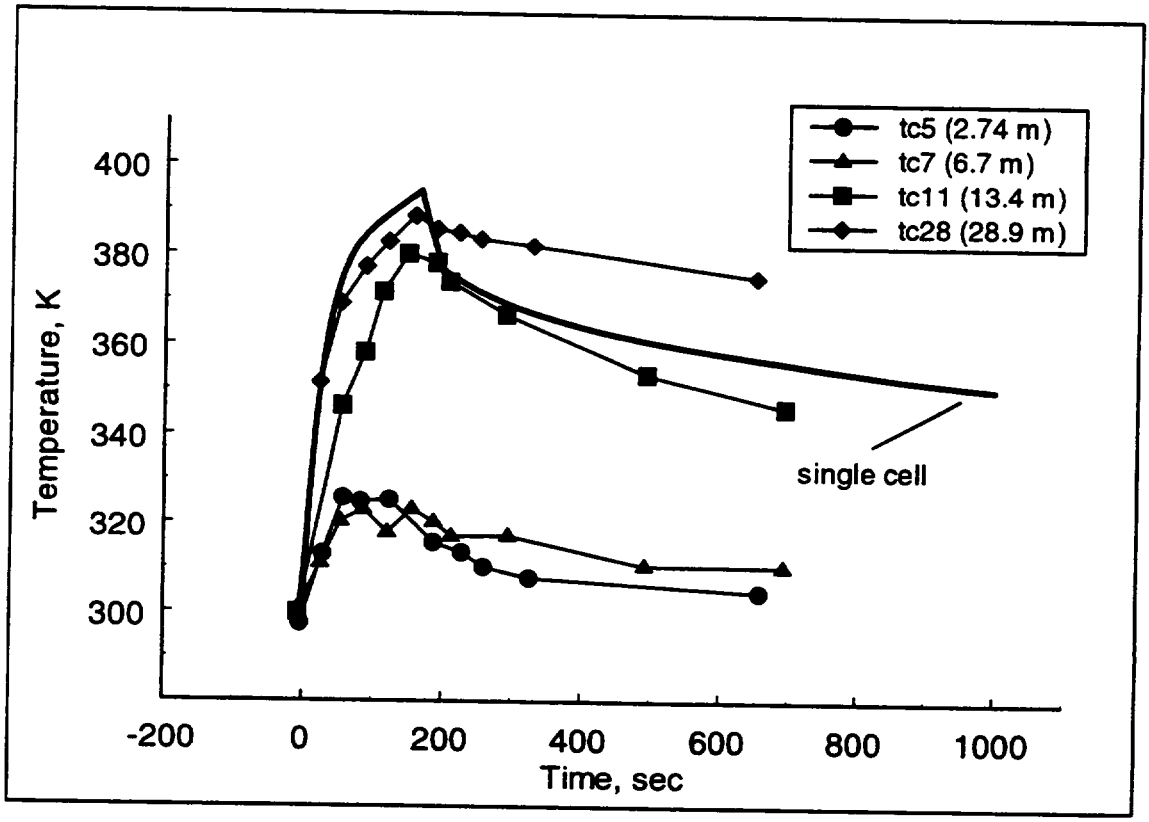

Figure 4.57 Comparison of measured and predicted gas temperatures for CVTR test #3.

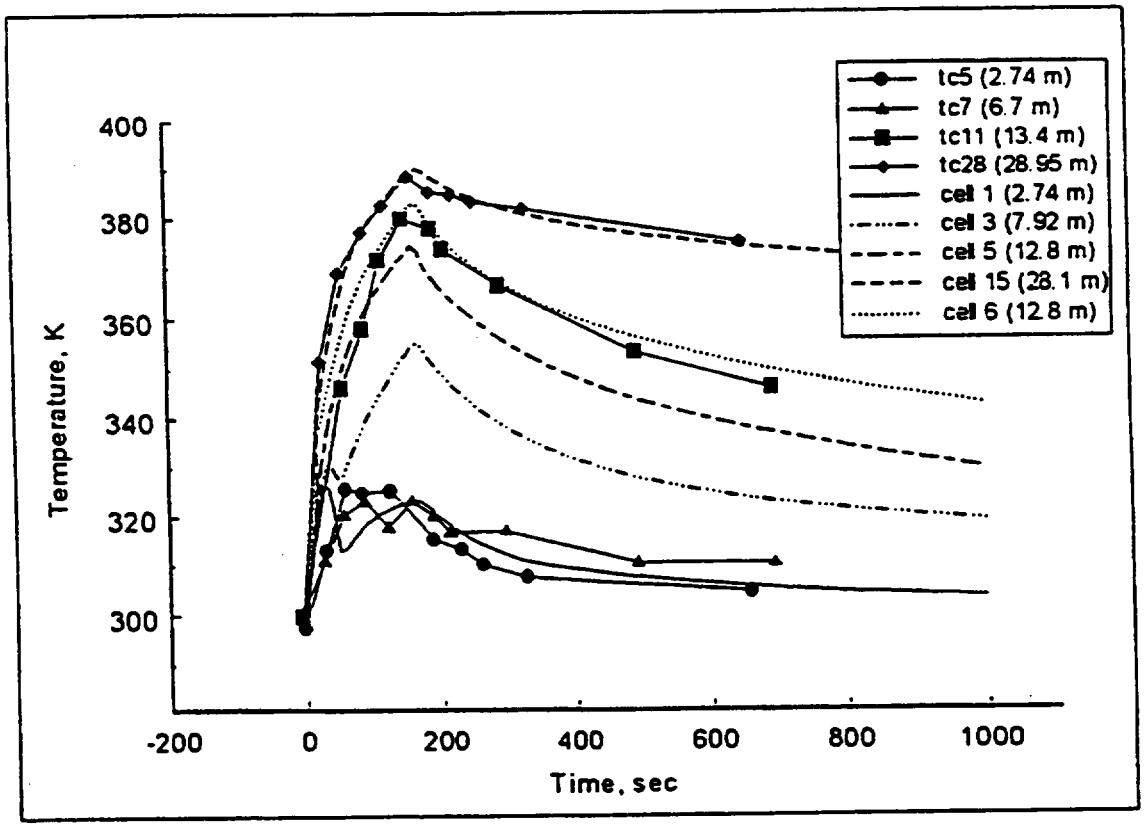

Figure 4.58 Comparison of measured and calculated temperatures in sensitivity case 4m for CVTR test #3. Calculated values are obtained using the 15-cell model of the CVTR facility.

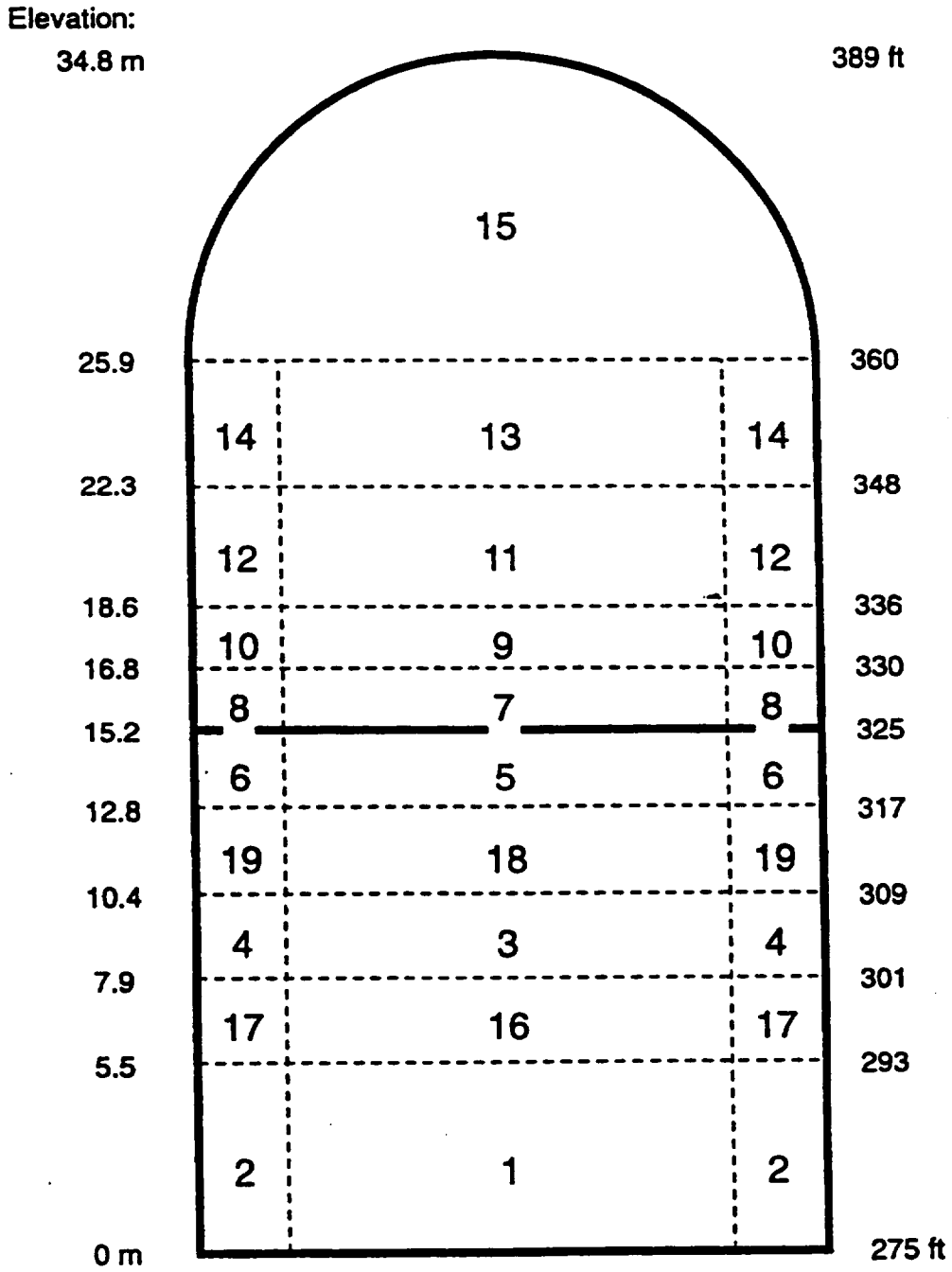

Figure 4.59 The 19-cell nodalization of CVTR.

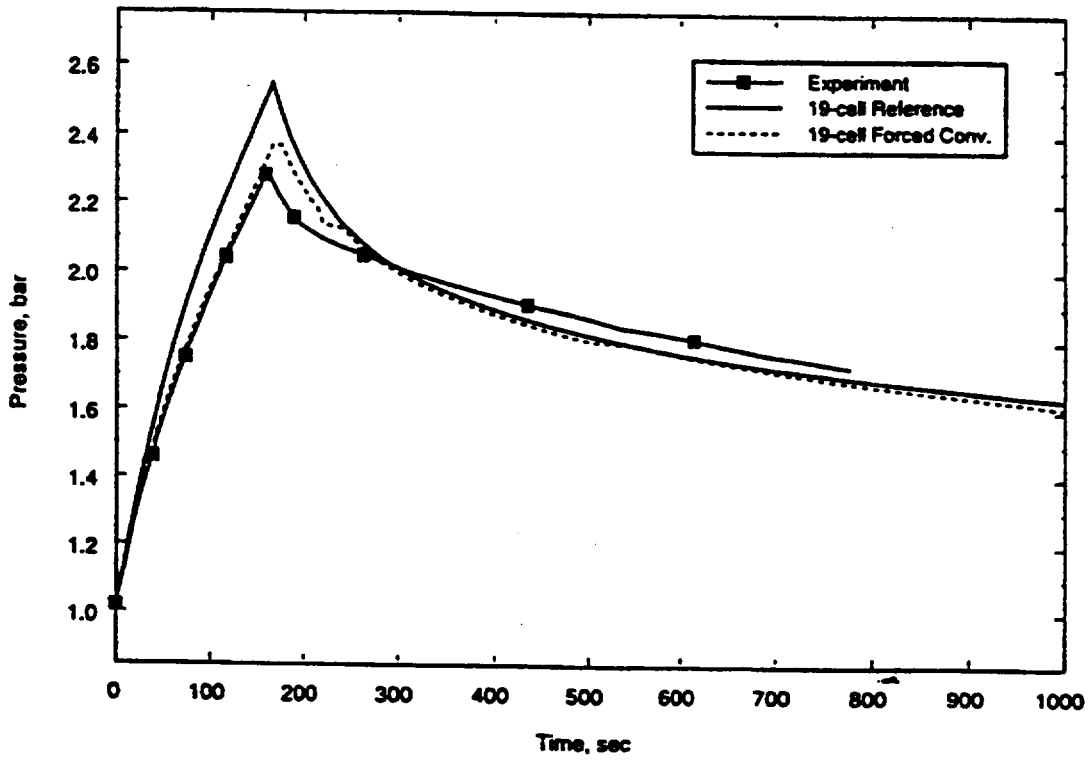

Figure 4.60 Comparison of measured and calculated pressures in the 19-cell reference case and the 19-cell forced convection case for CVTR test #3.

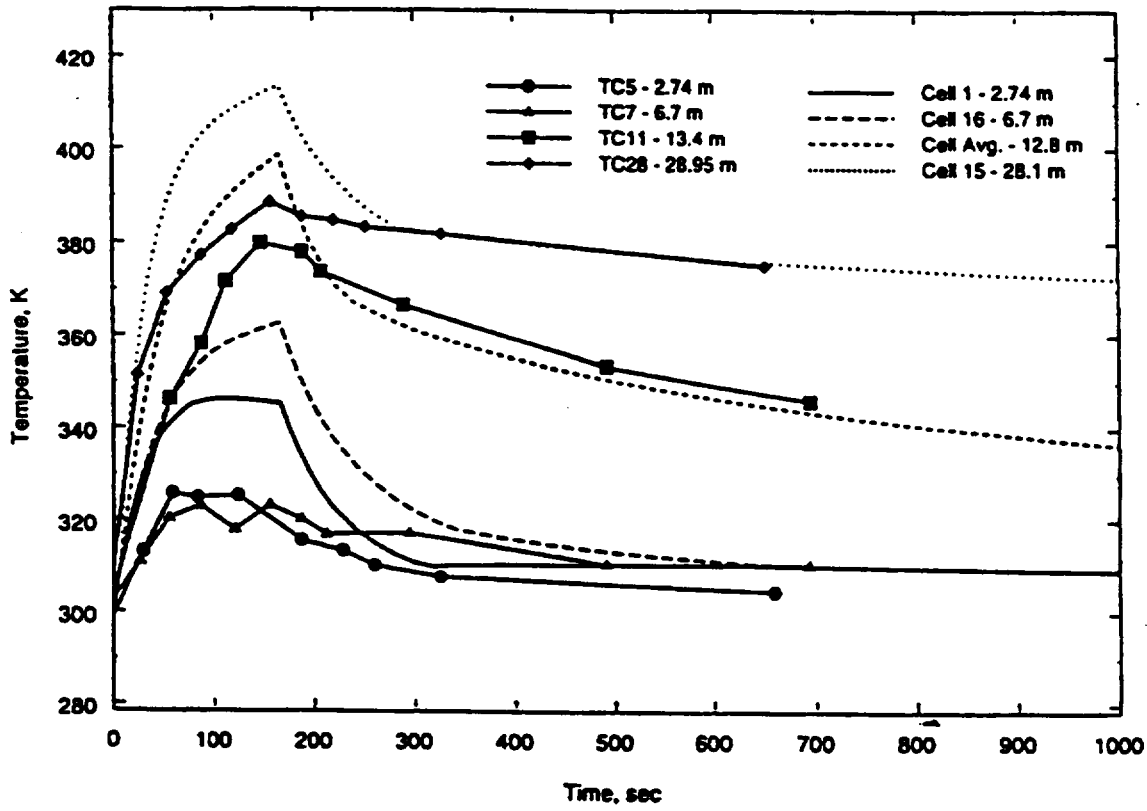

Figure 4.61 Comparison of measured and calculated gas temperatures in the CVTR 19-cell reference case.

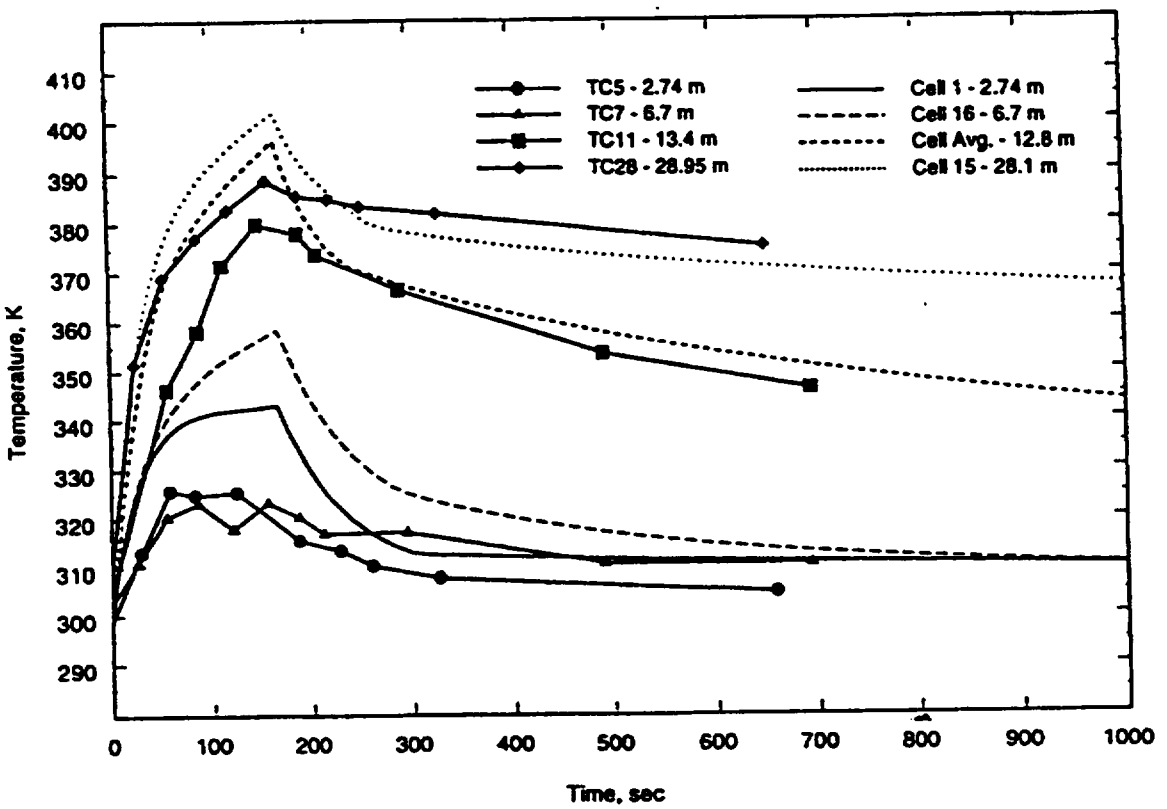

Figure 4.62 Comparison of measured and calculated gas temperatures in the CVTR 19-cell forced convection case.

4.2.3 NUPEC Tests

4.2.3.1 M-8-1 (mid-elevation injection, no sprays)

The M-8-1 experiment provides an example of a stable, fully developed stratification, for which, the hybrid flow solver limitations with respect to 1) neglect of momentum convection and 2) plume entrainment are minimized [Mur96]. In this subsection, thermal hydraulic results calculated with the hybrid flow solver (reference calculation for M-8-1) are compared with the "old solver" results obtained using the MSTABLE option in the code.

The pressures calculated with both the old and hybrid formulations are compared with the measured pressures in Figure 4.63. The calculated helium concentrations in the containment for the middle column of rooms (vertically in line with the steam generator tower) are compared with the measurements in Figures 4.64 and 4.65 for the old and hybrid flow solvers, respectively. The calculated and measured gas temperatures are similarly compared in Figures 4.66 and 4.67.

The effect of the flow solver on pressure calculations is seen to be small for this test, partially due to the short duration of the test and, with the lack of concrete structures, the inability to investigate long-term heat sink importance as a consequence of varying stratification predictions, and the compensating effect of over mixing on the total energy balance in the atmosphere. Nevertheless, these mixing effects are evident from a study of helium and local temperature comparisons presented in Figures 4.64 through 4.67. For example, in the case of the old solver, the under predicted helium concentration in the dome region (above the spring-line) and the over prediction in steam generator chimney are clear indicators of the over mixing induced by the old solver formulation. In contrast, the hybrid solver shows very good agreement with measurements. Predicted peak temperatures are slightly under predicted with the old solver.

Figures 4.68 and 4.69 show the vertical profile predicted by both formulations for helium and temperature at the end of the injection period. The calculations are presented in a step-wise manner because each cell is assumed to be well-mixed; measurements are shown as open symbols. Improvement is evident in both the containment helium concentration and temperature profiles with the hybrid solver. However, the most significant improvement is evident with the helium concentration, where we see that the old solver would under predict the peak concentration by about 30%, whereas the hybrid solver would under predict by only 5 %. Clearly, this improvement can be critical for postulated beyond design basis accidents when hydrogen is released inside containment.

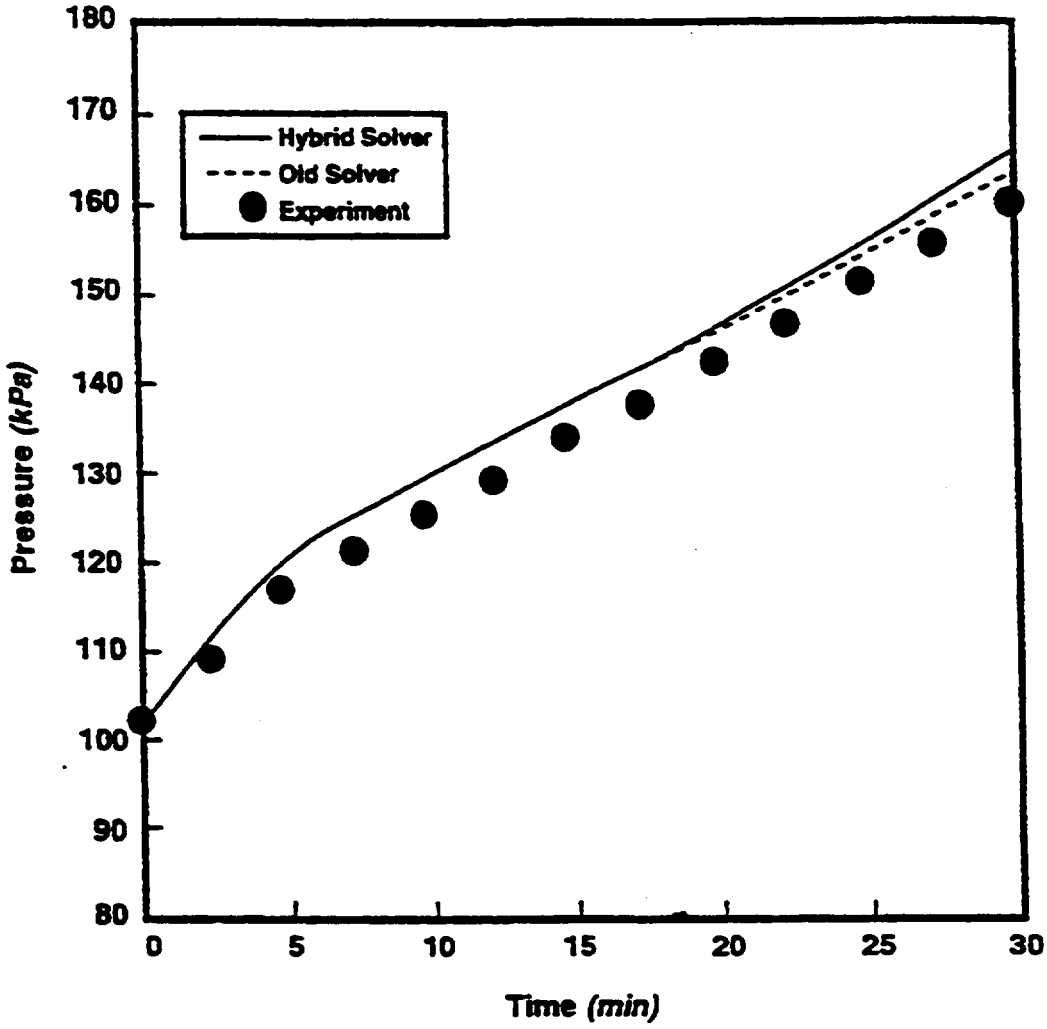

Figure 4.63 Comparison between the predicted pressures in the NUPEC facility for test M-8-1 and the experimental data[OECD94].

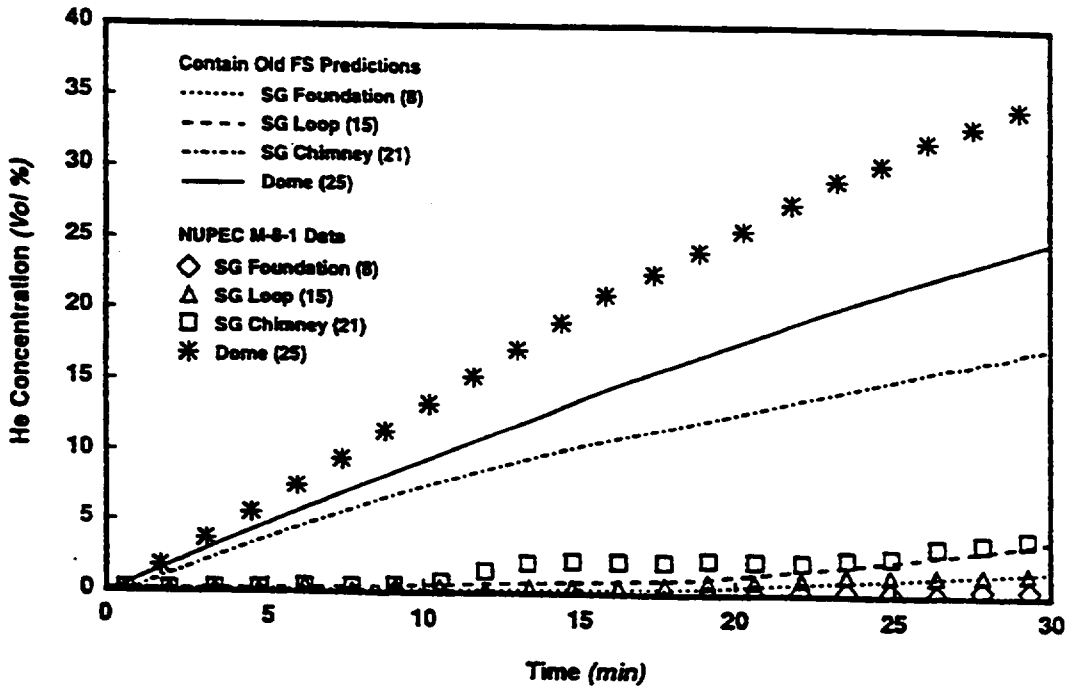

Figure 4.64 Comparison between the helium concentration predicted by the old gravitational head formulation in a middle column of rooms in the NUPEC facility and the experimental data for test M-8-1[OECD94].

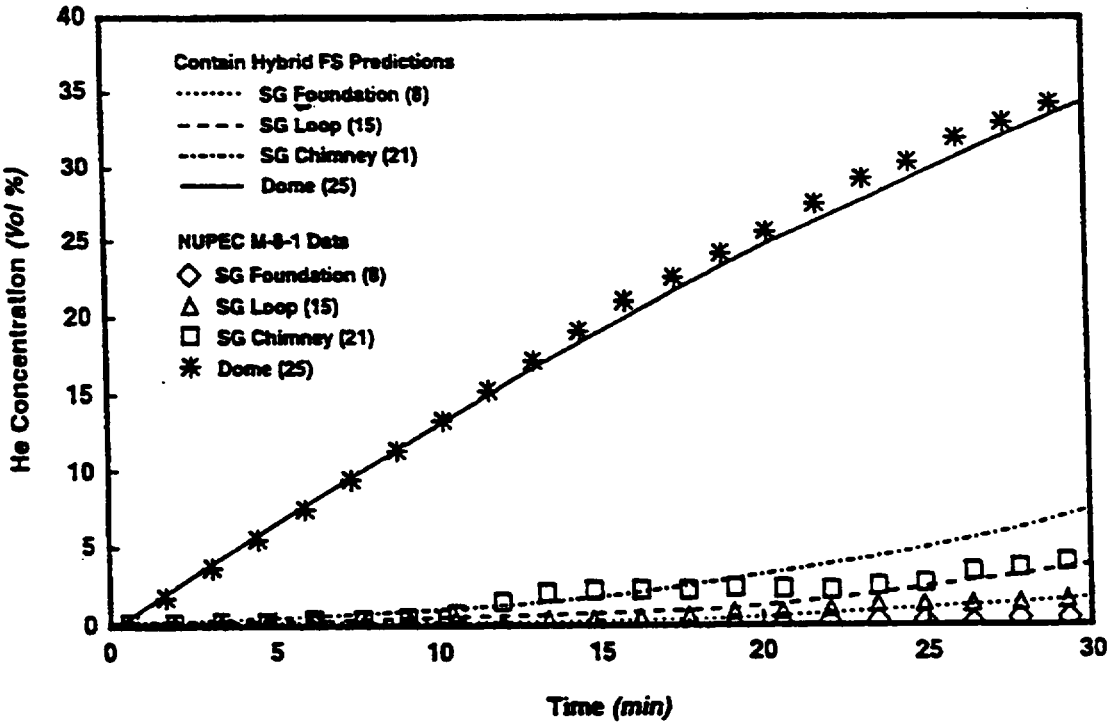

Figure 4.65 Comparison between the helium concentrations predicted by the hybrid gravitational formulation in a middle column of rooms in the NUPEC facility and the experimental data for test M-8-1[OECD94].

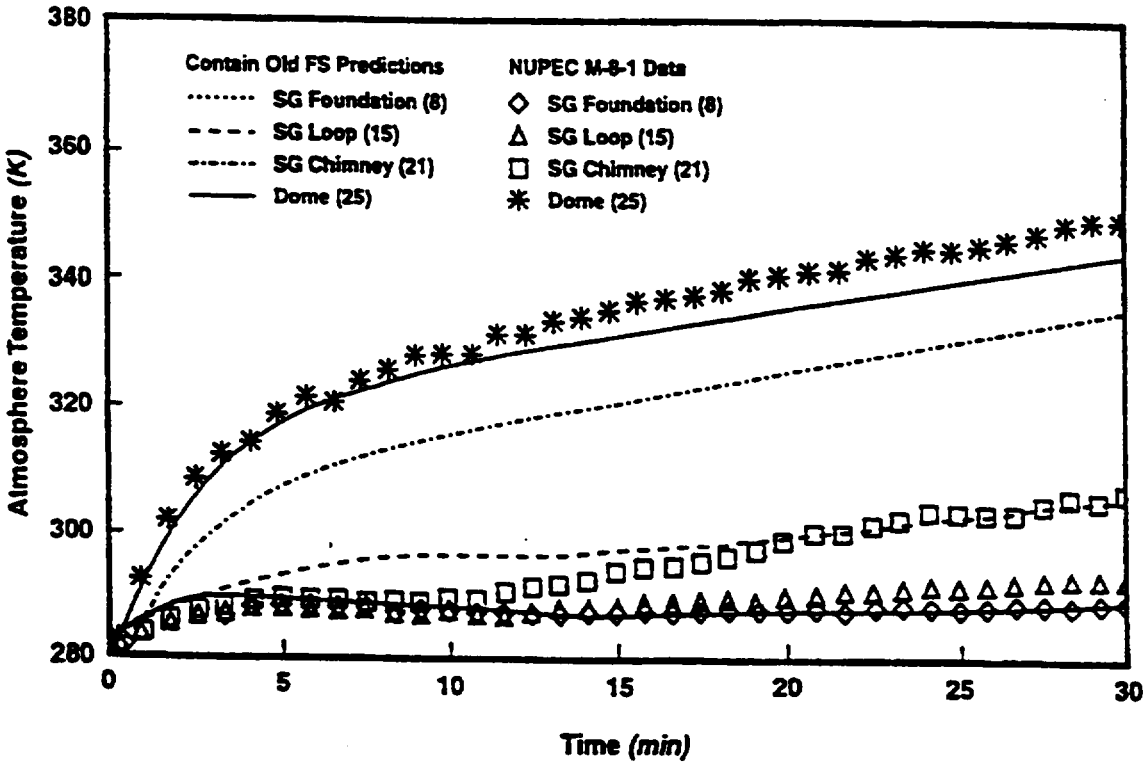

Figure 4.66 Comparison between the gas temperatures predicted by the old gravitational head formulation in a middle column of rooms in the NUPEC facility and the experimental data for test M-8-1[OECD94].

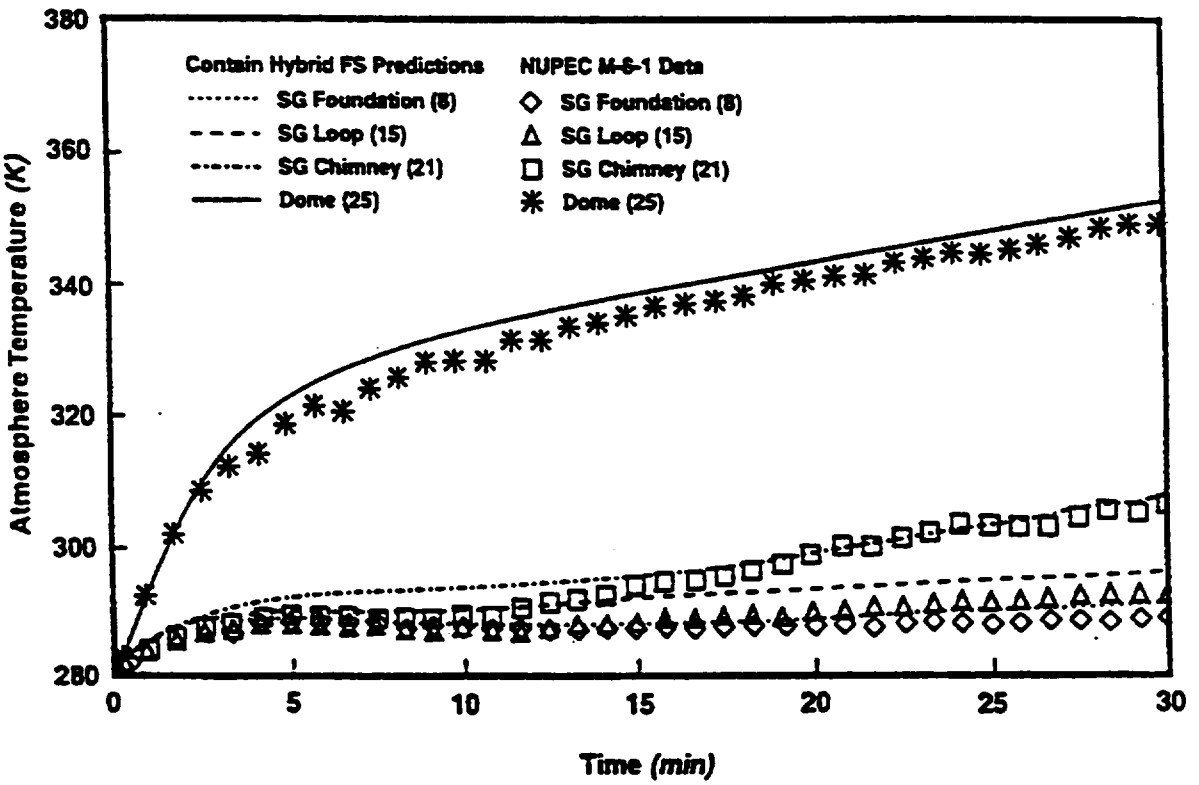

Figure 4.67 Comparison between the gas temperature predicted by the hybrid gravitational head formulation in a middle column of rooms in the NUPEC facility and the experimental data for test M-8-1[OECD94].

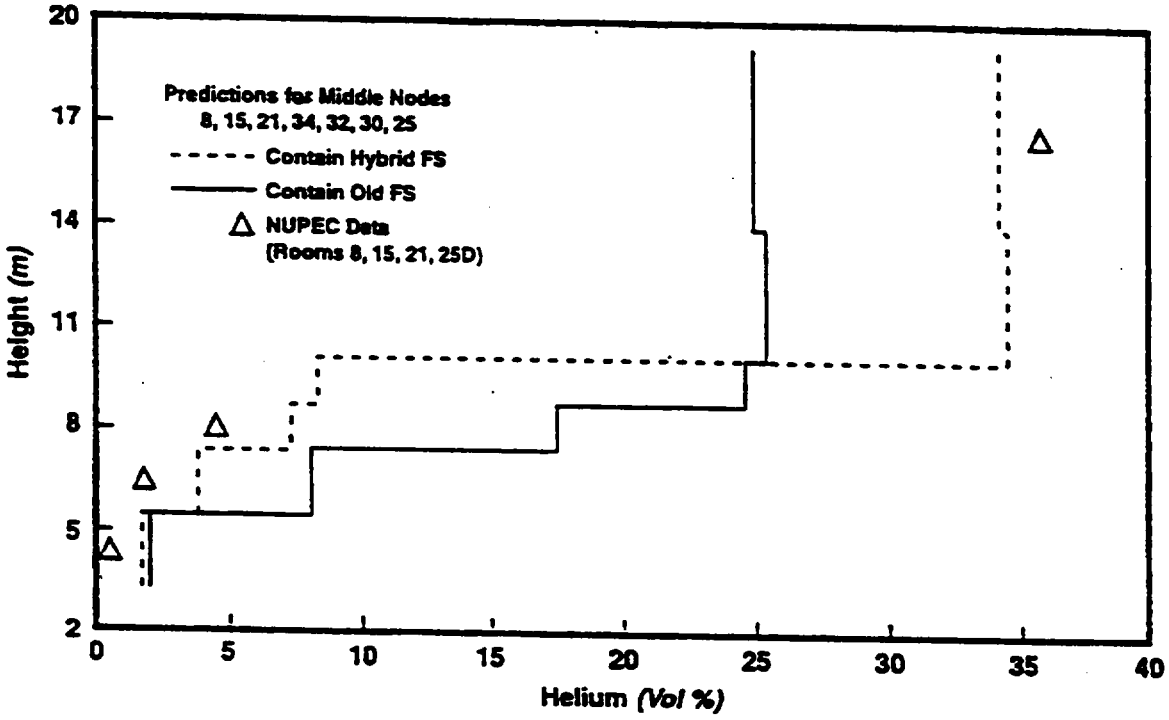

Figure 4.68 Comparison between the predicted helium distribution in a middle column of rooms in the NUPEC facility for test M-8-1 and the experimental data[OECD94].

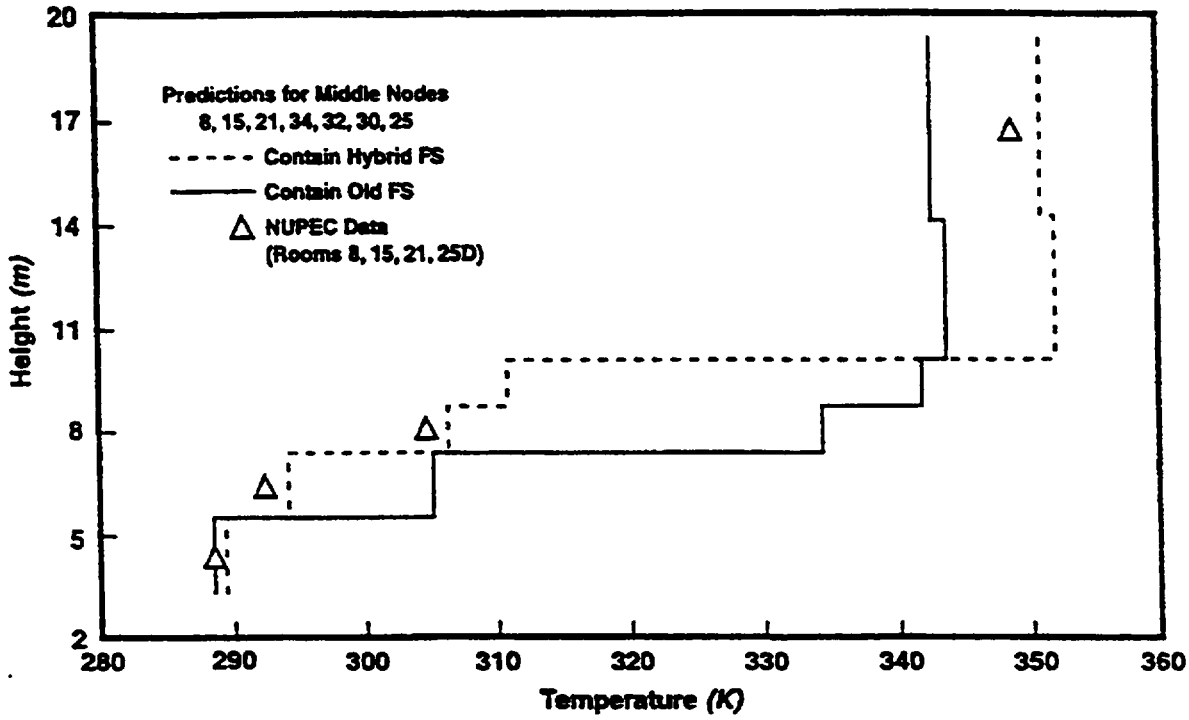

Figure 4.69 Comparison between the predicted gas temperature distribution in a middle column of rooms in the NUPEC facility for test M-8-1 and the experimental data[OECD94].

4.2.3.2 M-7-1 (mid-elevation injection, with sprays)

In the reference calculation, it was assumed that the interaction of sprays with the atmosphere create a vortex effect that induce air currents along the dome and cylinder walls. This effect was believed to produce a forced convective velocity of 14 m/s along the walls, as estimated by a simple power balance equation [Mar88]. As a result, the HMTA method was adjusted using the user supplied forced convective velocity for dome walls to simulate this effect in the reference calculation. Unfortunately, the few velocity sensors that were located in the containment were disabled by the wet conditions generated by the steam injection and spray activation. Consequently, there was no confirmation of the hypothesis that air currents of this magnitude existed in the dome region. Certainly, the environment in the containment during spray activation is quite turbulent in regions where the sprays are falling; there is substantial water carryover from cell-to-cell atmosphere as a result of droplet fall-through and entrainment, and from structure-to-structure transport by flowing water films. A number of sensitivity calculations are reported here to investigate the importance of some of the complexities in this environment with respect to atmospheric conditions and structural heat transfer. The sensitivities are intended to show improvements in the prediction of pressure, gas temperature, and wall temperatures for some conditions believed to be occurring in the facility both during and after the spray period. These sensitivities complement other case studies concerning atmospheric superheating in containment subcompartments during DBA-like conditions, as was previously noted in the CVTR sensitivity study. Shown in Table 4.18 are some of the sensitivities that have been carried out for the M-7-1 test. In each of the cases, the effects on hydrogen distribution is small, and therefore these comparisons will be omitted in deference to thermal hydraulic parameters.

Forced convective heat transfer modeling.

In the fall of 1993, Sandia submitted a blind calculation of M-7-1 as the official submittal for the ISP35 exercise [OECD94]. This submittal was based on a 28-cell nodalization of the NUPEC facility which was identical to the 35-cell nodalization of the reference calculation except that the dome was modeled with only one cell instead of the seven cells for the 35-cell nodalization. Additionally, the calculation had assumed no spray water impingement on walls or forced convection, and there was no spray water carryover into lower subcompartments. When the results of this submitted calculation and most other calculations by other participants in the ISP exercise were compared to measurements, it was noted that 1) the initial pressure reduction was overestimated, 2) late time pressures were over predicted, and 3) the dome and other internal wall temperatures were significantly over predicted. Later investigations comparing the 28 and 35 cell nodalization suggested that a refined nodalization scheme had very little to contribute to an improvement of these thermal hydraulic comparison; rather, through sensitivity studies it was found that spray water-structure interactions and forced convective flows have a significant effect on atmospheric thermal hydraulics and surface temperatures.

Shown in Figure 4.70 are the pressure comparisons for a case that represents the ISP35 blind

calculation (but using a 35-cell nodalization) which has no spray water impingement or forced convective heat transfer on the dome and internal wall structures. Figures 4.71 and 4.72 show temperature comparisons for the dome gas and dome wall, respectively. Clearly, the additional heat transfer from the forced convective process along the wall in the reference case significantly improves both pressure and temperature comparison to data. The improved results shown in the reference case, together with the analytical supporting evidence in Reference Mar88 concerning spray induced air currents, were important factors for selecting the reference case as a best-estimate calculation in two publications on the CONTAIN calculations of the NUPEC tests [OECD94, Sta95].

Spray water impingement.

Spray water impingement onto the dome wall (above the spring line) can not be excluded either by direct contact or as a result of entrainment and deposition from the turbulent air currents in the spray region. Shown in Figure 4.73 is the pressure comparisons for spray impingement where it is assumed that 15% of the injected spray water in the upper dome impinges directly on the dome walls; no forced convection on either the dome, cylinder or internal partition walls is assumed. The CONTAIN film flow tracking option is used to model the spray washdown effect. As was indicated in the JAERI multiple spray nozzle test, early pressure agreement is improved with a spray impingement effect. Figure 4.74 also indicates that the late time dome temperature response after the sprays are de-activated is also slightly improved with the assumption of impingement. The rapid temperature rise immediately following spray de-activation in the reference case represents a response of the atmosphere to energy transport from hot structures into the atmosphere (sensible heat) without the addition of evaporated water vapor; the result is that the hot walls produce a energy transfer condition that superheats the atmosphere. This post-spray effect, that is, sensible energy transfer to the gas following spray termination, was measured in a small region at the top of dome, well above the highest spray nozzle; the gas temperature location is denoted as RC025T in Figure 4.75. When the hot walls are cooled by a water film, energy transfer to the atmosphere is accompanied by vapor additions (through evaporation) which tend to keep the atmosphere near saturated, and subsequent depression in the rate of temperature increase. The effect of spray water impingement on atmospheric superheating can be seen in Figure 4.76, where the saturation ratios of the two CONTAIN calculations (cases 1 and 3) are plotted.

Unfortunately, the 15% spray impingement appears to also reduce the dome wall temperature too much, as seen in Figure 4.77. Therefore, another case has been considered where the spray impingement is reduced from 15 to 5% of the spray water injection. Figures 4.78 through 4.80 show the comparisons of cases 1 and 4, along with the measurement measured wall temperatures. Shown in Figure 4.81 are the locations of the dome wall measurements (tags 90-92). The 5% impingement case provides an improved early time pressure agreement with the measurements; dome gas temperature comparisons during the spray period are about the same; and most importantly, the dome wall temperature response is in agreement with the measurements. What

case 4 does not improve is the late time pressure comparisons, which now indicate a significant over estimation of the pressure. This is especially noticeable when the sprays are deactivated. One reason for this late time over estimated pressure response is that internal structures above the third floor (elevation 7325 mm, in Figure 4.81) have not been wetted by the sprays, and in addition, forced convection heat transfer along the vertical dome wall has been neglected. Figure 4.82 shows internal partitions in the facility, above the third floor (7325 mm).

Shown in Figures 4.83 through 4.85 are pressure and temperature comparisons for case 5 where the dome wall is assumed to have 5% spray water impingement, 10% spray water impingement on the internal wall structures above the third floor, and forced convection on the vertical dome walls (below the spring line) including the internal structures above the third floor. The internal partition structures are assumed to have a forced velocity of 3 m/s along surfaces, and for the dome and cylinder walls the velocity is assumed to be 14 m/s. The lower velocity profile for the internal partition structures reflects an understanding that obstructions will perturb and significantly reduce large loop air currents [Mar88]. One interesting response in this test that sheds some light on the question of spray water wetting of structures is the response of the atmosphere when the sprays are deactivated. In the reference case, all the structures are dry and hotter than the atmosphere when the sprays are deactivated. Hence, the calculated response of the atmosphere after deactivation is that it becomes superheated (approximately by 7 degrees). On the other hand, if the structures are wetted, structure energy is transferred to the atmosphere mainly by evaporation which keeps the atmosphere saturated. This method of energy transfer appears to be more consistent with the observed atmospheric response for both pressure and gas temperature.

Subcompartment modeling.

Below the third floor of the facility there are a number of subcompartments that are open to the spray region. If the sprays are not allowed to fall into these compartments the compartments will undergo significant superheating. For example, shown in Figure 4.86 are the gas temperature comparisons for the reference case with spray water fall-through into the cavity compartment (cell #19) and case 6 with no fall-through. The presence of spray water in the subcompartment keeps the atmosphere near saturation and closer to the measured temperatures. At the end of the spray period case 6 has a superheat of approximately 10 degrees. After the spray period, case 6 continues to show a substantial over prediction of temperature, but the reference case also shows a significant over prediction.

Although the reference case spray water falls into subcompartments with openings from the upper spray region, it does not assume washdown of the subcompartment walls by spray water entering the compartment, or washdown from the diversion of water from regions above. By assuming that the walls remain dry, and with no forced convective heat transfer, wall cooling is under estimated during the spray period, and when the sprays are deactivated, the sensible energy transfer from the walls to the compartment atmosphere causes an unrealistic superheating of the

atmosphere. Just as in case 5, we assume in case 7 a spray washdown of the compartment walls by 5% of the spray water entering the compartment; this case is shown in Figure 4.86. In another case, case 8, we add both spray washdown and a 3 m/s force convective velocity flow along the subcompartment walls. In still another case, case 9, we assume a 3 m/s convective velocity along the subcompartment walls, but no spray washdown. A review of the predicted gas temperatures in the subcompartment indicates that the case with both washdown and convective flow of 3 m/s gives a significant improvement between the predicted and measured subcompartment gas temperatures. When the subcompartment walls are dry yet have a convective flow assumed, the tendency to superheat the atmosphere remains both during the spray period and in the period following spray deactivation.

In Figure 4.87, the wall temperature measurement in SG C loop compartment (cell #14) that interfaces with the cavity subcompartment is compared to predictions from the reference calculation and case 8 above. It should be noted that there is spray fall-through into the loop compartment and there is a 5% spray washdown of the compartment walls. The plots in Figure 4.87 show that there is a significant improvement in the predicted wall temperature with a wall washdown effect.

Table 4.18 Sensitivity cases for CONTAIN calculations of NUPEC test M-7-1.	
Case #	Model description
1	Reference case : sprays are assumed to drive a large convection loop that concentrated the water drops into the center of the facility and enhanced wall-to-gas heat transfer (forced convection) for dome and cylinder walls
Dome region effects of washdown and forced convection:	
2	Uniform spray pattern is assumed in the region above the third floor level (7325 mm) with no spray impingement or forced convection
3	Spray pattern is based on flow in unconfined geometries with impingement of water sprays on the dome wall (15% spray water) – no forced convection
4	Case 2 with 5% spray water wetting the dome wall by direct impingement
5	Case 4 with 10% spray water wetting of internal partitions above third floor level (7325 mm) by direct impingement (that is, no interaction with the atmosphere)
Subcompartment effects of washdown and forced convection:	
6	Case 1, with no spray water fall through into the "cavity compartment", cell #19
7	Case 1, 5% washdown of vertical walls in SG compartment, C loop and cavity walls
8	Case 7, forced convective velocity of 3 m/s in the "cavity compartment"
9	Case 1, forced convective velocity of 3 m/s in "cavity compartment, no washdown of cavity walls

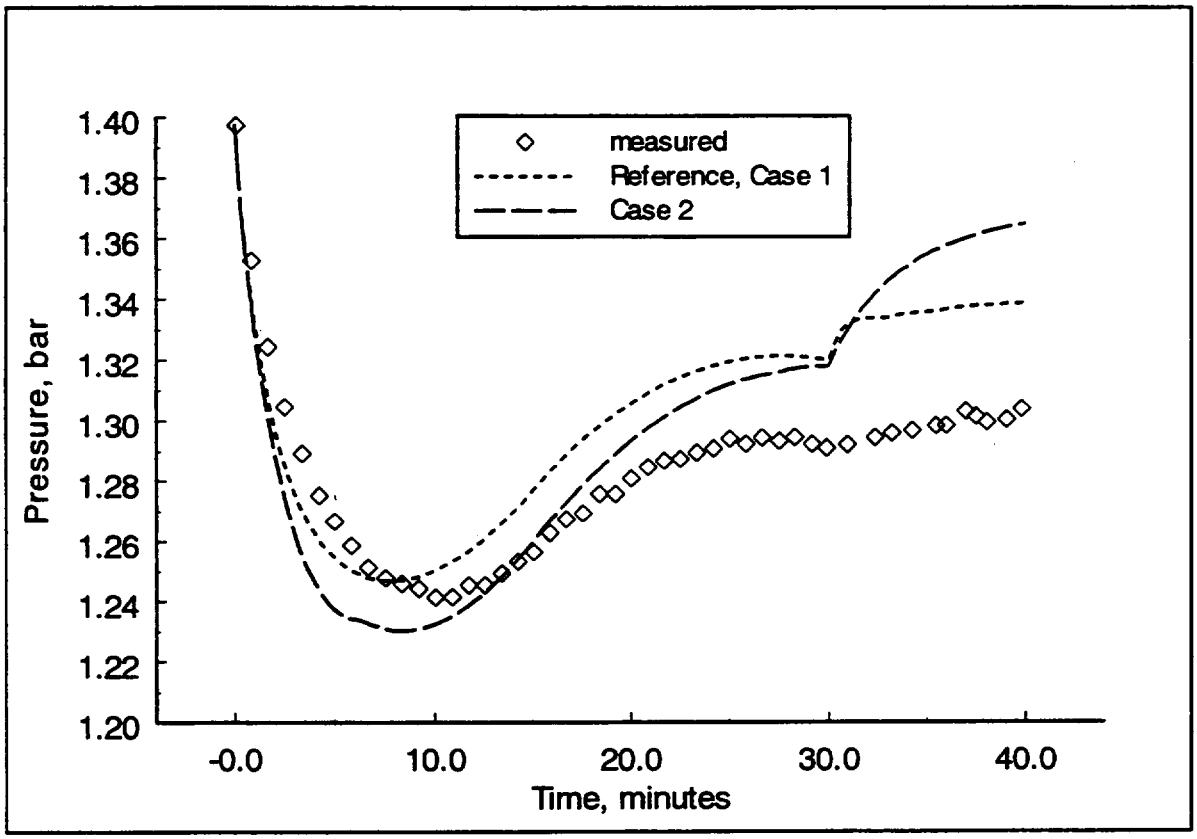

Figure 4.70 CONTAIN M-7-1 pressure comparisons for cases with (Case 1, 14 m/s) and without (Case 2) forced convective heat transfer on dome walls.

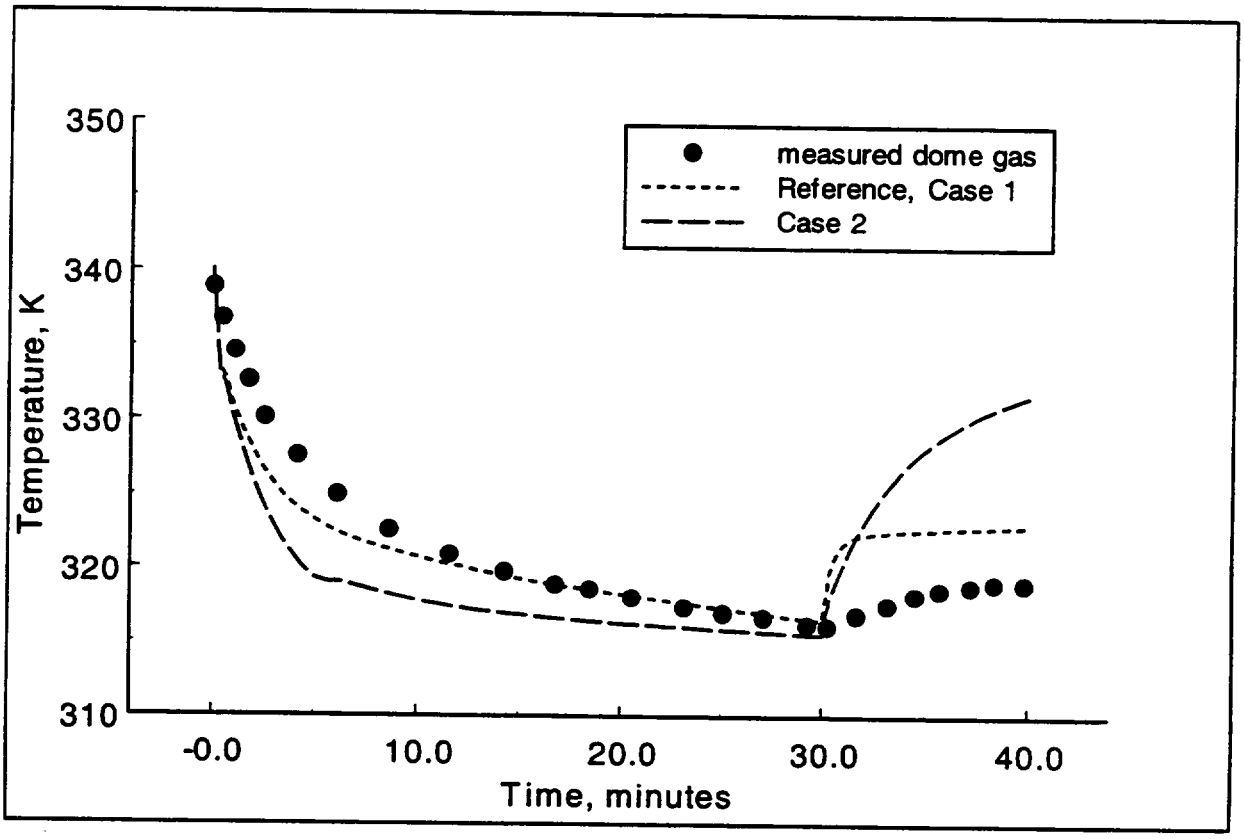

Figure 4.71 CONTAIN M-7-1 dome atmosphere temperature comparisons for cases with (Case 1, 14 m/s) and without (Case 2) forced convective heat transfer along dome walls.

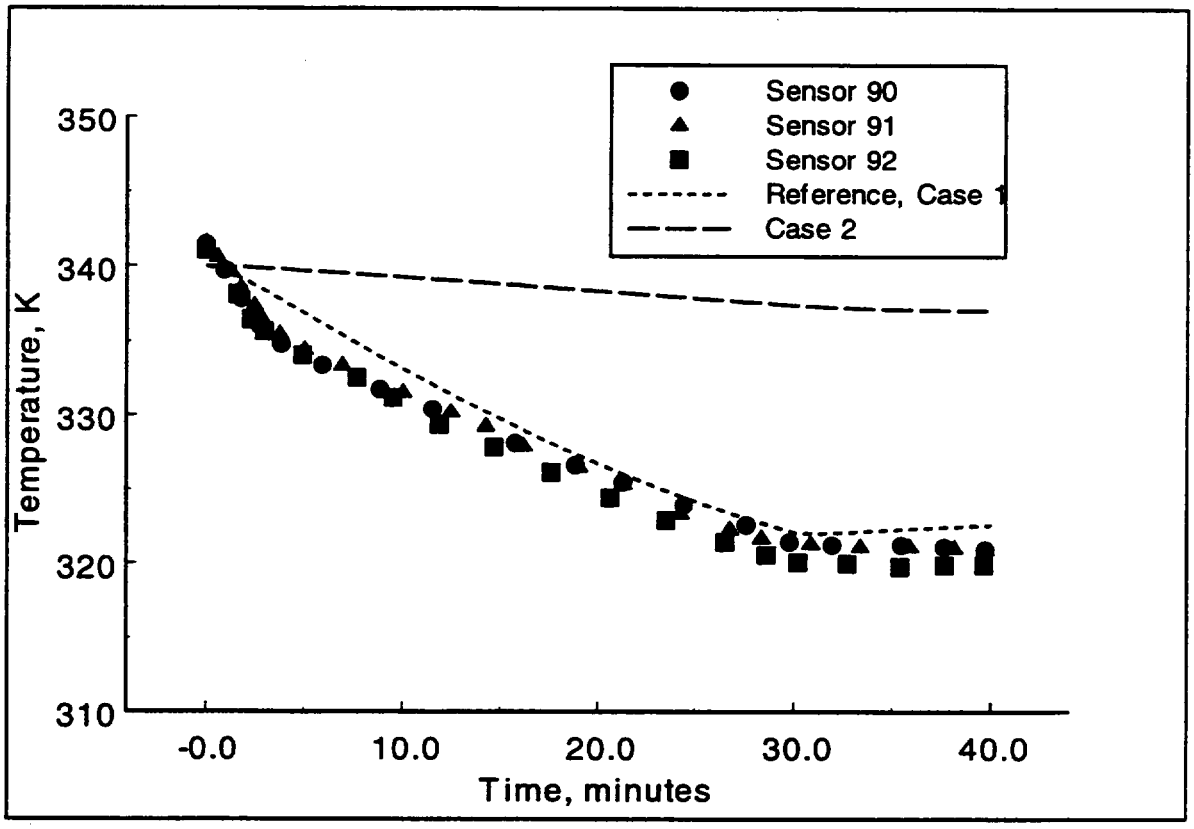

Figure 4.72 CONTAIN M-7-1 dome wall temperature comparisons for cases with (Case 1, 14 m/s) and without (Case 2) forced convective heat transfer along dome walls.

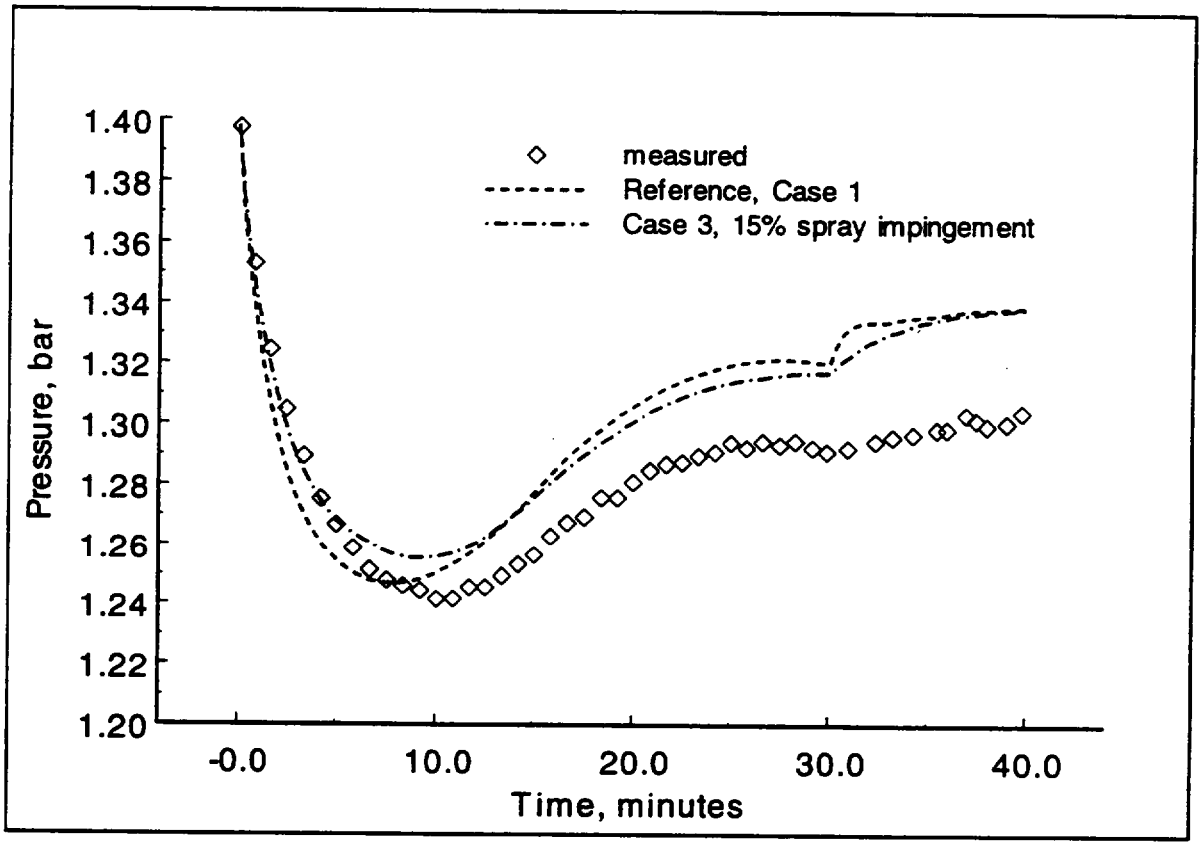

Figure 4.73 CONTAIN M-7-1 pressure comparisons for the reference case and a case with 15% spray water impingement on the facility dome walls.

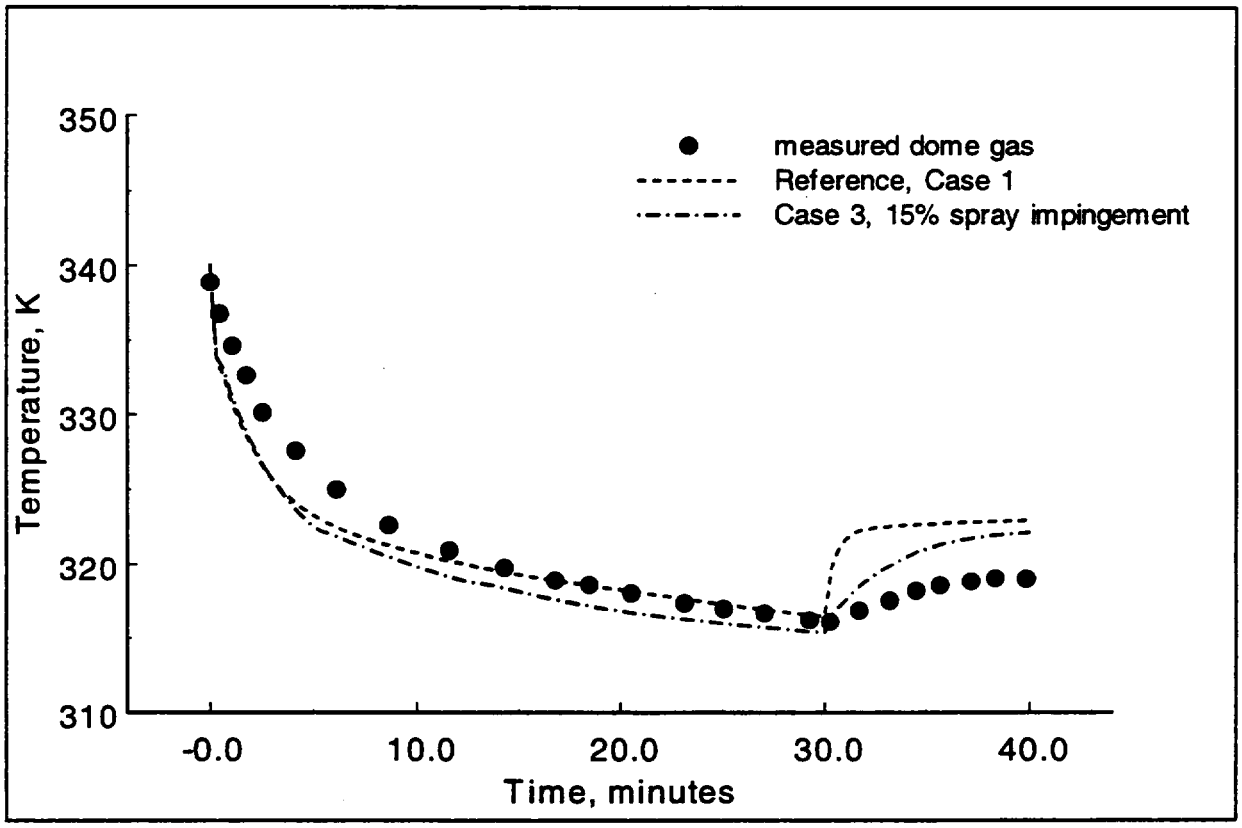

Figure 4.74 CONTAIN M-7-1 dome gas temperature comparisons for the reference case and a case with 15% spray water impingement on the facility dome walls.

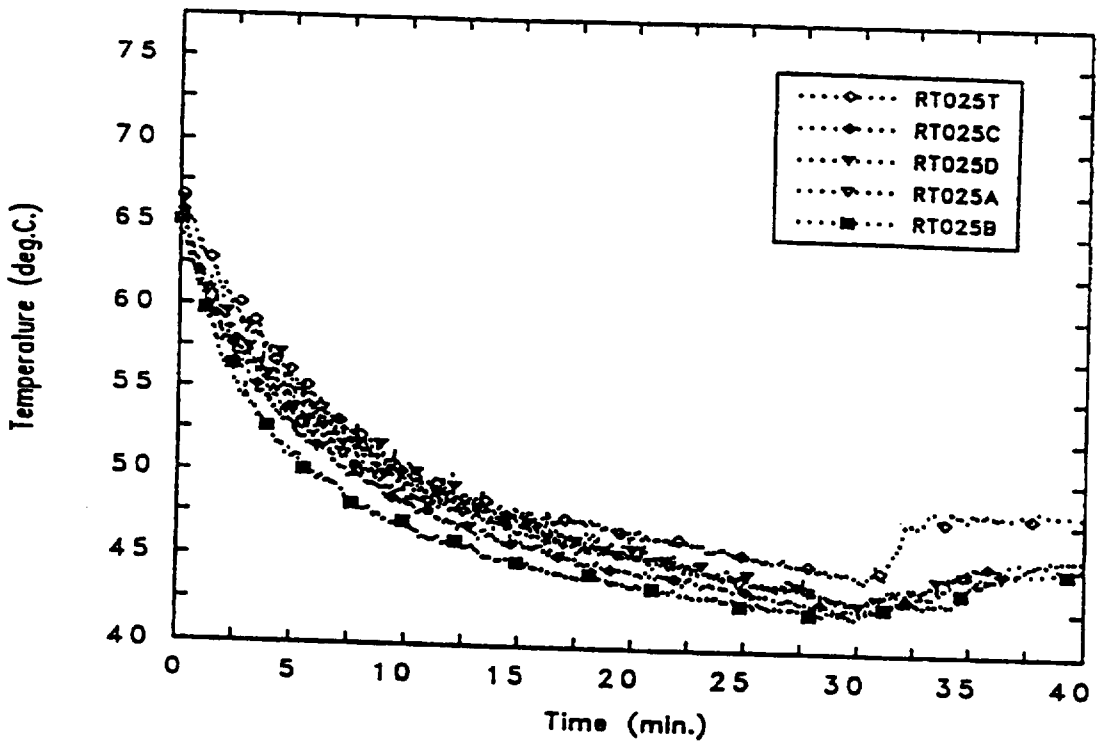

Figure 4.75 Dome compartment temperature measurements for NUPEC test M-7-1 [OECD94].

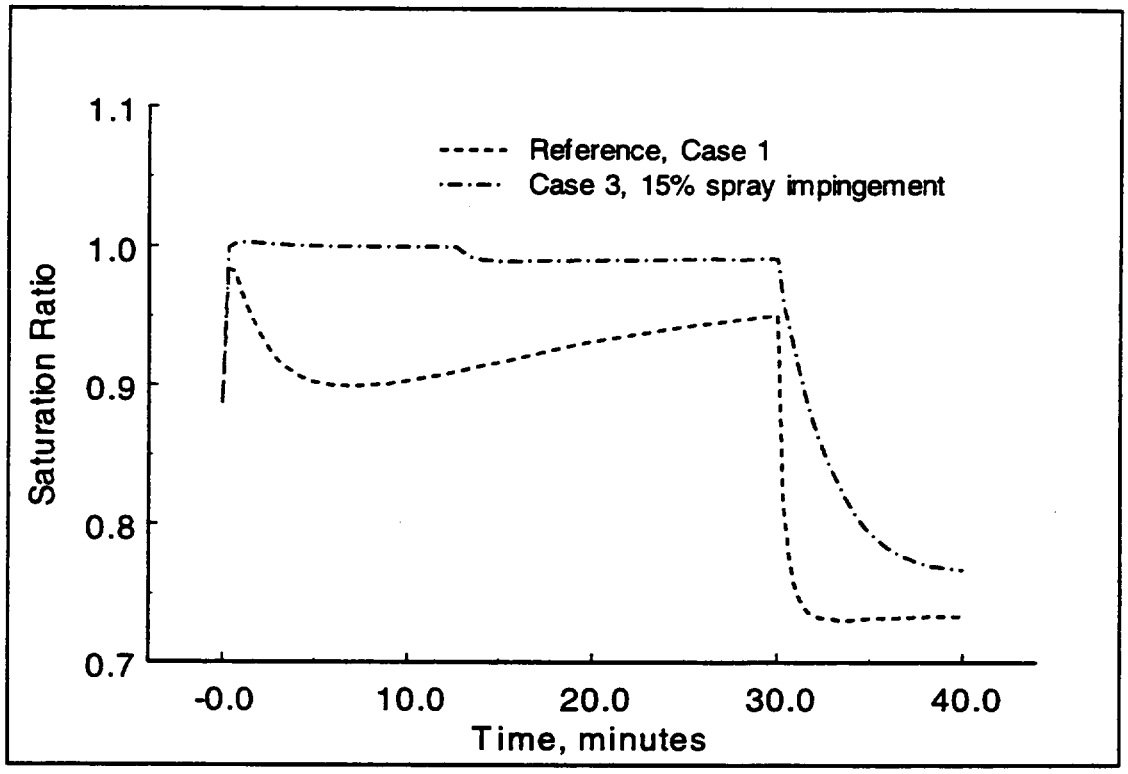

Figure 4.76 CONTAIN M-7-1 saturation ratio comparisons for the reference case and a case with 15% spray water impingement on the facility dome walls.

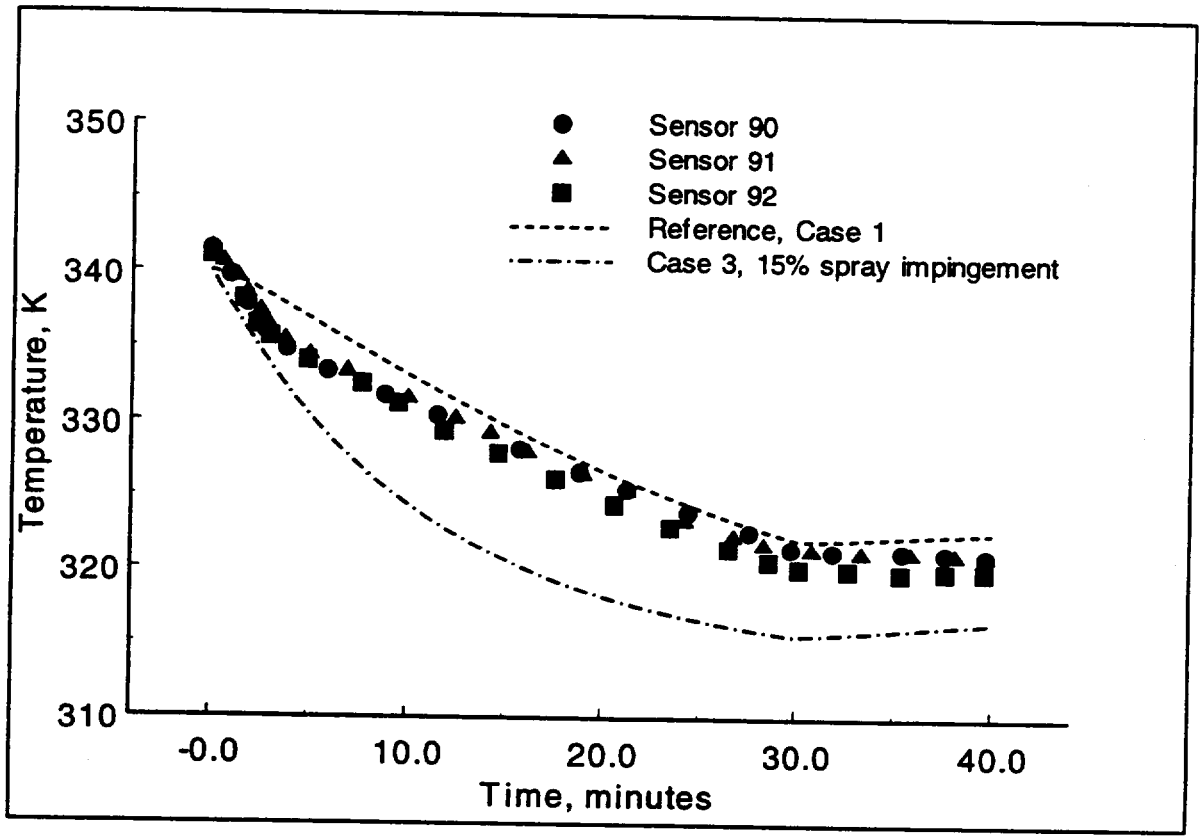

Figure 4.77 CONTAIN M-7-1 dome wall temperature comparisons for the reference case and a case with 15% spray water impingement on the facility dome walls.

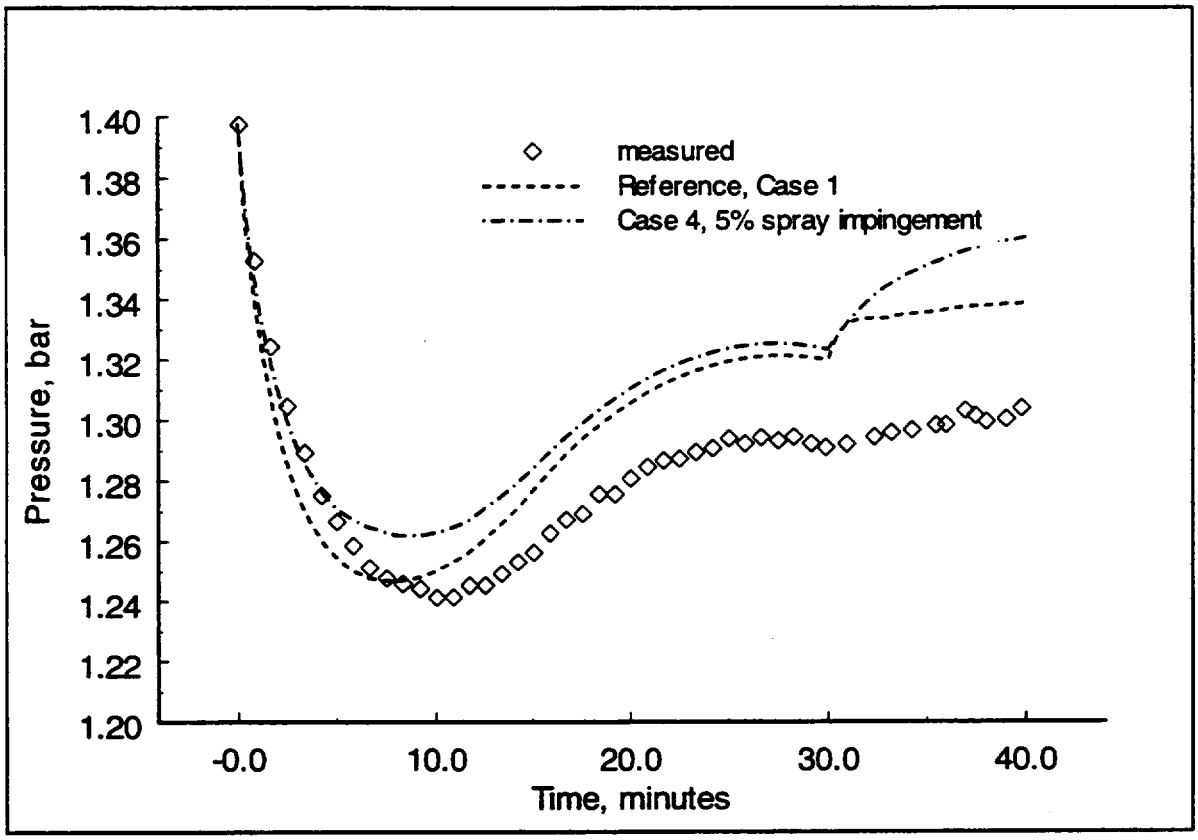

Figure 4.78 CONTAIN M-7-1 pressure comparisons for the reference case (Case 1) and a case with 5% spray water impingement on the dome walls (Case 4).

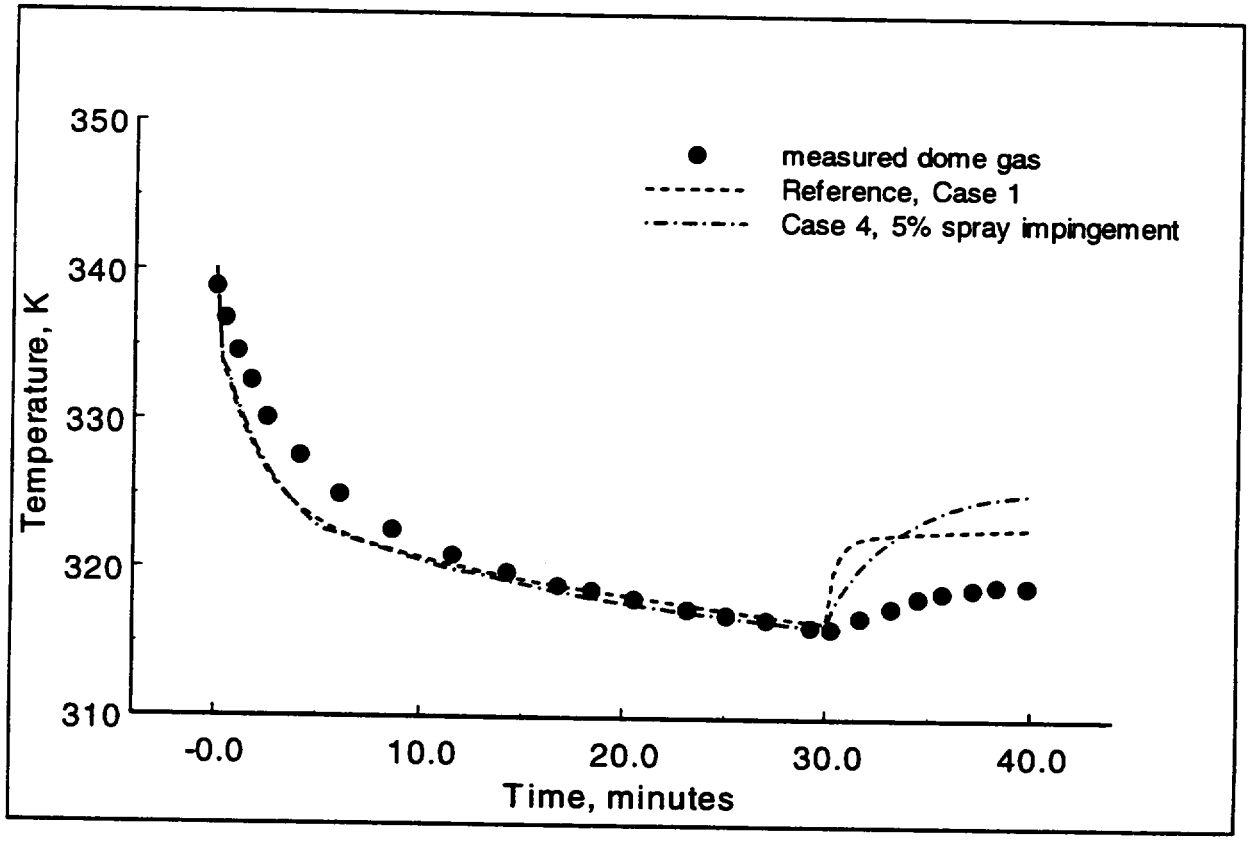

Figure 4.79 CONTAIN M-7-1 dome gas temperature comparisons for the reference case (Case 1) and a case with 5% spray water impingement on the dome walls (Case 4).

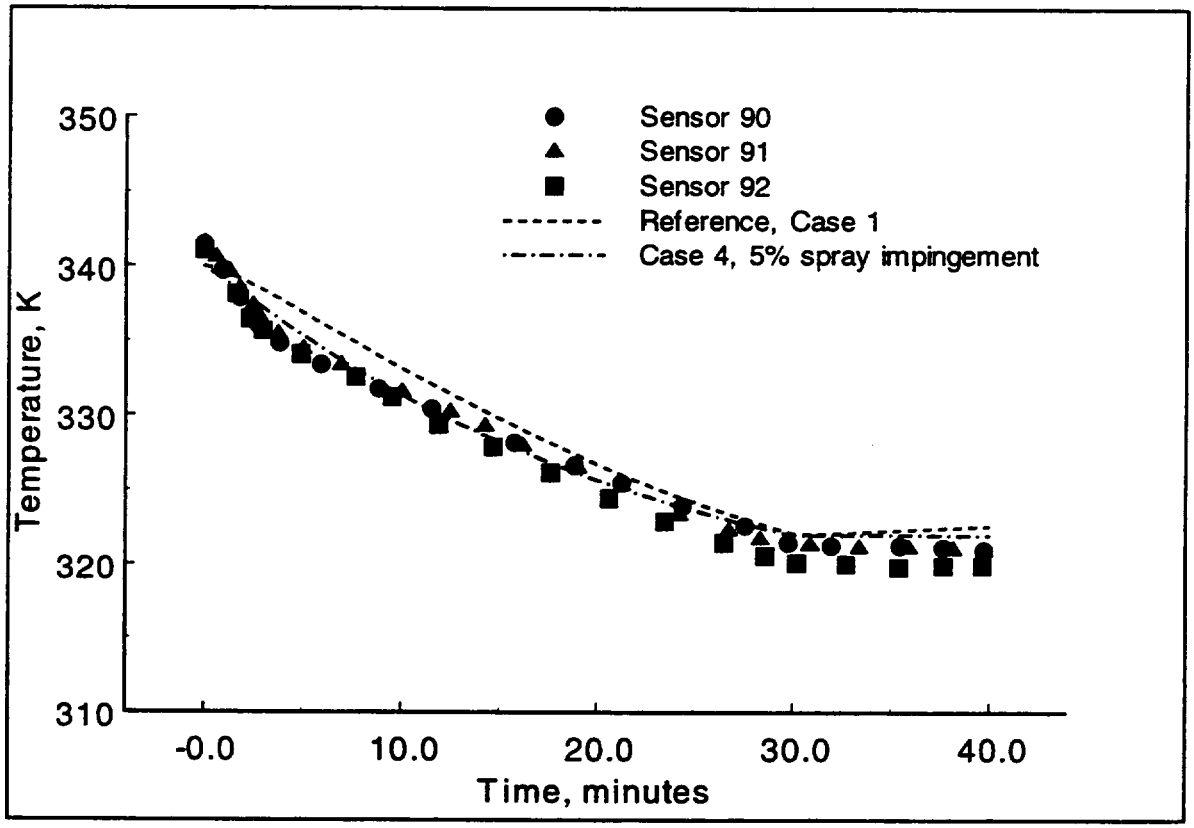

Figure 4.80 CONTAIN M-7-1 dome wall temperature comparisons for the reference case (Case 1) and a case with 5% spray water impingement on the dome walls (Case 4).

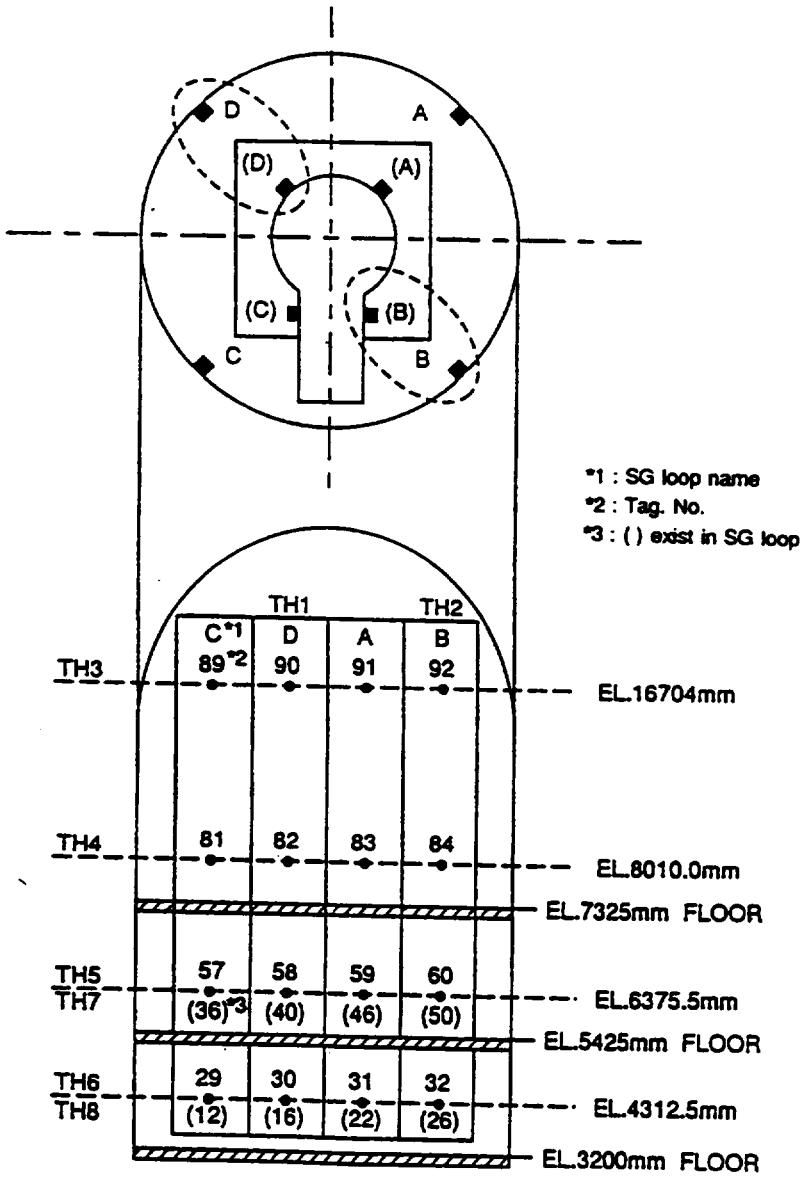

Figure 4.81 Locations of wall temperature measurements in the NUPEC facility [OECD94].

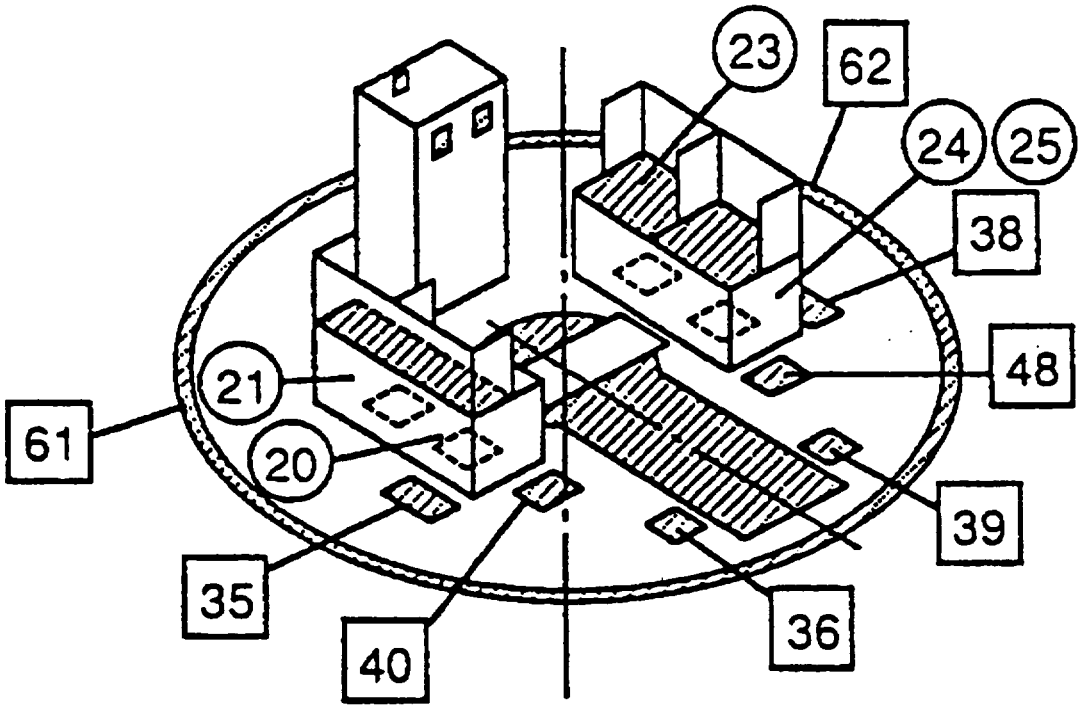

Figure 4.82 Internal metal partitions in the dome region (above the third floor) of the NUPEC facility [OECD94].

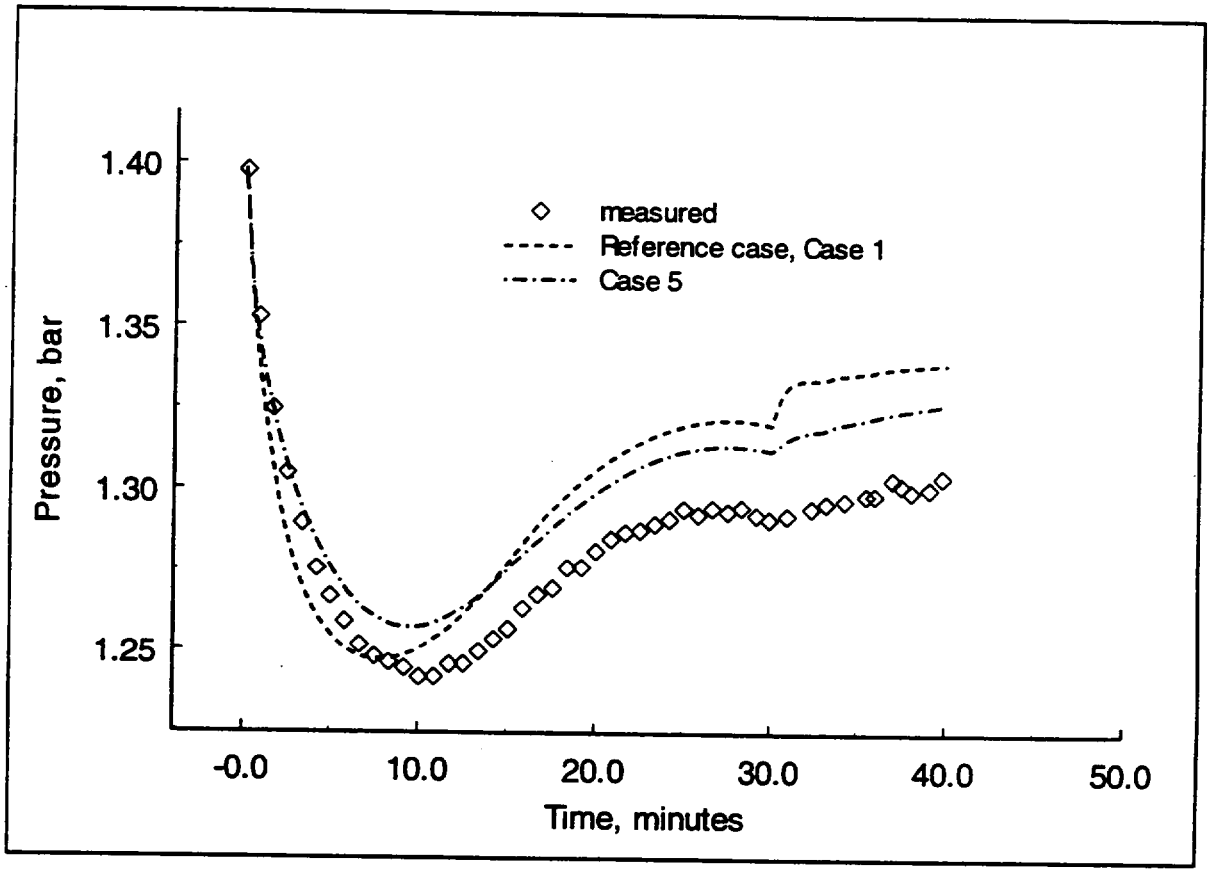

Figure 4.83 CONTAIN M-7-1 pressure comparisons for the reference case (Case 1) and a case with spray water impingement on dome and internal walls (above the first floor) and forced convective heat transfer (Case 5).

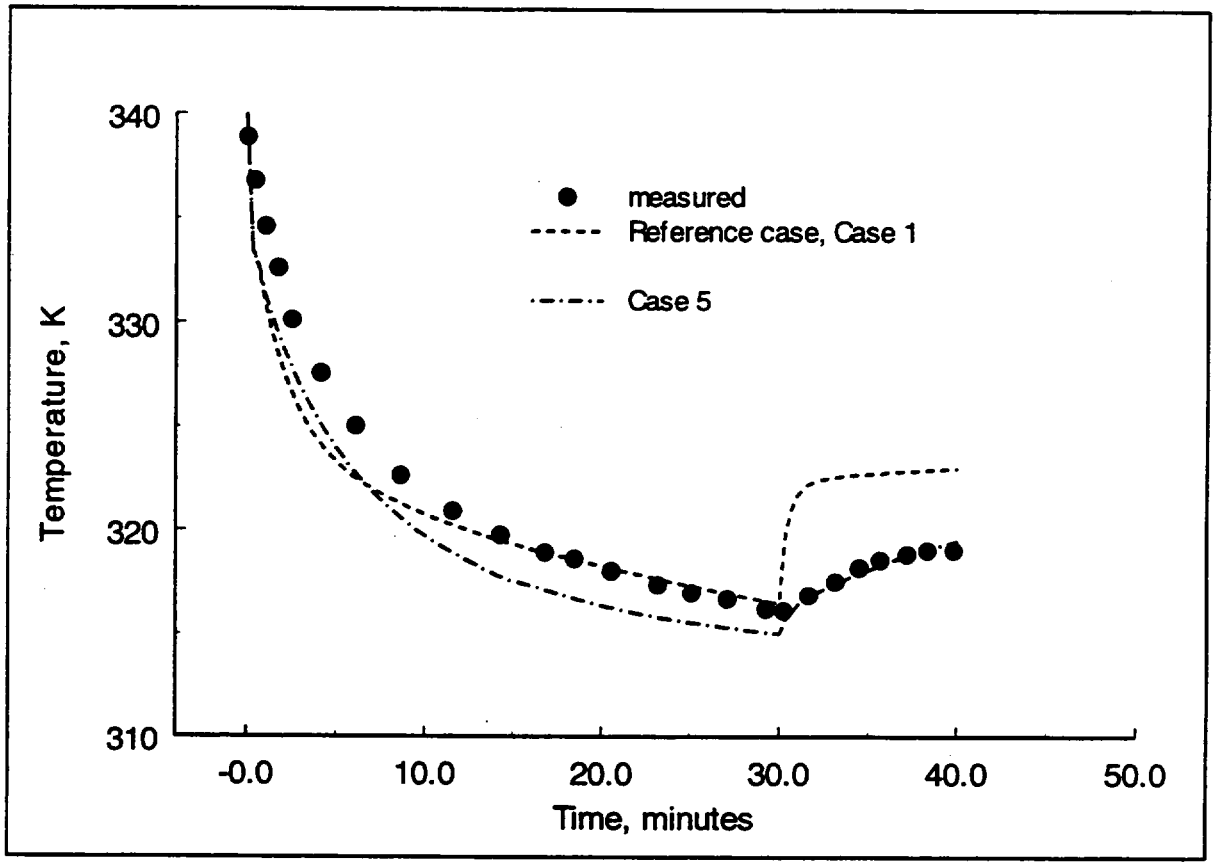

Figure 4.84 CONTAIN M-7-1 dome gas temperature comparisons for the reference case and a case with spray water impingement on the dome and internal walls (above the first floor) and forced convective heat transfer (Case 5).

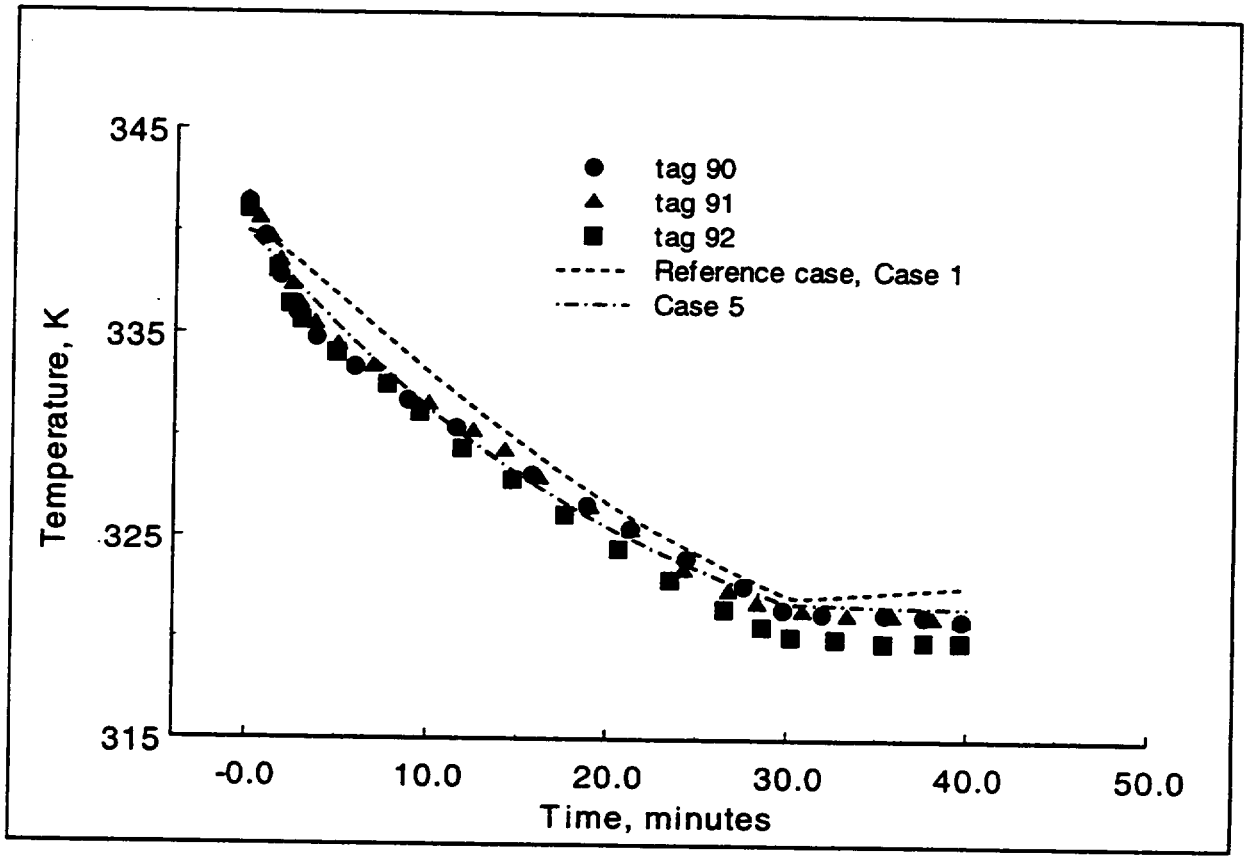

Figure 4.85 CONTAIN M-7-1 dome wall temperature comparisons for the reference case and a case with spray water impingement on the dome and internal walls (above the first floor) and forced convective heat transfer (Case 5).

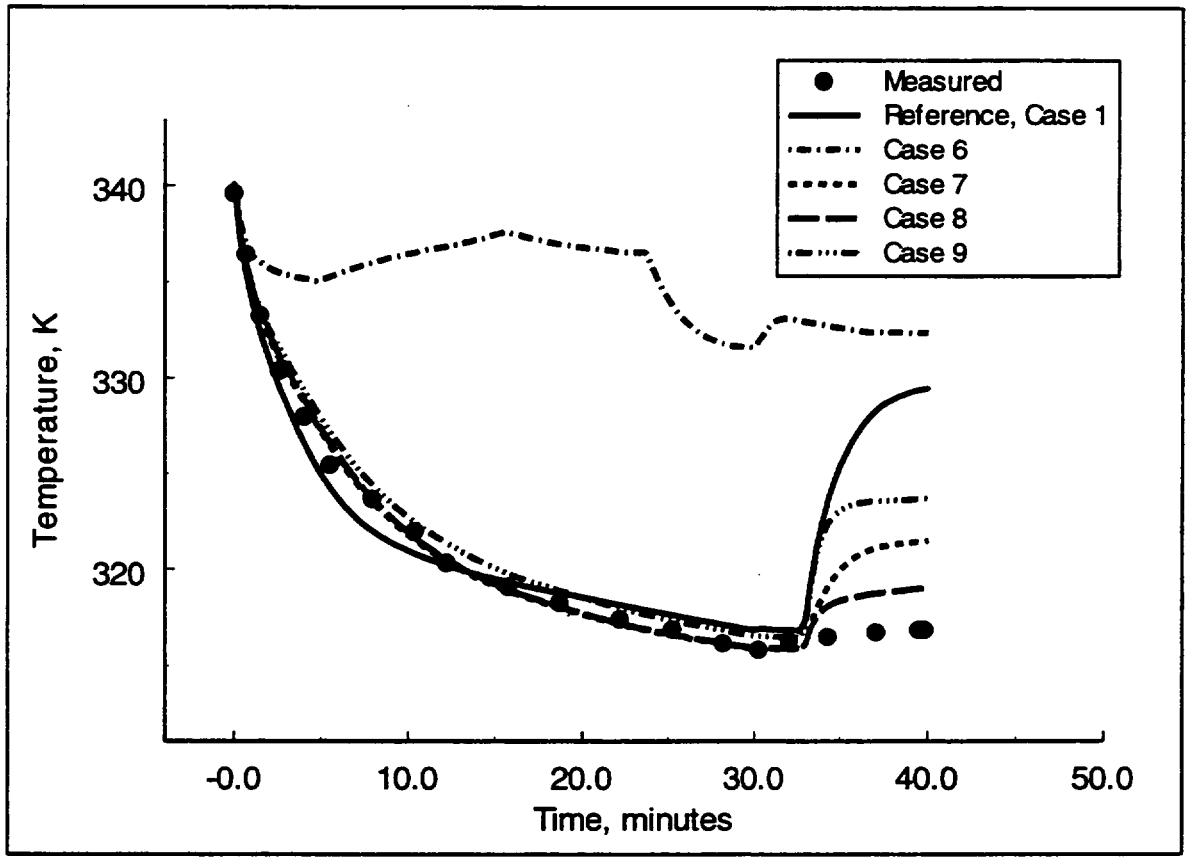

Figure 4.86 Comparison of measured and calculated local gas temperatures in the reactor cavity compartment (cell #19 in the CONTAIN 35-cell deck – compartment #19 in Figure 3.73) of the NUPEC facility, test M-7-1.

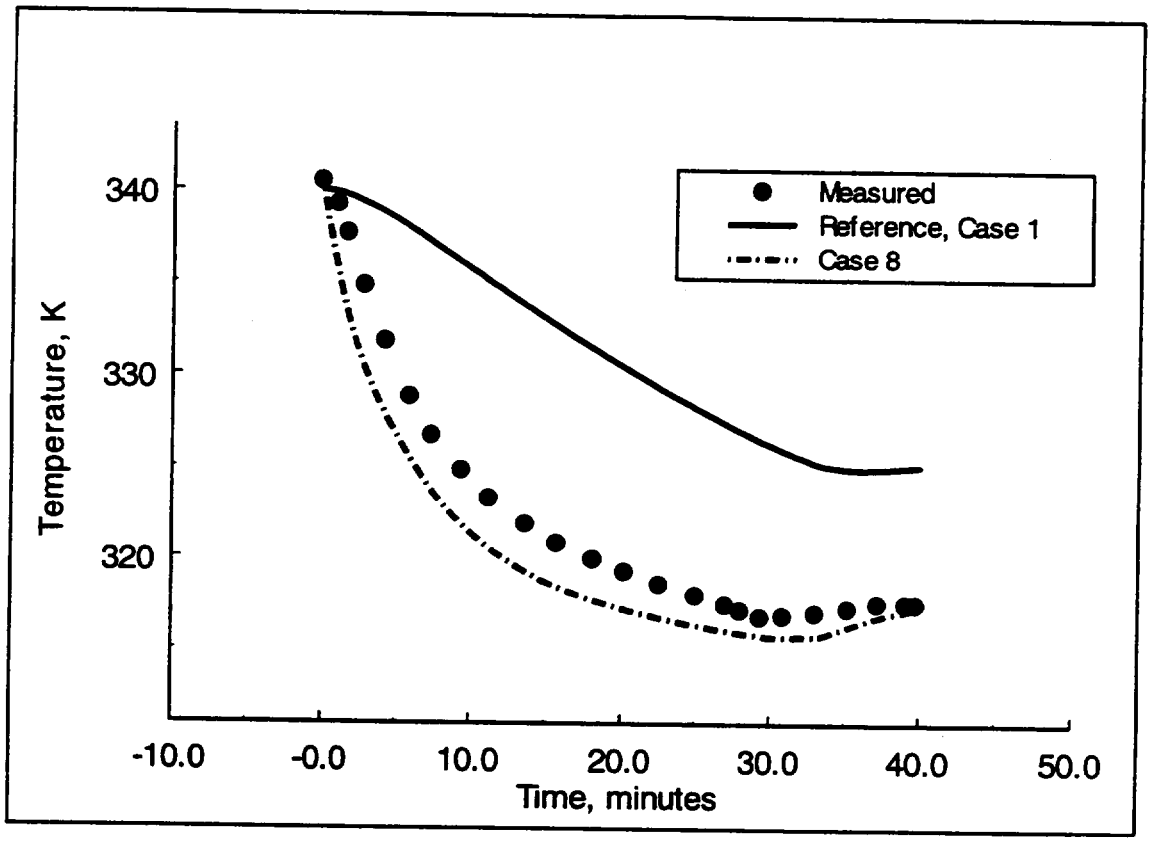

Figure 4.87 Comparison of measured and calculated wall temperature for SG compartment, C loop in the NUPEC facility.

5 Summary of Findings and Conclusions

This report has identified key containment phenomena for modeling thermal hydraulics and hydrogen distributions during design basis and beyond design basis accidents through the use of a PIRT methodology. These key phenomena and associated processes have been cross-referenced to 20 tests (separate and integral effects) to show that these tests provide a reasonable database for assessing the CONTAIN code's thermal hydraulic, mixing, and transport modeling. Reference calculations have been described for each test, and a series of over 80 sensitivity calculations have been completed to demonstrate the effect of code, user, and experimental uncertainties on predicted pressure, temperatures, and hydrogen concentrations. The result of this effort is that the CONTAIN code has been found to be a robust code, with scale-up physical modeling capable of providing reasonable predictions for a broad range of DBA-like scenarios. The applications have also shown that the complexity associated with building an analytical simulation model of a containment experiment or postulated accident, with implicit demands on the user knowledge base. A few modeling short-comings were identified, but these either involved low ranked phenomena, or were of a nature that conservative results were obtained.

Two of the more important phenomena investigated in the test series are condensation/evaporation heat transfer and gas transport. Each process has been assessed in reference to model reliability. Specifically, the CONTAIN HMTA method used for atmosphere-to-structure energy transport has been found to be an accurate modeling approach for predicting trends and absolute rates of energy transfers observed in tests. Also, the hybrid flow solver, which is used to model both well mixed and stratified atmospheres, has been shown to be an improved modeling method for predicting regional temperatures and concentrations within a containment. Pressure suppression by internal water spraying can be an important containment loads mitigating strategy. Processes associated with this strategy have been analyzed for a separate and two integral effects tests programs to show that the CONTAIN code model for spray effectiveness is reliably calculated. An auxiliary result of all these assessment efforts has been a compilation of user guidelines and remarks concerning the implications of the assessment to full-scale plant analyses.

5.1 Phenomena

Containment PIRTs have been developed for two phases of a PWR plant accident: the rapid pressurization phase, and the slow pressurization/depressurization (and the core damage phase) of postulated design basis or beyond design basis accidents. In the case of the short-term, rapid pressurization scenario, the number of processes involved reduces to essentially one phenomenon, multi-component gas compression and expansion. Since energy transfers by condensation require a certain amount of time to impact the containment thermal hydraulics, a typical rapid pressurization phase that lasts only a few seconds or 10's of seconds is relatively insensitive to transfer processes that remove a small amount of energy from the atmosphere. An

exception to this occurs in modeling non-prototypic blowdown experiments where the rate of pressurization is slower due to scale distortions. Some engineering safety systems, like sprays, are not activated soon enough to make a significant impact on blowdown loads. Although they can affect the peak pressures shortly after the blowdown, containment pressure and temperature profiles are typically affected more, in this time period, by the characteristics of two-phase water injection than by mitigating systems which are designed for longer term containment challenges. Mixing and transport processes are somewhat important, but when condensation processes are less important, so to are these processes.

The situation is quite different for the longer term processes that control the slow pressurization/depressurization phase of an accident where there are concerns for safety equipment overheating and potential hydrogen combustion. For these concerns, heat and mass transfer, gas transport and mixing processes are of high importance. Additionally, processes resulting from active pressure and temperature suppression systems, like sprays and fan coolers are important and must be reasonably modeled.

In summary, a list of processes have been identified that are highly important for DBAs and beyond DBAs. The list was constructed in a manner to reflect the highly transient nature of accidents where time is a major determinant of what processes are important for each phase of an accident. Time scales for processes are therefore significant considerations in extrapolating code performance in experiments to postulated accident simulations. The PIRTs presented here therefore point to issues involving scale of facilities and the time scaling involved in test procedures. Hence, the developed PIRTs not only serve to identify and rank, but also to place each phenomena in the context of a prototypical accident scenario. When reviewing the experimental database and calculational results, the PIRTs serve as an aid in maintaining a reasonable perspective on measured and calculationed differences. This perspective is used in this assessment to both emphasize and moderate our concerns regarding the reliability of the code for performing containment accident analyses.

5.2 Reference Calculations

The section on reference calculations first introduced a discussion on the various experimental facilities, test procedures, instrumentation, and a review of issues related to geometric and source scaling. The main body of the section explains important aspects of the CONTAIN input for various tests, and presents a comparison of measured and calculated results. The reference calculations are presented as baseline examples to introduce discussions on modeling while providing a reference for subsequent discussions involving sensitivity calculations. In most instances, the reference calculations are established using modeling choices that would typically be applied in the analysis of containment response to postulated accidents. However, they may not be described here as always representing a full plant, or even a "best-estimate" calculation.

Taking the lead from the PIRT discussions, this section focuses on two major code modeling

areas: energy transport from the atmosphere to structures – heat and mass transfer analogy modeling; and, gas transport and mixing within the containment by inter-cellular flows of gases – the hybrid flow solver model. These two areas are not independent, and therefore, integral effects testing results are used to investigate how well the interaction of these models are treated in the ASM. Separate effects tests are included to specifically address HMTA modeling, and pressure suppression by sprays which is also a highly important phenomenon for scenarios involving long term containment response. What is demonstrated in the separate effects calculations is that the HMTA methodology is a reliable physical modeling method for predicting condensation heat transfer for containment conditions that are characterized as natural convection dominated, or moderately affected by forced convective processes (1-3 m/s flow velocities). In the case of pressure suppression by internal sprays, the CONTAIN model for spray-atmosphere energy exchange, based also on the HMTA methodology, is a reliable modeling method. These separate effects findings are in concert with the need to have accurate models for the highly ranked energy exchange phenomena identified in the PIRT. A summary of results for the separate effects tests is presented in Table 5.1. (Comments in the table extend to various sensitivity calculations as summarized in Section 5.3.)

The reference calculations for integral effects showed the degree of conservatism associated with the natural convection condensation modeling during blowdown experiments, the dominant trends and good predictions of natural convection condensation for times after blowdown periods (via heat transfer coefficient comparisons), and the good predictions of steam and light gas concentrations with the hybrid flow solver for a variety of injection rates and injection locations within a facility. A summary of results for these integral effects test are given in Table 5.2.

In all the reference calculations, the maximum containment loads (pressure and temperature) were either calculated with very good accuracy, or in the case of blowdown pressure and temperatures, calculated with conservatism using the default options in the code. There were no cases where the maximum pressures were under predicted.

The reference calculations for regional hydrogen and temperature distributions in the HDR, CVTR, and NUPEC tests showed that the hybrid flow solver is capable of accurate (< 10-15% error) prediction of gas transport for a range of geometric scales, room configurations, source rates, and injection locations. The reference calculations also confirmed that the type of stability condition (fully developed stable stratification) that the CONTAIN code is most applicable to the dominant condition in the tests during the periods of observed maximum temperature and light gas concentration. Some noted but minor discrepancies concerned phenomena that were either not modeled in the code or neglected by the choice of user input. As an example of the former, during the initial injection periods of light gases (steam or hydrogen/helium) a buoyant plume or jet may form; these features are not modeled in the code, and as pointed out, the neglect is a major contributor to some very early under predictions of temperature and concentrations in regions above an injection. Treatment of water carryover is a type of modeling characterized mainly by user parametric input; in the process of water carryover, as a result of condensate

draindown or spray washdown, structures are cooled and the atmosphere is effectively desuperheated in certain regions. Since there is uncertainty associated with a parametric treatment of these processes, the reference calculations are presented as ones that neglect the effects of water carryover on lower compartment thermal hydraulics, except that pool-to-atmosphere interactions are considered.

From the perspective of full plant analyses, the distortion of geometric and source scaling in the tests generally benefit the viewpoint that CONTAIN is a reliably conservative computational tool for predicting containment responses to DBAs or beyond DBAs. It was shown that in both HDR and CVTR tests (HDR V44 and T31.5, and CVTR test #3) that the default option for the HMTA model results in significant (20-50%) over-predictions of maximum pressures during experimental blowdown events. In each facility and test procedure, however, the amount of short-term heat sinks and source rates were distorted in such a way that the energy transfer processes during the blowdown event are over emphasized. Therefore, the tendency of the code to over predict pressure (an indicator of atmospheric energy content) will be reduced for plant analyses as the importance of energy transfer to structures is also reduced due to geometric and time scaling. The over predictions that have been observed in this assessment report are therefore upper bounds on the degree of over prediction expected in plant analyses (assuming the default options for calculating flows along structures and the algorithm for mixed convection are used).

The good condensation heat transfer results that have been obtained for both small scale separate effects tests and in larger scale HDR testing is a significant measure of assurance that separate effects validations of the HMTA methodology as implemented in the code are also valid for scaled-up applications.

The HDR facility has been used as a testing platform for codes calculating gas transport processes. Its utility however for validation has probably been over emphasized in the literature, especially with respect to the severity of several gas distribution tests that, as a result of geometric scale distortions, are not considered representative of postulated conditions expected in domestic containments. This statement is applied to the elevated injection test of the E-series. We noted in the subsection on scaling the reasons: the HDR facility is 1) configured as a very complex, compartmentalized facility, with 2) a large aspect ratio, and 3) tested, in the case of the E11.2 test, using a procedure (location of the injection) and sensitive loop geometry (from the standpoint of gravitation heads and exposed heat sinks) that puts a great deal of importance on the requirements to model small circulating flows for prolonged periods. In comparison to U.S. containments, the HDR facility is too complex, having too high of an aspect ratio, and in the case of E11.2, used for a scenario that probably over emphasizes the impact of small circulating convection loops, compared to the types of postulated plant accident scenarios. The distribution test E11.2, therefore, is an interesting test for the extreme testing of gas transport and mixing code models. The non-prototypical aspects of the facility and test procedure are the principal factors that make the E11.2 test an extreme test. However, even as an extreme test, the

CONTAIN code with the default flow solver represents the data well in the reference calculation, and this should be viewed positively. The slight drawback, as indicated by sensitivity calculations, is the introduction of some degree of uncertainty in the modeling of this test due to user specified nodalization. In contrast to the HDR facility, the CVTR and NUPEC geometric scale and test procedures are more representative of the type of plants and accidents that a containment code should be tested for reliability in gas transport modeling. With respect to tests performed in these two facilities (sprays or without sprays), the reference calculations provided very good predictions of local and regional gas transport. Most importantly, nominal variations in the nodalizations used in the reference calculations verified the suitability of the nodalizations.

Each test characterized by a low injection points which exhibits good mixing and the CONTAIN calculated predictions of the thermal hydraulics and hydrogen distributions that were in very good agreement with data. In U.S. plants, the likely locations for injections initiated by LOCAs are situated low inside containment, and therefore the containment should be close to a well mixed environment. Accidents initiated by MSLBs can be classed as mid-elevation injections where a stratification profile can be expected. The gas distributions calculated for the two MSLB test scenarios (CVTR test#3 and NUPEC M-8-1) however have shown that the code results for gas distribution agree very well with measurements.

5.3 Sensitivity Calculations

No matter how well a code predicts experimental data through reference calculations, one can never be sure of the code's performance unless supplementary sensitivity calculations are performed. This is because the calculational results are the product of a simulation effort that involves code, user, and the variability of experimental initial and boundary conditions. Sensitivity calculations are performed to help gauge the relative importance of each component to the calculational assessment. We have presented many sensitivity calculations based on the referenced inputs for the tests reported in Section 3. Except for the separate effects tests, most of the sensitivities have involved user induced input and experimental initial and boundary condition uncertainties. In the more complicated integral case studies, the user induced uncertainties often dominate as the likely source of simulation uncertainty. Assessments of a simulation model is aided significantly by the modeling methodology in the code; that is a physically-based modeling method which is the foundation of the CONTAIN code (for example, the HMTA modeling method), allows for meaningful variation of physically identifiable parametric inputs.

In the CONTAIN studies, some of the more important user induced uncertainties involved parameter choices for phenomena not explicitly calculated by the code:

- forced convection during blowdown periods;
- spray impingement and washdown;
- liquid water carryover; and,

- water redistribution and interaction with portions of the atmosphere in the lower regions of containment.

Nodalization, another area of user influence, was quantitatively shown as affecting both short-term differential pressure calculations and long-term gas mixing behavior. In terms of the enhancement effects – that is, those that increase maximum containment loads – the default options were always found to result in the more conservative estimates. Some significant over predictions in lower compartment temperatures were observed when water redistribution and atmosphere interaction was neglected. These over predictions reflect on the difficulty associated with predicting degrees of superheat throughout a facility. Since these cases involved only small atmospheric energy increments, the local over predictions resulted in small incremental pressure deviations, and also imply small errors in postulated equipment heating. In summary, all of the sensitivities that dealt with atmospheric energy transfers and gas distributions confirmed the phenomena ranking given in the PIRTs.

The separate effects studies on the Wisconsin flat plate tests showed that the mixed convection algorithm used by default in the CONTAIN code gives good representation of both natural, forced and mixed convection condensation processes. Auxiliary calculations that removed the film correction factor in the CONTAIN HMTA, showed that the CONTAIN film correction for mass transfer at high transfer rates is important for accurate (<10% error) predictions of condensation under accident-like conditions. Variations on the natural convection Nusselt number correlation showed that the default correlation gives the best representation of natural convective condensation in the Phebus test. And for the JAERI spray tests, a default spray droplet diameter of 0.001 meters was found to be slightly too large, resulting in a tendency to predict a slight degree of superheating that was not observed in the tests. In addition, the neglect of spray impingement on hot containment metal surfaces – a user induced uncertainty – results in an under prediction of the pressures during the initial period when sprays are activated.

Overall, the sensitivity calculations confirmed that the code HMTA method of modeling heat and mass transfer for atmosphere-to-structure and atmosphere-to-spray droplets is a validated method for the conditions expected in containment atmospheres. This finding was made possible in part by user access to physically based parameter choices that are available in the code through input options. In all cases, default options were found appropriate for predicting the variety of mass and heat transfer conditions expected in U.S. plants during postulated accidents.

When we get to integral testing, there is a shift from single phenomenon assessment to dominant process modeling and the effects of model interactions. Integral tests are typically complex, costly, and difficult to instrument adequately compared to separate effects tests. Therefore, the tests are often best understood and models assessed through series of sensitivity calculations. In performing the sensitivity calculations we have investigated interactions between a number of processes:

- gas transport and condensation modeling;
- dispersed liquid water and pressure drops across pathways;
- spray-atmospheric cooling and spray water impingement on surfaces; and,
- condensate removal and condensate-atmospheric energy transfers.

The importance of transport and mixing on local temperature is shown, but the importance of transport processes to the prediction of light gas concentrations is shown to be even more important. Additionally, we have studied the effects of material property specifications and initial and boundary conditions on thermal hydraulic and gas distributions. For instance, the effect of too little steam circulation below the mid-elevation injection in the E11.2 experiment has been noted as one of the more probable reasons for late time over pressure prediction that has been repeatedly mentioned in the open literature. That, coupled with what appears to be an obvious problem regarding the use of low humidity thermal properties for concrete heat sinks that have deteriorated surface coatings, would improve the pressure comparisons presented for the reference calculation

Sensitivity studies on the HDR blowdown tests (V44 and T31.5) and the E-series led to some insights into process interaction. These studies also provided insights into the relationship between geometric and injection scale dependencies for subcompartment analyses. In this area, a weakness in the code's applicability was noted for phenomena associated with dispersed liquid water carryover and the associated estimation of transient, two-phase pressure drops for breakroom exit pathways. Predictions of differential pressures were possible for a test (V44) with the highest volumetric two-phase water injection rate, but only after pathway loss coefficients were adjusted for postulated phenomenological conditions within the breakroom, conditions that could not be determined a priori. The apparent scale dependency of these conditions, and lack of models for an important phenomena believed to be present suggests caution for using the code in this specific area of containment analysis.

Although a few sensitivities have been conducted using a single cell representation of test facilities, this simple geometric model is generally shown as being too inaccurate for the analyses required in most testing procedures. Multi-cell analyses is clearly preferred when the injection location is elevated (HDR V44, T31.5, and E11.2; CVTR tests 3, 4, and 5; NUPEC test M-8-1). In all studies where stratification was observed, the hybrid flow solver (which uses a combination of donor and average flow path density to determine gravity heads) performed well compared to an older method of formulating gravity heads by using averaged densities only. The over mixing of gases predicted by the old method has been simulated through a user input option and the improvement with the default hybrid flow solver has been confirmed. The studies on gas transport, especially as denoted by comparisons of measured and calculated steam and light gas concentrations, show that the lumped parameter (inter-compartmental) representation is adequate for performing containment safety analyses (in most cases, stable mixing conditions are expected to occur).

5.4 User Guidelines and Implications for Plant Analyses

One of the more useful aids to new users of a code are a set of input decks that transition from the simple to the more complex simulations that represent actual plant containments along with postulated accident scenarios. For this reason, and archival purposes, the input decks for all reference calculations are included as an appendix to this report. These decks may be consulted to acquire insights in determining the models and input that may be considered for performing plant containment analyses. Many of the input models in the CONTAIN code can be omitted when the accident analysis is limited to DBA or beyond DBA scenarios. The containment related experiments analyzed in this report focused on the core containment thermal hydraulic phenomenology, thereby omitting severe accident issues such as DCH and core-concrete interactions. Therefore, the CONTAIN input schemes mainly uses the HMTA models (STRUC block), the flow solver (FLOWS block), and pools (LOWER-CELL block), and minimal input for the aerosol model in the global input section. The user of the code should become familiar with these inputs and models as described in the CONTAIN code manual [Mur97].

In general, containments should be analyzed using a multi-cell representation of the free volume when local versus global features are an important factor (pressure differentials, equipment qualification, etc.). Maximum pressure predictions can often be calculated conservatively using a single cell representation of the containment; however, it was noted in this report that depressurization (i.e., the pressure relaxation period after the blowdown phase) may not be predicted conservatively with such a restrictive geometric model. Multi-cell models do not necessarily mean a large number of cells; most gas and liquid water transport effects of importance to DBA and beyond DBA assessments can be modeled with 15 to 20 cells - 3 to 6 cells in the open region above the operation deck is acceptable in most cases. Guidelines for proper orientation for these cells can be found in Mur96 –and in this report, the nodalization scheme used in the CVTR reference calculation, as modified for the sensitivity calculation, is a good example of how a plant nodalization may be constructed.

Variations in the values of pathway loss coefficients are generally in the range of C_{FC} = 1 to 1.5. Long-term gas mixing, driven by buoyancy forces does not appear sensitive to nominal variations in these coefficients. However, subcompartment analyses (differential pressures) may be more sensitive to these coefficients, and difficult to determine a priori since highly transient water carryover effects are not modeled in the code. For this reason an upper bound for loss coefficients (i.e., $C_{FC} \sim 1.5$) should be used for breakroom exit pathways. Most analyses performed during quasi-steady state periods however can be formulated using a $C_{FC} \sim 1$; this includes free (or open regions) and compartmentalized volumes.

It is recommended that sprays be modeled with a slightly smaller droplet size than the default option, such that droplet sizes ~ 0.0005 to 0.00075 meters should be used to avoid a tendency to generate superheating due to a possible mismatch of latent and sensible heat transfer for larger drop sizes.

Sensitivity calculations should always be performed to complement reference or baseline code calculations. To gain insights for the most important areas of sensitivities is by first performing a detailed energy partitioning study on the problem using the plot file output quantities listed for in the POSTCON code (the POSTCON code and input description is discussed in the CONTAIN manual [Mur97]). The most important quantities are pressure, local temperature, and steam mole fraction - plotted for each cell. More detailed analyses can be made using the flow path velocities and total surface energy transfers, also available on the CONTAIN plot file.

Table 5.1 CONTAIN Code Performance Summary for Separate Effects Tests (SETs)

Facility/Experiment Description	Highly Ranked Phenomena	CONTAIN Models Activated (ref. case)	Calculated Results Within Data Range			Comments
			Press %*	Temp deg	h (or condensation mass rates)	
Wisconsin Flat Plate - 6 Tests: steady state condensation downward flows, air/steam mixtures 1-3 m/s along a constant uniform flat plate. Flow is saturated.	-surface mass transfer (free and forced convection)	- HMTA - condensate Film Tracking	–	–	<10% **	default mixed convective algorithm accounts for natural and forced convective conditions modeling of high mass transfer rate effects shown to be in agreement with data film thickness insensitivity / diffusion layer dominant
Phebus - FPTO Steam (and some hydrogen) injected into steel vessel ($10m^3$); condensation restricted to selected areas, atmosphere is superheated.	- Multi-Component gas compression/expansion - Surface heat/mass transfer (natural convection)	- atmos. T/H - 1 cell model - HMTA - condensate film tracking - sensible conv. and rad. heat transfer	<8%	+/- 3	<15%	superheating of 25-30 degrees predicted in agreement with data film tracking (reference calc.) provides a slightly better results than default thickness default natural conv. Nusselt correlation shown to produce better results than other referenced correlations

* $(\Delta P_{calc} - \Delta P_{measured}) / \Delta P_{measured}$; $\Delta P_{measured} = P - P_0$ and $\Delta P_{calc} = P_{calc} - P_0$

** takes into account uncertainty band for instrumentation

Table 5.1 CONTAIN Code Performance Summary for Separate Effects Tests (SETs) continued

Facility/Experiment Description	Highly Ranked Phenomena	CONTAIN Models Activated (ref. case)	Calculated Results Within Data Range		Comments
			Press %*	Temp deg	
JAERI - PHS-1 & 6 Sprays injected into stagnant steam/air mixture. Steel vessel ($700m^3$) is insulated.	- multi-component gas compression /expansion - spray mass/energy exchange - spray dynamics (mixing) -buoyancy /stratification (regional) - surface heat/mass transfer (natural convection)	- atmos. T/H - 1 cell model - HMTA - condensate film tracking - sprays (droplet diameter, default value used) - PHS-1; 6 nozzles at 3/4h of vessel - PHS-6; 1 nozzle at near top of vessel - pool surface H.T.	<5%	<5**	smaller droplet diameter <.001m; about .0007m is more appropriate (to maintain saturation conditions) spray water impingement on hot wall surfaces required to obtain pressure and temperature accuracy for test PHS-1 which has multiple nozzles forced conv. cooling of walls without spray washdown results in superheating forced conv. cooling of walls without spray washdown and very small droplet diameters maintain saturation but increase pressure beyond measurements, i.e., error >5% sump modeling required for late time agreements

* $(\Delta P_{calc} - \Delta P_{measured}) / \Delta P_{measured}$; $\Delta P_{measured} = P - P_0$ and $\Delta P_{calc} = P_{calc} - P_0$

** within measurement height 7.5-16.5 meters

Table 5.2 CONTAIN code performance summary for Integrated Effects Tests

HDR Experiments:

Facility/Experiment Description *German PWR containment: ~70 compartments, complex configuration	Highly Ranked Phenomena	CONTAIN Models Activated (ref. case)	Calculated Results Within Data Range				Comments *Significant geometrical distortions relative to domestic PWR containment designs
			Press, max %*	Temp, max (deg.)	Press diff. %**	Gas conc. max %**	
ISP-16 (Test V44) 55 second two-phase blowdown in small, mid-elevation room	- Multi-component gas compression/expansion -Jet-plume gas interaction/entrainment - 1-D conduction - Surface H/M transfer (natural convection) - liquid water carry-over (transport)	* 5 cell nodalization * no water aerosols * default condensate film thickness * default conv. velocities	~50% [<20% (with forced convection, single cell modeling]***	<10 deg	>50% [<10% (with liquid water suspended; 33 cells; CFC = 1.5, from breakroom]		Small convective velocities calc with default conv. velocity; therefore, natural convection modeling is used Conservative pressure and temperature predictions improved differential pressure calc. with more detailed nodalization and suspended liquid water
ISP-23 (First 20 min T31.5) 55 second two-phase blowdown in larger (mid-elevation) room.	Same as above plus: -buoyancy	* 33 cell nodalization * water aerosols * default film thickness *default convective velocities * hybrid flow solver	<30% <20%[with forced conv.]	<10 deg	<10% [<20% with liquid water suspended]		improved pressure prediction with forced conv. during blowdown
T31.5 benchmark Gas injection 20 minutes after blowdown and lasted 15 minutes	-buoyancy -1-D conduction -Surface H/M transfer		<5% For ▷ 20min	<10 deg		<10% for max	improved conc. with hybrid flow solver

* $(\Delta P_{calc} - \Delta P_{measured}) / \Delta P_{measured}$; $\Delta P_{measured} = P - 1bar$ and $\Delta P_{calc} = P_{calc} - 1bar$

** $\Delta Pdiff_{calc} / Pdiff_{measured}$, $\Delta Xgas_{calc} / Xgas_{measured}$ where $\Delta = |calc. - measured|$

*** sensitivity study results

Table 5.2 CONTAIN code performance summary for Integrated Effects Tests (continued)

HDR Experiments:

Facility/Experiment Description	Highly Ranked Phenomena	CONTAIN Models Activated (ref. case)	Calculated Results Within Data Range				Comments
			Press, max %*	Temp, max deg.	Conc max %**	h (or condensation mass rates) %**	
ISP-29 (Test E11.2) 12 hour steam injection then 20 min gas injection (mid-elevation), then 3 hour steam injection in lower containment and about 4 hour outer spray cooling period	-Surface H/M transfer -1-D conduction -buoyancy	* 15 cell nodalization * water aerosols *hybrid flow solver	<40% [<14%, cooling line energy bounds and increased conductivity] ***	<10 upper <30 lower	<15%		- Significant uncertainties associated with experimental boundary conditions - Outer spray cooling not prototypical relative to domestic plants - hybrid flow solver improves prediction of maximum hydrogen concentration - results sensitive to relative elevation of injection source - increased nodalization (47 cells) does not improve results
Test E11.4 Similar to E11.2 but with 34 hour pre-heat. Steam and gas release into lower containment		* 48 cell nodalization * water aerosols * hybrid flow solver	<5%	<5 upper <15 lower	<5%	<10-30%	- using HDR concrete conductivity (lower than CONTAIN default) gives worst agreement for press.

* $(\Delta P_{calc} - \Delta P_{measured}) / \Delta P_{measured}$; $\Delta P_{measured} = P - 1bar$ and $\Delta P_{calc} = P_{calc} - 1bar$

** $(\Delta\_)_{calc} / (\_)_{measured}$, where $\Delta = |calc.-measured|$

*** sensitivity case

Table 5.2 CONTAIN code performance summary for Integrated Effects Tests (continued)

CVTR Experiments:

Facility/Experiment Description	Highly Ranked Phenomena	CONTAIN Models Activated (ref. case)	Calculated Results Within Data Range		Comments
			Press. max %*	Temp. max deg.	
CVTR - steel-lined concrete containment with internal sprays Above operating deck steam injection Test #3: no sprays	- multi-component gas compression/exp. - jet-plume gas interaction/entrainment - buoyancy/stratification (regional) - buoyancy (transport) - 1-D conduction - surface H/M transfer (natural convection) - liquid water carry over (transport)	- atmos. T/H - default conv. vel. - default condensate film thickness - atmos. rad. to structures - used upper bound est. of misc steel - sump pool formation - 15 cell nodalization	<20% <6%[forced conv. in upper region, with lower comp. water dispersed]** <14%[lower comp. water dispersed, 2.8% reduced enthalpy]	<26 (upper and lower compart.) <17[forced conv. in upper region with lower comp. water dispersed] <1 [lower comp. water dispersed, 2.8% reduced enthalpy]	- experiments to simulates MSLB with superheated steam - excellent long-term pressure relaxation - forced conv. along containment shell near injection, in the range of measured velocities, improves maximum pressure prediction -dispersed water (drain-down) in the lower containment reduces superheating - reduced injection enthalpy significantly reduces blowdown superheating in upper containment - single cell long term results (press and temp) below measurements
Test #4; sprays	Additional Phenomena: - spray mass/energy exchange - spray dynamics (mixing)	* 19 cell nodalization * default spray droplets	<5% spray period, relaxation pressures	<5 spray period, relaxation temperatures	- spray dominate mixing - comparisons for pressure and temperature in the spray region very good
Test #5; sprays, rate approx. twice test #4	same as Test #4	same as Test #4	<5% spray period	<7 spray period	

* $(\Delta P_{calc} - \Delta P_{measured}) / \Delta P_{measured}$; $\Delta P_{measured} = P - 1bar$ and $\Delta P_{calc} = P_{calc} - 1bar$

** sensitivity calculation

Table 5.2 CONTAIN code performance summary for Integrated Effects Tests (continued)

NUPEC Experiments:

Facility/Experiment Description	Highly Ranked Phenomena	CONTAIN Models Activated (ref. case)	Calculated Results Within Data Range (30 minute period)			Comments
			Press %*	Temp deg.	Conc. max %**	
NUPEC insulated steel containment, with internal sprays; short term tests only Test M-4-3; low-elevation steam/He injection	-multi-component gas compression/exp. - Jet-plume gas interaction/entrainment - buoyancy /stratification(regional) - buoyancy (transport) - 1-D conduction - surface H/M transfer (natural convection)	- atmos. T/H - default condensate film thickness - atmosphere rad. to structures - 35 cell nodalization - injection into cell 8	<11%	<1	<9%	- only steel internals (partitions) - geometrically scaled to typical PWR containment
Test M-8-1; mid-elevation steam/He injection		- injection into cells 22 and 35	<10%	<5	<3%	- hybrid flow solver improves stratification prediction
Test M-7-1 (ISP-35); low-elevation steam/He injection with sprays	- spray mass/energy exchange - spray dynamics (mixing)	- injection into cell 8 - spray droplet size = 0.0007 meters, specified conv. vel. to account for spray dynamic effects	<40%	<6	<8%	- spray dominated mixing - under estimate of energy removal from lower comp. partitions responsible for late time pressure over prediction - improved subcompartment results with spray carryover and spray water washdown of internal structures (sensitivity calc. with selected subcompartments))
Test M-8-2; mid-elevation steam/He injection with sprays		-injection into cells 22 and 35, 0.0007 meter droplet, specified conv. vel.	<80%	<10	<17%	- under estimate of energy removal from lower comp. partitions responsible for late time pressure over prediction

* $(\Delta P_{calc} - \Delta P_{measured}) / \Delta P_{measured}$; $\Delta P_{measured} = P - P_0$ and $\Delta P_{calc} = P_{calc} - P_0$

** $(\Delta\_)_{calc} / (\_)_{measured}$, where $\Delta = |calc. - measured|$

6 References

Boy90 Boyack, B.E., et al., "Quantifying Reactor Safety Margins, Part 1: An Overview of the Code Scaling, Applicability, and Uncertainty Evaluation Methodology," Nuclear Engineering Design, 119, pp. 1-15, 1990.

Boy95 Boyack, B.E., Corradini, M.L., Denning, R.S., Khatib-Rahbar, M., Loyalka, S.K., and Smith, P.N., "CONTAIN Independent Peer Review," LA-12866, UC-000, Los Alamos National Laboratory, Los Alamos, NM, January 1995.

Wil96 Wilson, G.E. and Boyack, B.E., " The Role of the PIRT Process in Identifying Code Improvements and Executing Code Development," OECD Meeting, Annapolis, Maryland, November 5-8, 1996.

Til96a Tills, J., "Calculations and Analyses for the Large-Scale Passive Containment Cooling System (PCS) Tests," SAND96-1089, (Proprietary), Sandia National Laboratories - Contractor Report, Albuquerque, NM, May 1996.

Til96b Tills, J., et al., "User Guidance on the CONTAIN Code for Advanced Light Water Reactors," SAND96-0947, (Proprietary), Sandia National Laboratories, Albuquerque, NM, April 1996.

Huh93 Huhtiniemi, I.K. and Corradini, M.L., "Condensation in the Presence of Noncondensable Gases," Nuclear Engineering Design, 141, pp. 429-446, 1993.

Phe93 "Phebus FP Programme - Final Report on the 4th Period," Phebus Report No. IP/93/195, Institut de Protection et de Surete Nucleaire, CEA, France, June 1993.

Phe94 "Phebus PF FPT0 Preliminary Report, Part C - Degradation Phase," Phebus Report No. IP/94/211, Institut de Protection et de Surete Nucleaire, CEA, France, May 1994.

Phe94a "Phebus-FP Information Meeting - Proceeding," Phebus Report No. IP/94/224, Institut de Protection et de Surete Nucleaire, CEA, France, November 1994.

Kit78 Kitani, S., "Containment Spray Experiments for Pressure Suppression," presentation at 1st International Conference on Liquid Atomization and Spray Systems, Tokyo, Japan, August 27-31, 1978.

Fir85 Firnhaber, M., "ISP16: Rupture of a Steam Line within the HDR-Containment Leading to an Early Two-Phase Flow - Results of the Post-Test Analyses," CSNI Report No. 112, June 1985.

Val83 Valencia, L. and Kanzleiter, T. F., "Blowdown Investigation in a Reactor Containment - Rupture of a Steam Pipe - Quick Look Report for Tests V42, V43, and V44," Technical Report PHDR 38-83, Kernforschungszentrum, Karlsruhe, Germany, May 1983.

Wol83 Wolf, L., Valencia, L., and Kanzleiter, T., "Overview of the HDR-containment tests," NUREG/CP-0048, Vol. 3, *Proceedings of the U.S. Nuclear Regulatory Commission Eleventh Water Reactor Safety Research Information Meeting*, Gaithersburg, Maryland, October 24-28, 1983.

Kar89 Karwat, H., "ISP23: Rupture of a Large-Diameter Pipe within the HDR-Containment," Vol. 1 and 2, CSNI Report No. 160, Committee on the Safety of Nuclear Installations - OECD Nuclear Energy Agency, Paris, France, 1989.

Val89 Valencia, L., "HDR Hydrogen Distribution Test after Large LOCA," *Proceedings of the 10th SMIRT Conference*, Anaheim, California, August 1989.

Wol89 Wolf, L. and Valencia, L., "Experimental Results of the Preliminary HDR-Hydrogen Distribution Test T31.5, *Proceedings of the 4th International Topical Meeting on Nuclear Reactor Thermal Hydraulics*, Karlsruhe, Germany, Vol. 2, p. 967, October 10-13, 1989.

Wol89b Wolf., L. and Valencia, L., "Hydrogen Mixing Experiments in the HDR-facility," NUREG/CP-0105, *Proceedings of the U.S. Nuclear Regulatory Commission Seventeenth Water Reactor Safety Research Information Meeting*, Rockville, MD October 1989.

Kar92 Karwat, H., "OECD-CSNI-ISP29, Distribution of Hydrogen within the HDR-Containment under Severe Accident Conditions - Final Comparison Report," Organization for Economic Cooperation and Development - Committee on the Safety of Nuclear Installations, August 1992.

Til92 Tills, J., "Analysis of the HDR Test E11.2," Letter Report to USNRC from Department 6421, Sandia National Laboratories, Albuquerque, NM, May 1992.

Mur96 Murata, K. K. and Stamps, D. W., "Development and Assessment of the CONTAIN Hybrid Flow Solver," SAND96-2792, Sandia National Laboratories, Albuquerque, NM, 1996.

Mur97 Murata, K.K., et al., "Code Manual for CONTAIN 2.0: A Computer Code for Nuclear Reactor Containment Analysis," NUREG/CR-6533, SAND97-1735, Sandia National Laboratories, Albuquerque NM, December 1997.

Roy95 Royl, P., Muller, C., Travis, J.R., and Wilson, T., "Validation of GASFLOW for Analysis of the Steam/Hydrogen Transport and Combustion Processes in Nuclear Reactor Containments," *Proceedings of the 13th Conference on Structural Mechanics in Reactor Technology*, Porto Alegre, RS, Brazil, August 13-18, 1995.

Wen87 Wenzel, H.H., et al., "Blowdown- und Wasserstoffvertieilungsversuche Versuchsgruppe CON Versuch T31.5," PHDR 3.520/88, Kernforschungszentrum, Karlsruhe, Germany, December 1987 (in German).

Wen91 Wenzel, H.H., et al., "Quality Considerations of Major Direct and Indirect Measured Quantities During the Experiments of Test-Group E11," PHDR-Working Report No. 10.025/91, Kernforschungszentrum, Karlsruhe, Germany, June 1991.

Val92 Valencia, L., et al., "Design Report - Hydrogen Distribution Experiments, E11.1-E11.5," PHDR-Working Report No. 10.004/89, Kernforschungszentrum, Karlsruhe, Germany, August 1992.

Gre92 Green, J. and Almenas, K., "Modeling of the HDR E11.4 Experiment Using CONTAIN 1.12," Report to USNRC from College of Engineering, Nuclear Engineering Program, Materials and Nuclear Engineering, University of Maryland, College Park, Maryland, March 1992.

Gre94 Green, J., "The Impact of Bulk Atmospheric Motion Upon Condensation Heat Transfer in the Presence of Noncondensable Gases," MDNE-93-005, Materials and Nuclear Engineering, University of Maryland, College Park, Maryland, May 1994.

Gre96 Green, J. and Almenas, K., "An Overview of the Primary Parameters and Methods for Determining Condensation Heat Transfer to Containment Structures," Nuclear Safety, Vol. 37, No. 1, January-March, 1996.

Lee99 Lee, S.J., et al., "Benchmark of the Heiss Dampf Reaktor E11.2 Containment Hydrogen-Mixing Experiment Using the MAAP4 Code," Nuclear Technology, Vol. 125, pp.182-195, February 1999.

Sch70 Schmitt, R.C., Bingham, G.E., and Norberg, J.A., "Simulated Design Basis Accident Tests of the Carolinas Virginia Tube Reactor Containment - Final Report," IN-1403, UC-80, Idaho Nuclear Corporation, National Reactor Testing Station, Idaho Falls, Idaho, December 1970.

Car81 Carbajo, J. J., "Heat Transfer Coefficients Under LOCA Conditions in Containment Buildings," Nuclear Engineering Design, Vol 65, pp. 369-386, 1981.

Kro78 Krotiuk, W. J. and Rubin, M.B., "Condensing Heat Transfer Following a Loss-of-Coolant Accident," Nuclear Technology, Vol 37, pp. 118-128, February 1978.

Eco87 Economos, C., et al., "Condensation Heat Transfer Modelling for Containment Environmental Response Calculations - a Reappraisal for the Standard Review Plan: Main Report," BNL Technical Report A-3719, Brookhaven National Laboratory, Associated Universities, Inc., Upton, Long Island, New York, June 1987.

Tak91 Takumi, K., et al., "Proving Test on the Reliability for Reactor Containment Vessel, Hydrogen Mixing and Distribution Test," Proceedings of a Workshop on Hydrogen Behavior and Mitigation in Water-Cooled Nuclear Power Reactors, Brussels, Belgium, 1991 March 4-8, pp. 96-101.

Tak92 Takumi, K. and Nonaka, A., "Overview of NUPEC Containment Integrity Project," 5th Workshop on Containment Integrity for Nuclear Power Plants, Washington, DC, 1992 May 12-14, pp. 367-380.

Mar88 Marx, K.D., "Analysis and Computer Simulation of Confined Ring Vortices Driven by Falling Sprays", Physics of Fluids, Vol. 31, No. 2, pp.263-77, February,1988.

Sta95 Stamps, D.W., "CONTAIN Assessment of the NUPEC Mixing Experiments," SAND94-2880, UC-505, Sandia National Laboratories, Albuquerque, NM, August 1995.

Sta98 Stamps, D.W., "Analyses of the Thermal Hydraulics in the NUPEC 1/4 Scale Model Containment Experiments," Nuclear Science and Engineering, Vol. 128, pp. 1-27, 1998.

OECD94 "Final Comparison Report on ISP-35: NUPEC Hydrogen Mixing and Distribution Test (Test M-7-1)," Organization for Economic Co-Operation and Development (OCDE) report, OCDE/GD/(95)29, NEA/CSNI/R(94)29, Paris, France, December 1994.

APPENDIX A

Listing of Reference CONTAIN Input Files

[Electronic Storage Data]